DIRECTIONAL CODING OF BACKWARD COMPATIBLE HIGH DYNAMIC RANGE (HDR) IMAGE CODING RESIDUES

A THESIS SUBMITTED TO
THE GRADUATE SCHOOL OF NATURAL AND APPLIED SCIENCES
OF
MIDDLE EAST TECHNICAL UNIVERSITY

BY

KUTAN FEYIZ

IN PARTIAL FULFILLMENT OF THE REQUIREMENTS
FOR
THE DEGREE OF MASTER OF SCIENCE
IN
ELECTRICAL AND ELECTRONICS ENGINEERING

JANUARY 2018

Approval of the thesis:

DIRECTIONAL CODING OF BACKWARD COMPATIBLE HIGH DYNAMIC RANGE (HDR) IMAGE CODING RESIDUES

submitted by **KUTAN FEYIZ** in partial fulfillment of the requirements for the degree of **Master of Science in Electrical and Electronics Engineering Department, Middle East Technical University** by,

Prof. Dr. Gülbin Dural Ünver
Dean, Graduate School of **Natural and Applied Sciences** _____

Prof. Dr. Tolga Çiloğlu
Head of Department, **Electrical and Electronics Engineering** _____

Assoc. Prof. Dr. Fatih Kamışlı
Supervisor, **Electrical and Electronics Eng. Dept., METU** _____

Dr. Alper Koz
Co-supervisor, **Center for Image Analysis (OGAM), METU** _____

Examining Committee Members:

Prof. Dr. Abdullah Aydın Alatan
Electrical and Electronics Eng. Dept., METU _____

Assoc. Prof. Dr. Fatih Kamışlı
Electrical and Electronics Eng. Dept., METU _____

Prof. Dr. Gözde Bozdağı Akar
Electrical and Electronics Eng. Dept., METU _____

Assoc. Prof. Dr. Ahmet Oğuz Akyüz
Computer Eng. Dept., METU _____

Assist. Prof. Dr. Hakkı Alparslan Ilgın
Electrical and Electronics Eng. Dept., Ankara University _____

Date: _____

I hereby declare that all information in this document has been obtained and presented in accordance with academic rules and ethical conduct. I also declare that, as required by these rules and conduct, I have fully cited and referenced all material and results that are not original to this work.

Name, Last Name: KUTAN FEYIZ

Signature :

ABSTRACT

DIRECTIONAL CODING OF BACKWARD COMPATIBLE HIGH DYNAMIC RANGE (HDR) IMAGE CODING RESIDUES

Feyiz, Kutan
M.S., Department of Electrical and Electronics Engineering
Supervisor : Assoc. Prof. Dr. Fatih Kamışlı
Co-Supervisor : Dr. Alper Koz

January 2018, 120 pages

High dynamic range (HDR) image and video formats are proposed to overcome limitations of widely accepted standard 8-bit low dynamic range (LDR) image and video representations. The main aim of these formats is to encode the whole luminance range of real world scenes which changes from extreme darkness (10^{-6} cd/m^2) to bright sunshine (10^8 cd/m^2), and to generate and store such scenes independent from the display technology. To achieve a successful transition from LDR to HDR technology, backward compatible image and video representation formats are proposed so that both LDR and HDR displays can use the same representation to show LDR and HDR versions of the same content. This is typically achieved by including in the representation an LDR base layer, and an HDR enhancement layer that includes a method to predict HDR content from the LDR content in the base layer and possibly residue data to correct the HDR prediction. The main focus of this thesis is to implement a more efficient coding method for backward compatible HDR image coding residues, which are defined as the differences between original HDR images and their predictions from the corresponding base layer LDR images. As the first stage, analyses of similarities between spatial characteristics of backward compatible HDR image coding residues and LDR motion-compensated (MC) prediction residuals, for which directional coding methods were proposed, are performed. These analyses are followed by an implementation of suitable directional transforms which model spatial

characteristics of backward compatible HDR image coding residues more efficiently. Rate-distortion performance of the proposed method for coding of backward compatible HDR image coding residues are evaluated with objective and perceptual quality metrics. Results indicate that the proposed coding method can perform better than the standard coding methods for the coding of backward compatible HDR image coding residues.

Keywords: High dynamic range image, backward compatible coding, spatial characteristics, statistical analyses, residue 8-bit conversion, residue coding, directional coding

ÖZ

GERİYE UYUMLU YÜKSEK DİNAMİK ORANLI (YDO) GÖRÜNTÜ KODLAMA KALINTILARININ YÖNLÜ KODLAMASI

Feyiz, Kutan
Yüksek Lisans, Elektrik ve Elektronik Mühendisliği Bölümü
Tez Yöneticisi : Doç. Dr. Fatih Kamışlı
Ortak Tez Yöneticisi : Dr. Alper Koz

Ocak 2018 , 120 sayfa

Yüksek dinamik oranlı (YDO) görüntü ve video biçimleri, gelişen dünyanın teknolojik ihtiyaçlarının gerektirdiği görsel içerikleri temsil etmekte yetersiz kalmakta olan yaygın bir şekilde kabul görmüş standart 8-bit alçak dinamik oranlı (ADO) gösterimin getirdiği sınırlamalarla başa çıkmak için önerilir. Bu biçimlerin başlıca amacı aşırı karanlıktan (10^{-6} cd/m^2) parlak güneş ışığına (10^{8} cd/m^2) kadar değişen gerçek dünya sahnelerinin tüm parlaklık aralığını kodlamaktır, ve sonuç olarak bir sahneyi ekran gösteriminden bağımsız olarak üretmek ve depolamaktır. ADO'dan YDO teknolojisine başarılı bir geçişi gerçekleştirmek için, geriye uyumlu görüntü ve video gösterim biçimleri önerilir, böylece aynı içeriğin ADO ve YDO versiyonlarını göstermek için hem ADO hem de YDO ekranlar aynı gösterimi kullanabilir. Bu tipik olarak gösterimin içerisine bir ADO temel katmanı, ve temel katman içerisindeki ADO içeriğinden YDO içeriğinin tahmin edildiği bir yöntem ve YDO tahminini düzeltmek için mümkün olduğunca kalıntı verisi içeren bir YDO yükseltme katmanı dahil edilerek gerçekleştirilir. Bu tezde, orijinal YDO görüntüleri ve onların temel katman ADO görüntülerine karşılık gelen tahminleri arasındaki farklar olarak tanımlanan geriye uyumlu YDO görüntü kodlama kalıntıları için daha verimli bir kodlama yöntemi uygulanmasına odaklanılmıştır. İlk aşamada, geriye uyumlu YDO görüntü kodlama kalıntılarının ve yönlü kodlama yöntemleri önerilmiş olan ADO hareket-telafili tahmin kalıntılarının uzamsal karakteristiklerinin aralarındaki benzerliklerin analizleri

gerçekleştirilmiştir. Bu analizleri, geriye uyumlu YDO görüntü kodlama kalıntılarının uzamsal karakteristiklerini daha verimli modelleyen uygun yönlü dönüşümlerin uygulanması takip etmiştir. Geriye uyumlu YDO görüntü kodlama kalıntılarının kodlaması için önerilen yöntemin oran-bozulma performansı tarafsız ve algısal nitelik metriklerine göre değerlendirilmiştir. Sonuçlar, önerilen kodlama yönteminin geriye uyumlu YDO görüntü kodlama kalıntılarının kodlaması için standart kodlama yöntemlerinden daha iyi performans gösterebileceğini ortaya koymuştur.

Anahtar Kelimeler: Yüksek dinamik oranlı görüntü, geriye uyumlu kodlama, uzamsal karakteristikler, istatistiksel analizler, kalıntı 8-bit dönüşümü, kalıntı kodlama, yönlü kodlama

To science...

ACKNOWLEDGMENTS

First of all, I would like to express my sincere thanks to my supervisor Assoc. Prof. Dr. Fatih Kamışlı for his valuable guidance, and positive suggestions in order to make this thesis work more realistic. It has been such an honor to be the graduate student of him. I would also like to acknowledge Dr. Alper Koz as a co-supervisor.

I would like to thank to Prof. Dr. A. Aydın Alatan for the research environment Center for Image Analysis (OGAM) that he has provided.

I would like to acknowledge Dr. Frederic Dufaux and Dr. Giuseppe Valenzise of Laboratoire des Signaux et Systémes (L2S), CNRS, CentraleSupélec, Université Paris-Sud, Paris, France, and Emin Zerman of LTCI, Télécom ParisTech, Université Paris-Saclay, Paris, France for their valuable suggestions and contributions on this thesis work.

I would also like to acknowledge the Scientific and Technological Research Council of Turkey (TÜBİTAK) and the French Ministry of Foreign Affairs under the common program BOSPHORUS with the project number 115E830 for the scholarship they have provided to me throughout my thesis research.

Finally, I would like to thank to my father, grandmother and aunt specially for their constant supports and encouragements during my thesis study.

TABLE OF CONTENTS

ABSTRACT v

ÖZ vii

ACKNOWLEDGMENTS x

TABLE OF CONTENTS xi

LIST OF TABLES xiv

LIST OF FIGURES xv

LIST OF ABBREVIATIONS xx

CHAPTERS

1 INTRODUCTION 1

1.1 Previous Research 3

1.2 Goals of the Research 5

1.3 Outline of the Thesis 5

2 GENERAL SCHEME FOR PROPOSED BACKWARD COMPATIBLE CODING OF HIGH DYNAMIC RANGE (HDR) IMAGE 7

2.1 Base Layer Operations 9

2.2 Residue Layer Operations 14

3 AUTO-COVARIANCE (AC) ANALYSES OF BACKWARD COMPATIBLE HDR IMAGE CODING RESIDUES 17

3.1 AC Analyses 18

3.1.1 AC Models 24

3.1.2 Estimation of the Parameters of AC Models 26

4 EXPERIMENTAL RESULTS FOR THE AC ANALYSES OF BACKWARD COMPATIBLE HDR IMAGE CODING RESIDUES 29

4.1 Experimental Setup 29

4.2 AC Analyses Results 33

5 PROPOSED CODING METHOD FOR BACKWARD COMPATIBLE HDR IMAGE CODING RESIDUES 57

5.1 8-bit Conversion of Backward Compatible HDR Image Coding Residues 57

5.1.1 The Sigmoid Function of the Adaptive Residual Mapping Method for Backward Compatible HDR Image Coding Residues 58

5.1.2 The Logit Function of the Adaptive Residual Mapping Method for Backward Compatible HDR Image Coding Residues 65

5.1.3 Adaptation of the Optimum Tone Mapping Method to Backward Compatible HDR Image Coding Residues 73

5.2 Directional Coding of 8-bit Backward Compatible HDR Image Coding Residues and Details of the Utilized Directional Codec 81

6 EXPERIMENTAL RESULTS FOR THE PROPOSED CODING METHOD FOR BACKWARD COMPATIBLE HDR IMAGE CODING RESIDUES 89

6.1 Experimental Setup 89

6.2 Rate-Distortion Performance Results 90

6.2.1 Rate-Distortion Performance Results for the 8-bit Conversion of Backward Compatible HDR Image Coding Residues 91

6.2.2 Rate-Distortion Performance Results for the Coding of 8-bit Backward Compatible HDR Image Coding Residues 98

7 CONCLUSIONS 111

7.1 Summary 111

7.2 Conclusions 113

7.3 Future Work 114

REFERENCES 117

LIST OF TABLES

TABLES

Table 5.1 The codewords in order to represent the selected transforms for both the 4x4-pixel 8-bit backward compatible HDR image coding residue blocks and the 8x8-pixel 8-bit backward compatible HDR image coding residue blocks [33] 87

LIST OF FIGURES

FIGURES

Figure 2.1 The General Scheme for the Proposed Backward Compatible Coding of HDR Image 8

Figure 2.2 The parameterization of the tone mapping curve in [6]. The barplot is the log luminance histogram of an HDR image. 12

Figure 2.3 Illustration of the Base Layer Operations 13

Figure 3.1 (a) Tone mapped (method Mai *et al.*) log luminance (L) image of original HDR image *LasVegasStore*, (b, c, d, e) Its HDR image coding residues with different base layer quantization parameters, respectively, QP = 22, 27, 32, 37. 21

Figure 3.2 (a) Tone mapped (method Mai *et al.*) log luminance (L) image of original HDR image *AirBellowsGap*, (b, c, d, e) Its HDR image coding residues with different base layer quantization parameters, respectively, QP = 22, 27, 32, 37. 23

Figure 3.3 (a) Frame 10 of *mobile* sequence at CIF resolution, (b) Its LDR MC residual predicted from frame 9 using ful-pel motion estimation with 8x8-pixel blocks in [33]. 24

Figure 3.4 (a) Frame 118 of *basket* sequence at CIF resolution, (b) Its LDR MC residual predicted from frame 117 using ful-pel motion estimation with 8x8-pixel blocks in [33]. 24

Figure 3.5 Comparison between the separable AC model and the generalized AC model [33]. 26

Figure 4.1 The selected HDR images (tone mapped versions) for the experiments. 32

Figure 4.2 Characteristics of the selected HDR images for the experiments [38]. 32

Figure 4.3 The tone mapped (method Mai *et al.*) log luminance (L) images of the selected HDR image set. 36

Figure 4.4 The absolute backward compatible HDR image coding residues for the selected HDR image set with a fixed base layer quantization parameter, QP = 37. 38

Figure 4.5 The AC analyses results for the HDR image *LasVegasStore* with a fixed base layer quantization parameter, QP = 27. 40

Figure 4.6 The absolute backward compatible HDR image coding residues for the HDR image *LasVegasStore* with different base layer quantization parameters, respectively, QP = 22, 27, 32, 37. 43

Figure 4.7 The absolute backward compatible HDR image coding residues for the HDR image *RedwoodSunset* with different base layer quantization parameters, respectively, QP = 22, 27, 32, 37. 45

Figure 4.8 The AC analyses results with the separable AC model for the HDR image *LasVegasStore* with different base layer quantization parameters, respectively, QP = 22, 27, 32, 37. 46

Figure 4.9 The AC analyses results with the separable AC model for the HDR image *RedwoodSunset* with different base layer quantization parameters, respectively, QP = 22, 27, 32, 37. 47

Figure 4.10 The AC analyses results with the generalized AC model for the HDR image *LasVegasStore* with different base layer quantization parameters, respectively, QP = 22, 27, 32, 37. 48

Figure 4.11 The AC analyses results with the generalized AC model for the HDR image *RedwoodSunset* with different base layer quantization parameters, respectively, QP = 22, 27, 32, 37. 49

Figure 4.12 The histograms of the estimated angles (θ) with the generalized AC model for the HDR image *LasVegasStore* with different base layer quantization parameters, respectively, QP = 22, 27, 32, 37. 50

Figure 4.13 The histograms of the estimated angles (θ) with the generalized AC model for the HDR image *RedwoodSunset* with different base layer quantization parameters, respectively, QP = 22, 27, 32, 37. 51

Figure 4.14 The AC analyses results with the separable AC model for all the selected HDR images with a fixed base layer quantization parameter, QP = 27. 53

Figure 4.15 The AC analyses results with the generalized AC model for all the selected HDR images with a fixed base layer quantization parameter, QP = 27. 54

Figure 5.1 An illustration of the optimum s parameter value selection in the Sigmoid function of the adaptive residual mapping method for each of the selected five HDR images. 62

Figure 5.2 8-bit backward compatible HDR image coding residues obtained with the Sigmoid function of the adaptive residual mapping method using the optimum s parameter values with a fixed base layer quantization parameter, QP = 27. 65

Figure 5.3 An illustration of the optimum s parameter value selection in the Logit function of the adaptive residual mapping method for each of the selected five HDR images. 69

Figure 5.4 An illustration of 8-bit conversion curves obtained with the optimum s parameter values and the histogram of the normalized backward compatible HDR image coding residue in the Sigmoid (blue) and the Logit (red) functions of the adaptive residual mapping method for each of the selected five HDR images. 70

Figure 5.5 8-bit backward compatible HDR image coding residues obtained with the Logit function of the adaptive residual mapping method using the optimum s parameter values with a fixed base layer quantization parameter, QP = 27. 73

Figure 5.6 An illustration of the optimum δ parameter value selection in the adaptation of the optimum tone mapping method for the selected five HDR images. 77

Figure 5.7 An illustration of 8-bit conversion curve obtained with the optimum δ parameter value and the histogram of the normalized backward compatible HDR image coding residue in the adaptation of the optimum tone mapping method for each of the selected five HDR images. 78

Figure 5.8 8-bit backward compatible HDR image coding residues obtained with the adaptation of the optimum tone mapping method using the optimum δ parameter values with a fixed base layer quantization parameter, QP = 27. 81

Figure 5.9 The 8 1-D directional transforms defined on the 4x4-pixel 8-bit backward compatible HDR image coding residue blocks [33]. 82

Figure 5.10 The 16 1-D directional transforms defined on the 8x8-pixel 8-bit backward compatible HDR image coding residue blocks [33]. 83

Figure 5.11 The designed alternative scans used in entropy coding of the quantized 1-D directional transform coefficients defined on the 4x4-pixel 8-bit backward compatible HDR image coding residue blocks [33]. 85

Figure 5.12 The designed alternative scans used in entropy coding of the quantized 1-D directional transform coefficients defined on the 8x8-pixel 8-bit backward compatible HDR image coding residue blocks [33]. 86

Figure 6.1 HDR-MSE (log_{10}) vs. bitrate (bits/pixel) rate-distortion performance plot results for the different 8-bit conversions (Mai *et al.* (black) and Mir *et al.* (f_s) (blue)) of backward compatible HDR image coding residues for the selected five HDR images coded with the standard codec in the residue layer and with a fixed base layer quantization parameter, QP = 27. 95

Figure 6.2 HDR-MSE (log_{10}) vs. bitrate (bits/pixel) rate-distortion performance plot results for the different 8-bit conversions (Mai *et al.* (black) and Mir *et al.* (f_s) (blue)) of backward compatible HDR image coding residues for the selected five HDR images coded with the directional or in other words the 1-D codec in the residue layer and with a fixed base layer quantization parameter, QP = 27. 97

Figure 6.3 HDR-MSE (log_{10}) vs. bitrate (bits/pixel) rate-distortion performance plot results for the coding (the standard coding (blue) and the directional coding (red)) of 8-bit backward compatible HDR image coding residues for the selected five HDR images coded with the 8-bit conversion method of Mai *et al.* in the residue layer and a fixed base layer quantization parameter, QP = 27. 101

Figure 6.4 PU-PSNR [dB] vs. bitrate (bits/pixel) rate-distortion performance plot results for the coding (the standard coding (blue) and the directional coding (red)) of 8-bit backward compatible HDR image coding residues for the selected five HDR images coded with the 8-bit conversion method of Mai *et al.* in the residue layer and a fixed base layer quantization parameter, QP = 27. 104

Figure 6.5 HDR-VDP (Q) vs. bitrate (bits/pixel) rate-distortion performance plot results for the coding (the standard coding (blue) and the directional coding (red)) of 8-bit backward compatible HDR image coding residues for the selected five HDR images coded with the 8-bit conversion method of Mai *et al.* in the residue layer and a fixed base layer quantization parameter, QP = 27. 106

Figure 6.6 HDR-VQM vs. bitrate (bits/pixel) rate-distortion performance plot results for the coding (the standard coding (blue) and the directional coding (red)) of 8-bit backward compatible HDR image coding residues for the selected five HDR images coded with the 8-bit conversion method of Mai *et al.* in the residue layer and a fixed base layer quantization parameter, QP = 27. 109

LIST OF ABBREVIATIONS

HDR	High Dynamic Range
LDR	Low Dynamic Range
MC	Motion-Compensated
AVC	Advanced Video Coding
HEVC	High Efficiency Video Coding
MSE	Mean Square Error
PU	Perceptually Uniform
DCT	Discrete Cosine Transform
AC	Auto-Covariance
QP	Quantization Parameter
CST	Color Space Transformation
ICST	Inverse Color Space Transformation
TMO	Tone Mapping Operation/Operator
ITMO	Inverse Tone Mapping Operation/Operator
Norm	Normalization
Inv Norm	Inverse Normalization
HD	High Definition
CIF	Common Intermediate Format
HVS	Human Visual System
UVLC	Universal Variable Length Coding
CABAC	Context Adaptive Binary Arithmetic Coding
HDR-MSE	High Dynamic Range-Minimum Square Error
PU-PSNR	Perceptually Uniform-Peak Signal to Noise Ratio
HDR-VDP	High Dynamic Range-Visible Differences Predictor
HDR-VQM	High Dynamic Range-Video Quality Measure
VDP	Visible Differences Predictor

CHAPTER 1

INTRODUCTION

Image content which is represented by 8-bit per pixel has been commonly accepted in many applications and areas such as mobile phones, personal computers, tablets, televisions, internet/video streaming, digital film industry, medical imaging and etc. Such a wide acceptance of 8-bit representation is mainly because of the compact representation of one pixel value as a byte for the storage in memory chips and the sufficiency of 256 levels in order to implicate the luminance range of widely used low dynamic range (LDR) displays. However, display technology has evolved in recent years and displays with much higher dynamic range (*with up to 1,000,000:1 dynamic range and 4000 cd/m^2 peak luminance, and etc.*) than conventional LDR displays are becoming available. For these new displays, the 8-bit representation of visual content provides inadequate fidelity or visual quality.

In the last ten years, high dynamic range (HDR) image formats (*such as the Radiance RGBE (.hdr) [1], the OpenEXR (.exr) [2], the LogLuv [3] TIFF (.tiff), and etc.*) have been proposed and developed to encode the whole luminance range of real world scenes which changes from extreme darkness (10^{-6} cd/m^2) to bright sunshine (10^{8} cd/m^2) [4]. The main goal of this HDR technology is to capture, and to store or to transmit exact physical luminance values rather than the 8-bit intensities, and to generate and store a scene independently from the display technology [5]. Such a technology is expected to overcome the limitations of standard 8-bit representations for new generation cameras and displays possessing HDR utility and provide a much better perceived image quality for consumers in many applications and areas ranging from digital film industry to medical imaging [4-6].

A major challenge for HDR, which is represented in floating point real numbers, is an efficient compression scheme to store, transmit or manipulate these formats because of their bigger storage sizes and bigger transmission bandwidths compared to standard 8-bit LDR formats. Especially, for HDR video which requires more storage size and transmission bandwidth than standard 8-bit LDR video considerably. For example, the size of the HDR video, which was captured by the first HDR camera and displayed at the yearly ACM SIGGRAPH conference in 2009, was reported as 42 GB for only one minute demonstration compared to just 9 GB for its corresponding LDR [4]. In addition, backward compatibility to the existing 8-bit displays for such a compression scheme is an essential requirement for a wide acceptance of this technology by the users. Also, the previous research [7] shows that, the backward compatible coding approach or in other words the layer-based coding approach may outperform the single-layer coding approach in terms of HDR quality.

The objective of this thesis is to design an HDR image coding system, which is backward compatible with widely used standard 8-bit LDR displays, with the aim of providing successful transition from LDR to HDR technology. To achieve a successful transition from LDR to HDR technology, backward compatible image and video representation formats are proposed so that both LDR and HDR displays can use the same representation to show LDR and HDR versions of the same content. This is typically achieved by including in the representation an LDR base layer, and an HDR enhancement layer that includes a method to predict HDR content from the LDR content in the base layer and possibly residue data to correct the HDR prediction. The main focus for this objective is to implement a more efficient coding method for backward compatible HDR image coding residues, which are defined as the differences between original HDR images and their predictions from the corresponding base layer LDR images. In particular, analyses of similarities between spatial characteristics of backward compatible HDR image coding residues and LDR motion-compensated (MC) prediction residuals, for which directional coding methods were proposed, are performed. These analyses are followed by an implementation of suitable directional transforms, which model spatial characteristics of backward compatible HDR image coding residues more efficiently. Rate-distortion performance of the proposed method for coding of backward compatible HDR image coding residues are evaluated by ob-

jective and perceptual quality metrics as well.

1.1 Previous Research

In the literature, in order to handle the coding of high dynamic range (HDR) image, there exists mainly two coding approaches based on the current low dynamic range (LDR) codecs (*such as the Advanced Video Coding H.264/AVC [8] and the High Efficiency Video Coding (HEVC) [9]*). The first coding approach is the single-layer coding approach [10-12] and it exploits the advantages of the high profiles of those codecs, which can support higher bit-depths, in particular up to 14 bits. The second coding approach is the backward compatible coding approach [6, 13-29] or in other words the layer-based coding approach. This approach provides backward compatibility with the existing standard 8-bit LDR displays.

The ratio based method and the residual based method are some well-known layer-based coding approaches. In the ratio based method [16-18], set of parameters, which are the ratio between an original HDR image and its tone mapped LDR version, is sent as side information to the decoder in an auxiliary stream. The HDR image at the decoder side is reconstructed by multiplying the decoded LDR image and the ratio image, which is obtained from the set of parameters sent as side information to the decoder in the auxiliary stream.

In the residual based method [6, 15, 19-22, 27, 28], firstly, HDR images are tone mapped into 8-bit represented LDR images and after that these tone mapped images (*8-bit represented LDR images*) go through the standard 8-bit encoding-decoding process by using an existing codec (*such as H.264/AVC, HEVC, or etc.*). Finally, these coded 8-bit represented LDR images are inverse tone mapped in order to reconstruct HDR images, which are represented in floating point real numbers. These are the first layer or in other words the base layer operations.

In the enhancement layer, or in other words, in the residue layer, firstly, backward compatible HDR image coding residues are obtained by taking the difference between original HDR images and their predictions from the corresponding base layer LDR images. After that, these backward compatible HDR image coding residues

go through the standard 8-bit image encoding-decoding process by using an existing codec. Finally at the decoder side, HDR images are obtained by adding these coded backward compatible HDR image coding residues, which come from the enhancement layer, and the predicted HDR images (*predicted by inverse tone mapping of coded 8-bit represented LDR images of the base layer*).

Mai *et al.* have derived a closed-form solution for optimum tone mapping operation, which minimizes the mean square error (MSE) between an original HDR image and its prediction from the corresponding base layer LDR image [6]. Their solution is mainly based on a statistical model, which approximates the distortion in the sequence of tone mapping, encoding, decoding, and inverse tone mapping. The optimized tone mapping method of Mai *et al.* was improved in [19, 20] by using perceptually uniform (PU) luminance values in order to map the wide luminance range of HDR content rather than the logarithmic values and by also inserting the quality of the produced LDR images into the optimization problem as a constraint. Recent studies further explore the optimization of tone mapping curves by taking the rate of both the base layer and the enhancement layer or in other words the residue layer into account [29]. These methods, which perform the tone mapping operation for each frame independently, are replaced with tone mapping of successive video frames based on motion compensation [30].

While these previous methods mainly focus on the rate-distortion optimization of the base layer, the coding of the enhancement layer has received less attention compared to these previous approaches. Even though some recent studies [21, 22] specifically handle the coding of backward compatible HDR image coding residues by means of developing global tone mapping curves based on the histogram of them, they do not take local characteristics of residue blocks into account. It is however verified in the previous research on the LDR motion-compensated (MC) video coding [31-34] that residue blocks exhibit local anisotropic characteristics, which allows the use of directional transforms for more efficient coding of the residue than with the traditional 2-D discrete cosine transform (DCT) [35, 36].

1.2 Goals of the Research

In this thesis, firstly whether backward compatible high dynamic range (HDR) image coding residues exhibit also local anisotropic characteristics or not, as in the case of low dynamic range (LDR) motion-compensated (MC) prediction residuals [31-33] is investigated. To this aim, auto-covariance (AC) analyses on backward compatible HDR image coding residues are performed with respect to different bitrates (different quantization parameters (QPs)), spatial activities and dynamic ranges as the main variables in the HDR image coding. The resulting AC model parameters for a particular image and then the behaviours of these parameters are analyzed. After the verification of existence of such local anisotropic characteristics in backward compatible HDR image coding residues, rate-distortion performance results of different 8-bit conversion methods and different coding methods are examined comparatively.

1.3 Outline of the Thesis

The outline of the thesis is given as follows:

In **Chapter 2**, a general scheme of proposed backward compatible coding of high dynamic range (HDR) image with base layer and enhancement/residue layer is presented, and operations, which are accomplished for each stage of the both layers, are explained in detail.

In **Chapter 3**, auto-covariance (AC) analyses of backward compatible HDR image coding residues are presented and explained in detail.

In **Chapter 4**, experimental results for the AC analyses of several backward compatible HDR image coding residues, which have different bitrates (different quantization parameters (QPs)), spatial activities and dynamic ranges as the main variables in the HDR image coding, are given and interpreted.

In **Chapter 5**, proposed coding method for backward compatible HDR image coding residues are presented and explained in detail. In addition, details of the codec, which is utilized for this proposed coding method, are discussed.

In **Chapter 6**, experimental results for the proposed coding method for several backward compatible HDR image coding residues, which have different bitrates (different QPs), spatial activities and dynamic ranges as the main variables in the HDR image coding, are given, compared and interpreted.

In **Chapter 7**, summary of the thesis, conclusions and future work are provided.

CHAPTER 2

GENERAL SCHEME FOR PROPOSED BACKWARD COMPATIBLE CODING OF HIGH DYNAMIC RANGE (HDR) IMAGE

In this chapter, a general scheme for proposed backward compatible coding of high dynamic range (HDR) image with base layer and enhancement/residue layer is presented, and operations, which are performed in each stage of both layers, are explained in detail.

Figure 2.1 illustrates the general scheme for the proposed backward compatible coding of HDR image. The backward compatible, or in other words, the layer-based structure, which is used in this thesis, is composed of two layers. The first layer is called as *base layer* and the second layer is called as *enhancement layer* or *residue layer*. After this point, the second layer will be expressed as *residue layer* for simplicity.

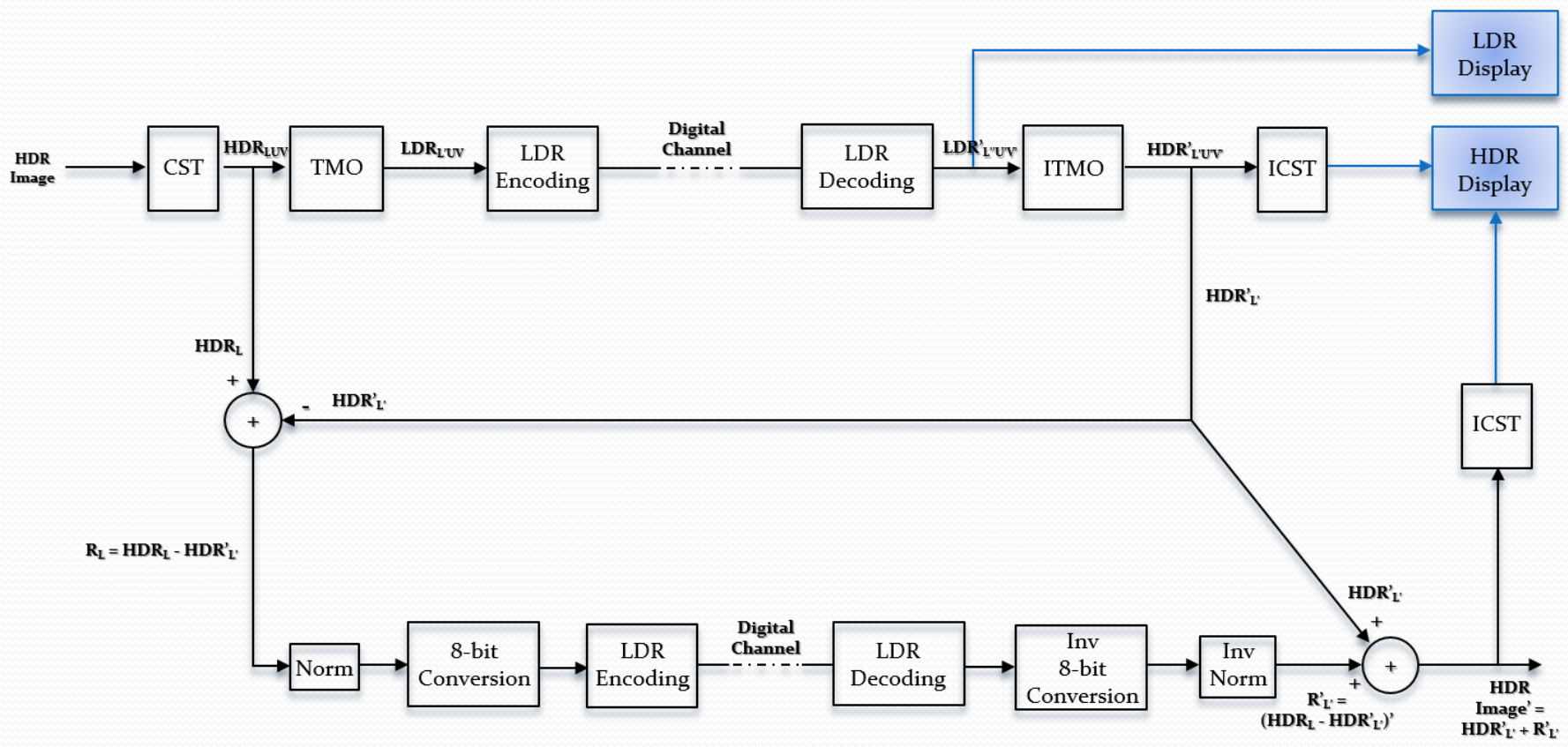

Figure 2.1: The General Scheme for the Proposed Backward Compatible Coding of HDR Image

2.1 Base Layer Operations

In the base layer, as seen from Figure 2.1, firstly, color space transformation (CST) is performed on high dynamic range (HDR) images which are in floating point real valued RGB format. The LogLuv transform, which is proposed by Larson [3], is used as a CST in order to transform floating point real RGB values into XYZ color space which is device independent. Note that XYZ values are also in floating points at this stage. After that, the X and Z components are used to calculate the 8-bit integer valued chroma components u_e and v_e in order to provide the 8-bit requirement of the codec that will be used in the base layer encoding-decoding operations. On the other hand, the Y component is held and the logarithm (log_{10}) of this Y component is computed (in order to map the wide dynamic range of luminance to the computationally more significant range), which is referred as *log luminance*, before the base layer tone mapping operation (TMO). In general, TMOs are constructed only for the luminance channel of HDR images, and the chroma channels are kept unchanged. After this point, *log luminance* will be used in order to refer to the logarithmic (log_{10}) values of the luminance for simplicity.

The utilized forward transformation equations in the CST block from RGB color space to LogLuv color space are as follows:

$$\begin{bmatrix} X \\ Y \\ Z \end{bmatrix} = \begin{bmatrix} 0.497 & 0.339 & 0.164 \\ 0.256 & 0.678 & 0.066 \\ 0.023 & 0.113 & 0.864 \end{bmatrix} \begin{bmatrix} R \\ G \\ B \end{bmatrix} \tag{2.1}$$

$$x = \frac{X}{X + Y + Z} \tag{2.2}$$

$$y = \frac{Y}{X + Y + Z} \tag{2.3}$$

$$u_e = \left\lfloor 410 \frac{4x}{-2x + 12y + 3} \right\rfloor \tag{2.4}$$

$$v_e = \left\lfloor 410 \frac{9y}{-2x + 12y + 3} \right\rfloor \tag{2.5}$$

$$L = log_{10}(Y) \tag{2.6}$$

The utilized inverse transformation equations in the inverse color space transformation (ICST) block from LogLuv color space to RGB color space are as follows:

$$Y = 10^L \tag{2.7}$$

$$u = \frac{u_e + 0.5}{410} \tag{2.8}$$

$$v = \frac{v_e + 0.5}{410} \tag{2.9}$$

$$x = \frac{9u}{6u - 16v + 12} \tag{2.10}$$

$$y = \frac{4v}{6u - 16v + 12} \tag{2.11}$$

$$X = \frac{Yx}{y} \tag{2.12}$$

$$Z = \frac{Y(1 - x - y)}{y} \tag{2.13}$$

$$\begin{bmatrix} R \\ G \\ B \end{bmatrix} = \begin{bmatrix} 2.690 & -1.276 & -0.414 \\ -1.022 & 1.978 & 0.044 \\ 0.061 & -0.224 & 1.163 \end{bmatrix} \begin{bmatrix} X \\ Y \\ Z \end{bmatrix} \tag{2.14}$$

Secondly, a TMO is applied on floating point real valued log luminance components (L) of HDR images. There are several tone mapping operators (TMO) for different

usages and they can be classified as *local*, *global*, *fixed*, *adaptive* or *etc.* with respect to their utilization specifics. A global tone mapping curve is a transformation function that maps floating point real valued HDR luminance pixel values to 8-bit represented low dynamic range (LDR) luminance pixel values regardless of the neighborhood relation between pixels. The optimum tone mapping method, which is derived by Mai *et al.* [6], is utilized as a TMO for the proposed backward compatible coding of HDR image. The optimum tone mapping method of Mai *et al.* minimizes the mean square error (MSE) between the log luminance of original HDR image and the log luminance of its prediction from the corresponding base layer LDR image. Given that the log luminance of HDR image and the pixel values of its tone mapped LDR version are denoted as *l* and *v* respectively, the tone mapping curve is first parameterized as a piece-wise linear function with nodes (l_k, v_k) as shown in Figure 2.2. Each segment k between two nodes (l_k, v_k) and (l_{k+1}, v_{k+1}) has a constant width in HDR values equal to δ (*selected as 0.1*).

The tone mapping curve is then uniquely specified by a set of slopes:

$$s_k = \frac{v_{k+1} - v_k}{\delta} \tag{2.15}$$

which forms a vector of the tone mapping parameters. Mai *et al.* have developed a statistical distortion model for the error on the tone mapping, coding, decoding and inverse tone mapping and have derived a closed-form solution for the optimum tone mapping curve in terms of slopes, s_k. Their eventual closed form solution minimizing the MSE between the log luminances of original and inverse tone mapped HDR images is found as:

$$s_k = \frac{v_{max} . p_k^{\frac{1}{3}}}{\delta . \sum_{k=1}^{N} p_k^{\frac{1}{3}}} \tag{2.16}$$

where p_k is the summation of the normalized histogram of the log luminance values for the *k*'th bin, *N* is the total number of bins in the histogram, and v_{max} is the maximum LDR pixel value.

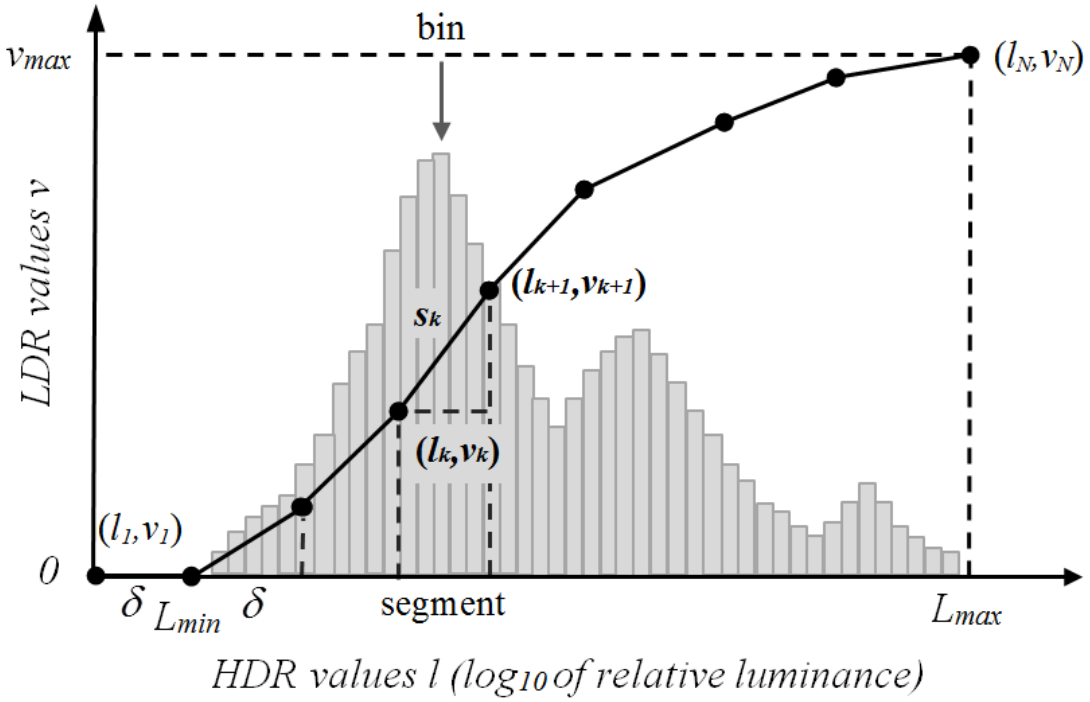

Figure 2.2: The parameterization of the tone mapping curve in [6]. The bar-plot is the log luminance histogram of an HDR image.

After the TMO, as shown in Figure 2.1, tone mapped HDR images (8-bit represented LDR versions) go through the encoding-decoding operation. As a codec, the H.264/AVC JM reference software encoder-decoder [8] is used for the proposed backward compatible coding of HDR image. Later the encoding-decoding operation, inverse tone mapping operation (ITMO), which is the inverse operation of the utilized TMO, is applied on these encoded-decoded tone mapped HDR images. As seen from Figure 2.1, if ICST is performed on these encoded-decoded inverse tone mapped HDR images, the resultant reconstructed HDR images are displayed on a HDR screen. As the other option, if there is not any HDR screen, these encoded-decoded tone mapped HDR images are displayed on a LDR screen directly without performing the ITMO and ICST operations.

The base layer operations are illustrated in more detail in Figure 2.3.

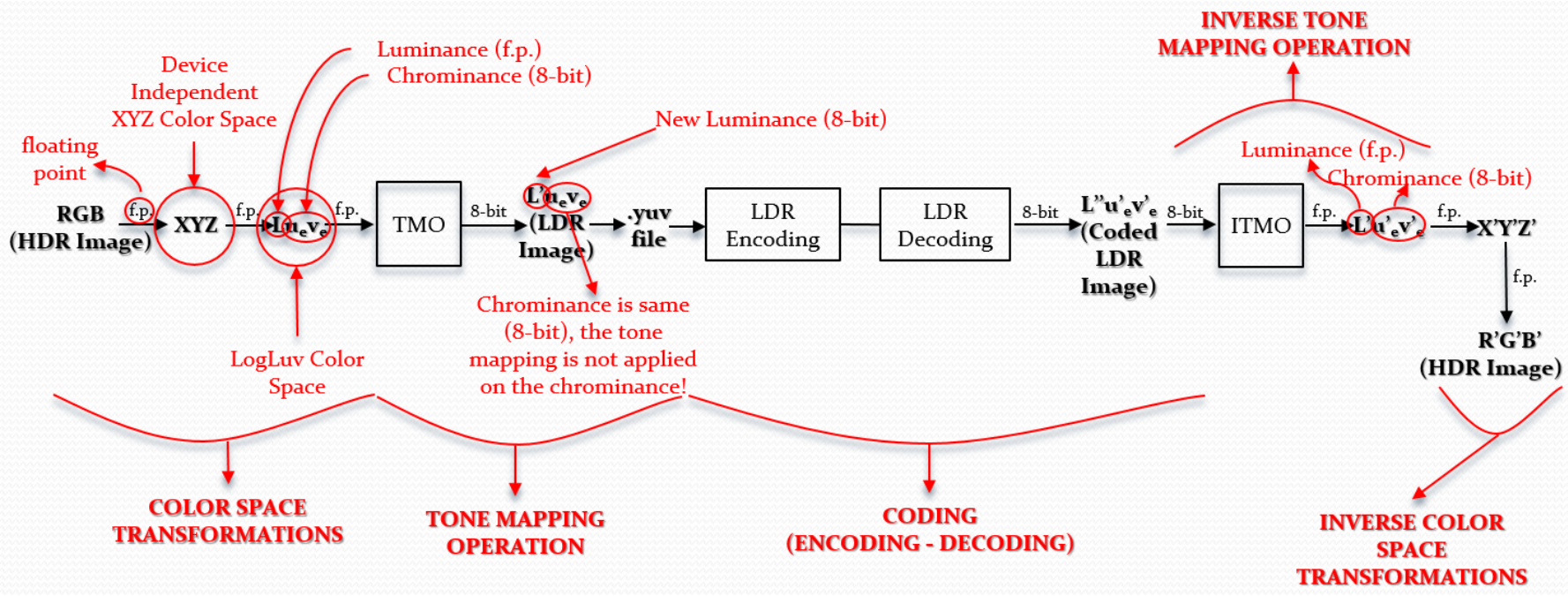

Figure 2.3: Illustration of the Base Layer Operations

2.2 Residue Layer Operations

In the residue layer, backward compatible high dynamic range (HDR) image coding residues are obtained by taking the difference between log luminance components (L) of original HDR images and log luminance components of their predictions, which are obtained by inverse tone mapping the corresponding base layer low dynamic range (LDR) images. Each pixel value in backward compatible HDR image coding residues is represented in floating point real numbers and backward compatible HDR image coding residues are single channel, which is the log luminance (L) only.

As seen from Figure 2.1, firstly, due to the fact that backward compatible HDR image coding residues' pixel values are represented in floating point real numbers, they should be converted into 8-bit format before the encoding-decoding operation in the residue layer. 8-bit conversion requires two operations: normalization (Norm) of backward compatible HDR image coding residues and then their conversion to 8-bit. For the 8-bit conversion of backward compatible HDR image coding residues, two 8-bit conversion methods are used (Mai *et al.* [6] and Mir *et al.* [22]). In Chapter 5, these utilized 8-bit conversion methods will be explained in detail.

After the 8-bit conversion of backward compatible HDR image coding residues, these 8-bit backward compatible HDR image coding residues go through the encoding-decoding operation. In the residue layer, two codecs are used and compared for this purpose. The first one is the standard or in other words the typical codec, which is the standard H.264/AVC JM reference software encoder-decoder [8], and the other one is the modified H.264/AVC JM reference software, which also includes 1-D directional transforms, in the encoder and decoder [32, 33]. In Chapter 5, these coding methods and utilized codecs will be explained in detail.

Finally at the decoder side, inverse 8-bit conversion is applied on the decoded 8-bit backward compatible HDR image coding residues. Inverse 8-bit conversion requires two operations: inverse 8-bit conversion of the decoded 8-bit backward compatible HDR image coding residues to the floating point real valued representation again and inverse normalization (Inv Norm) of these decoded floating point real valued backward compatible HDR image coding residues.

In conclusion, coded HDR images are obtained by adding the HDR images which are predicted by inverse tone mapping LDR images from the base layer and the reconstructed HDR image coding residues which come from the residue layer. As seen from Figure 2.1, if inverse color space transformation (ICST) is performed on these coded HDR images, they can be displayed on a HDR screen.

CHAPTER 3

AUTO-COVARIANCE (AC) ANALYSES OF BACKWARD COMPATIBLE HDR IMAGE CODING RESIDUES

In this chapter, auto-covariance (AC) analyses of backward compatible high dynamic range (HDR) image coding residues are presented and explained in detail. Before proposing an efficient coding method for backward compatible HDR image coding residues, it is necessary to study characteristics of them in order to code them more efficiently. For this purpose, it is investigated whether backward compatible HDR image coding residues exhibit also local anisotropic (*i.e., property of being directionally dependent, which implies different properties in different directions [37]*) characteristics or not as in the case of low dynamic range (LDR) motion-compensated (MC) prediction residuals in [31-33] with respect to different bitrates (different quantization parameters (QPs)), spatial activities and dynamic ranges as the main variables in the HDR image coding. Analyses methods are similar to those used in [32, 33] for analyzing LDR MC prediction residuals. At first, spatial characteristics of backward compatible HDR image coding residues and spatial characteristics of LDR MC prediction residuals are associated with each other by visual inspection. Then, utilized AC models in order to quantify the visually inspected similarities between spatial characteristics of backward compatible HDR image coding residues and LDR MC prediction residuals are explained, and estimation procedure of the parameters of utilized AC models are given at the end.

3.1 AC Analyses

Before proposing an efficient coding method for backward compatible high dynamic range (HDR) image coding residues, which are found by taking difference between the log luminances of original HDR images and their predictions from the base layer, with the aim of coding them more efficiently, it is necessary to study their characteristics. In this section, with this purpose, on account of understanding whether backward compatible HDR image coding residues exhibit also local anisotropic characteristics or not, as in the case of low dynamic range (LDR) motion-compensated (MC) prediction residuals, spatial characteristics of backward compatible HDR image coding residues and LDR MC prediction residuals are associated with each other based on visual inspection.

Figures 3.1 and 3.2 show tone mapped (method Mai *et al.* [6]) log luminance (L) images of their corresponding original HDR images and their backward compatible HDR image coding residues with different base layer quantization parameters, respectively, QP = 22, 27, 32, 37. They are all in high definition (HD) (1920x1080) resolution. Figures 3.3 and 3.4 show some LDR frames and their LDR MC prediction residuals. Figure 3.3 shows frame 10 of *mobile* sequence at common intermediate format (CIF) (352x288) resolution and Figure 3.4 shows frame 118 of *basket* sequence at CIF resolution. From Figures 3.1 and 3.2, it can be observed that, a substantial portion of the information in backward compatible HDR image coding residues with different base layer quantization parameters concentrates along edges, object boundaries and textured regions mostly, forming 1-D structures along them as in the case of LDR MC prediction residuals as seen from Figures 3.3 and 3.4.

Consequently, characteristics of backward compatible HDR image coding residues differ around edges, object boundaries and textured regions considerably. These different characteristics of backward compatible HDR image coding residues may arise because some effects alike the quantization noise that can be caused by the base layer tone mapping operation (TMO) and inverse tone mapping operation (ITMO). As mentioned before, a great portion of the backward compatible HDR image coding residues concentrates along edges, object boundaries and textured regions mostly, and forming 1-D structures along them. Thus, backward compatible HDR image coding residues

concentrating on these 1-D structures have 1-D characteristics.

(a)

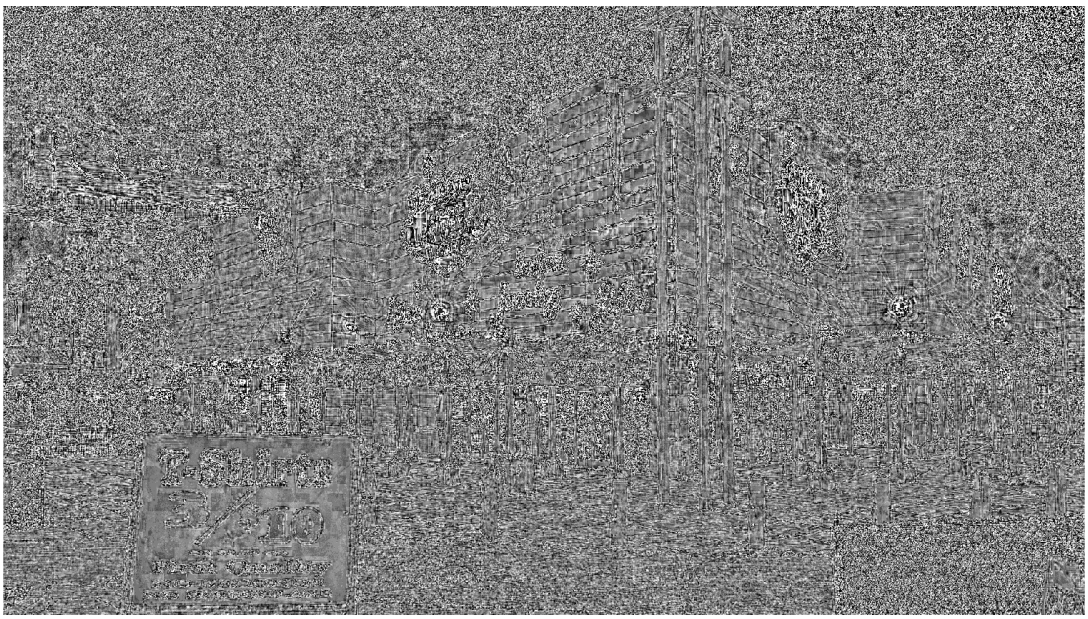

(b)

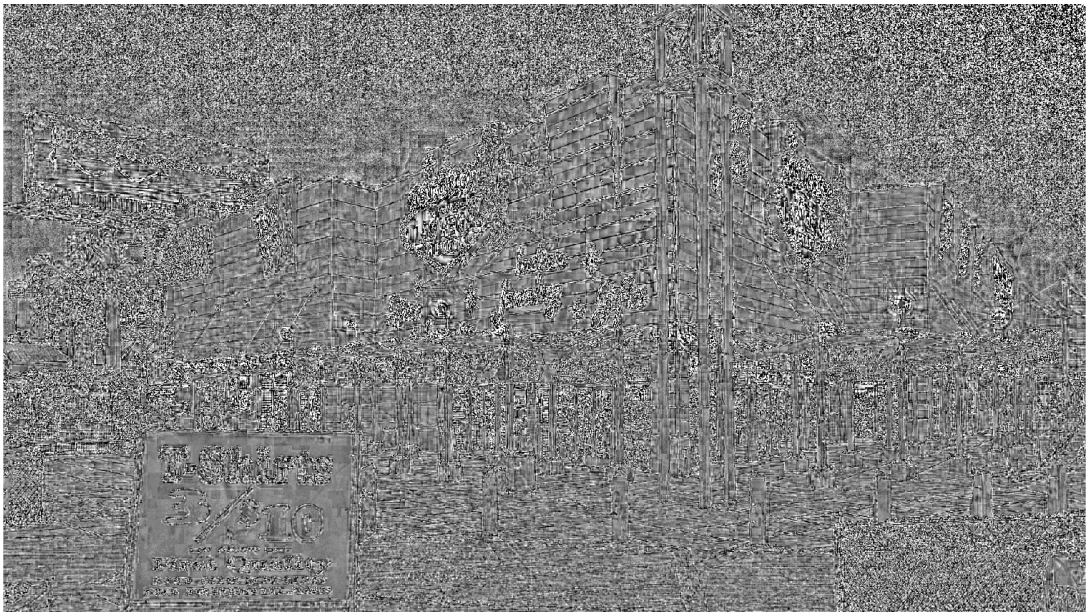

(c)

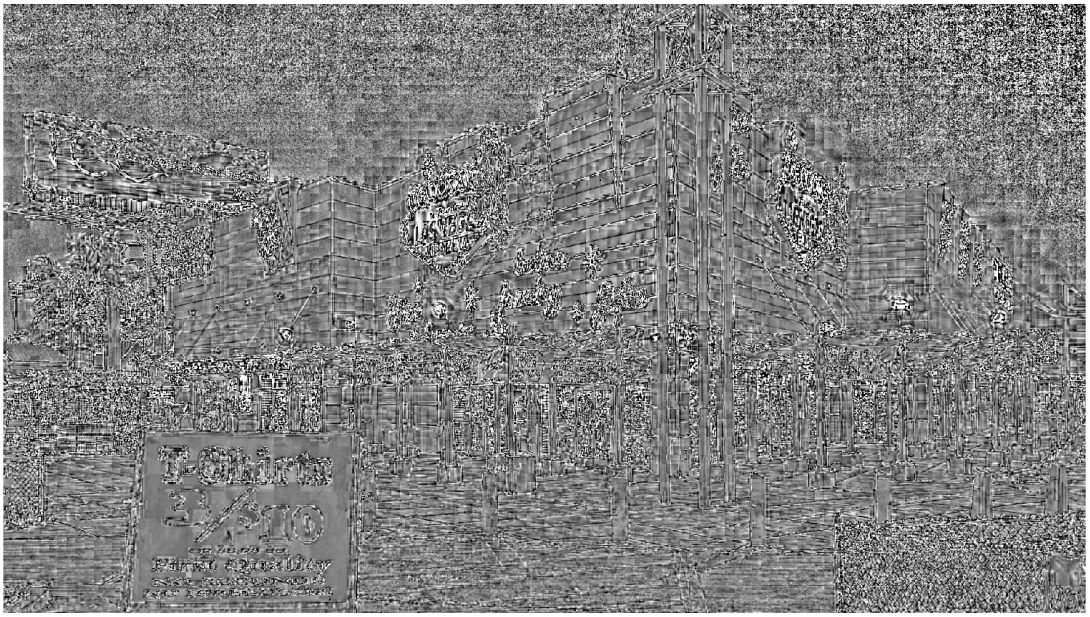

(d)

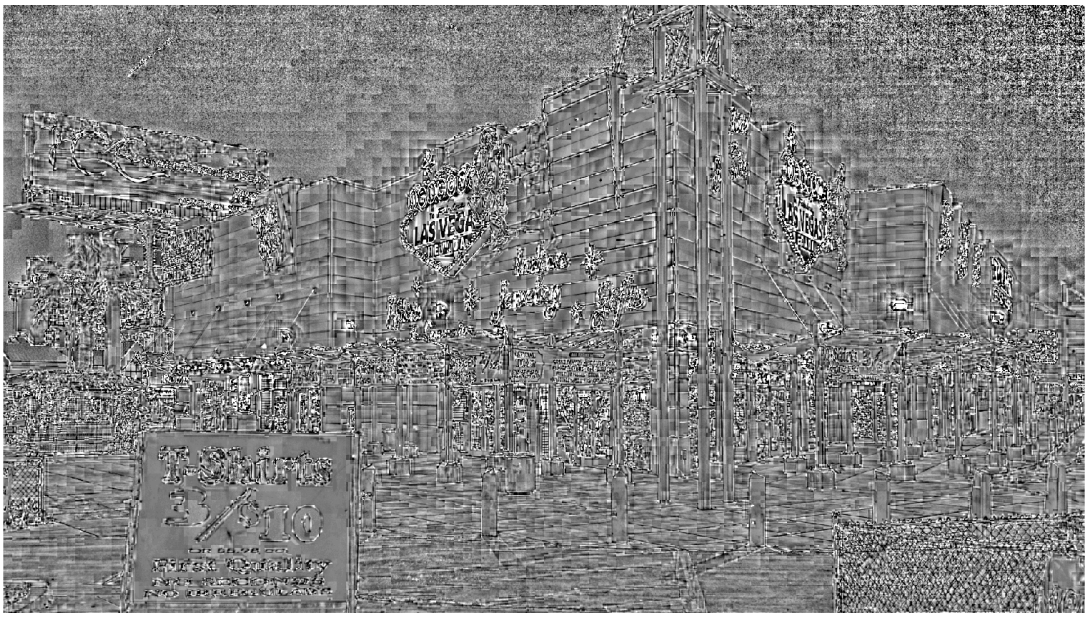

(e)

Figure 3.1: (a) Tone mapped (method Mai *et al.*) log luminance (L) image of original HDR image *LasVegasStore*, (b, c, d, e) Its HDR image coding residues with different base layer quantization parameters, respectively, QP = 22, 27, 32, 37.

(a)

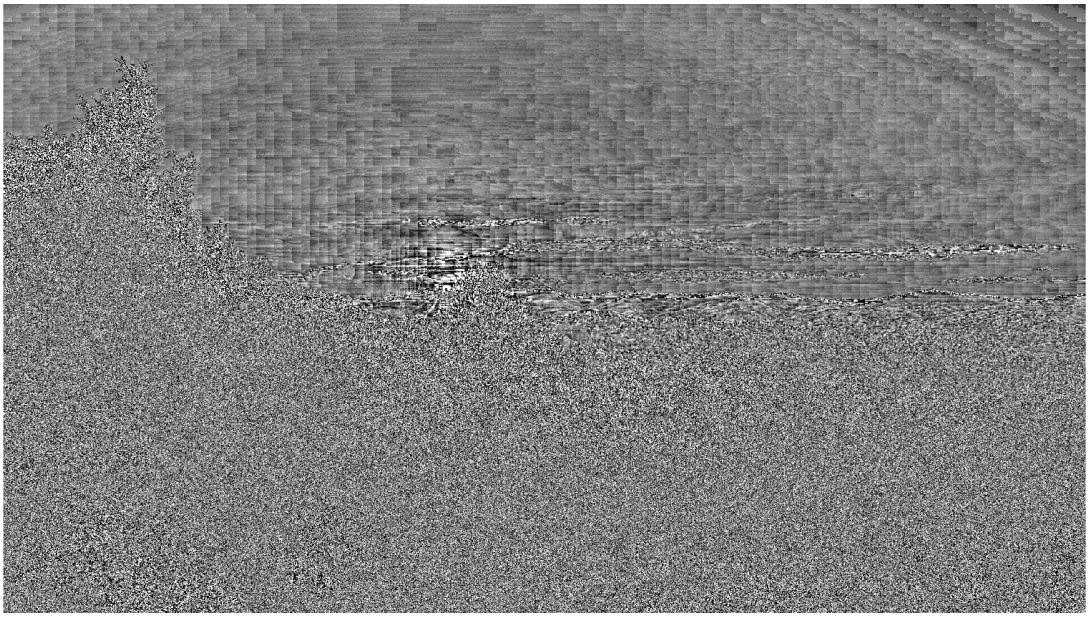

(b)

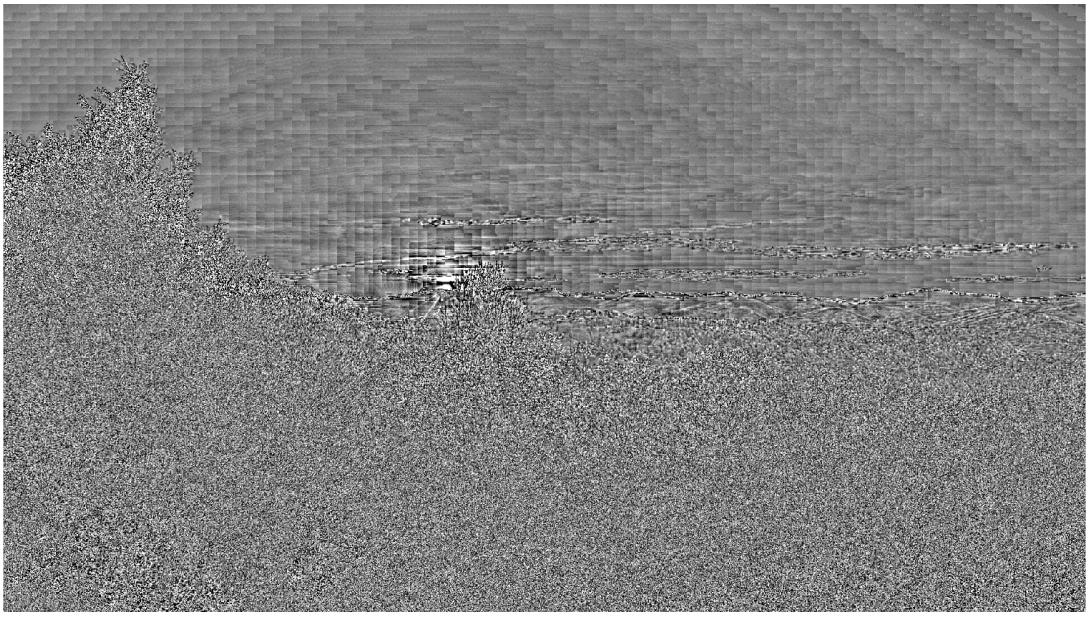

(c)

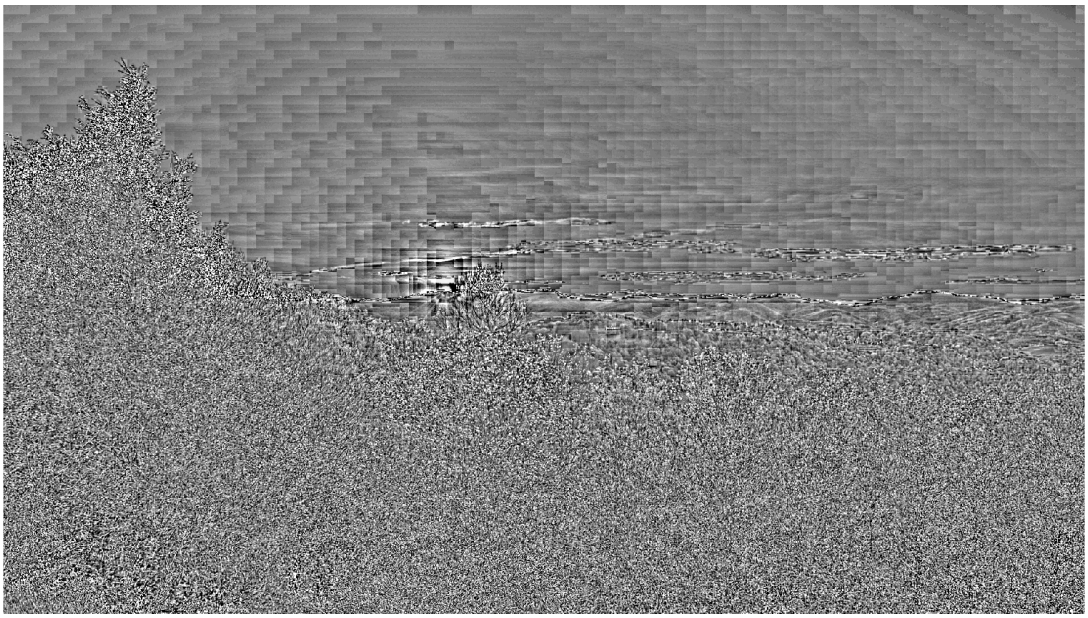

(d)

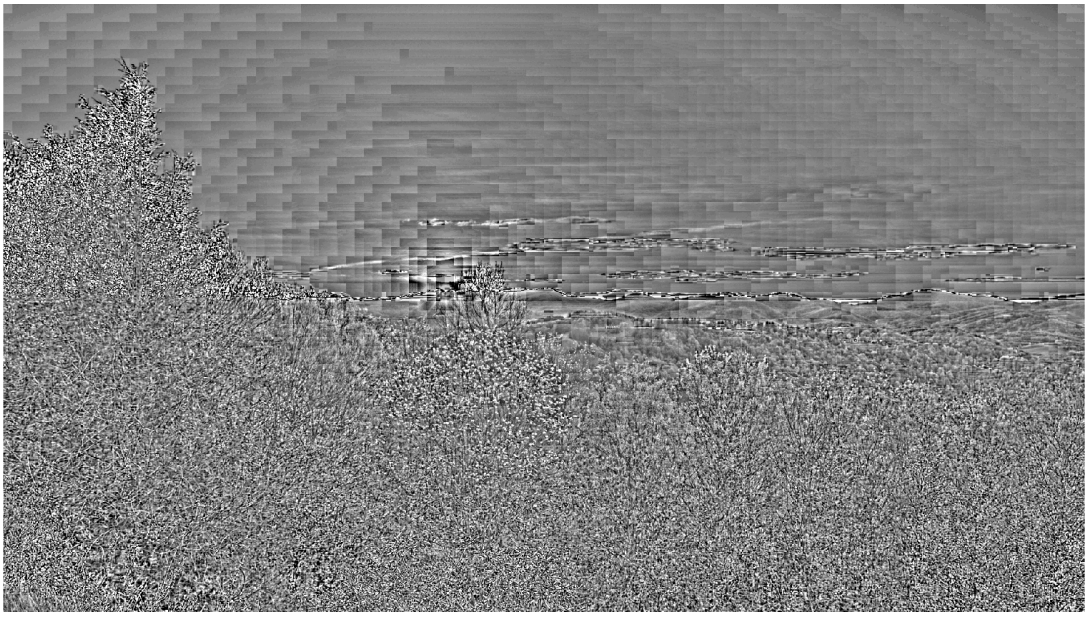

(e)

Figure 3.2: (a) Tone mapped (method Mai *et al.*) log luminance (*L*) image of original HDR image *AirBellowsGap*, (b, c, d, e) Its HDR image coding residues with different base layer quantization parameters, respectively, QP = 22, 27, 32, 37.

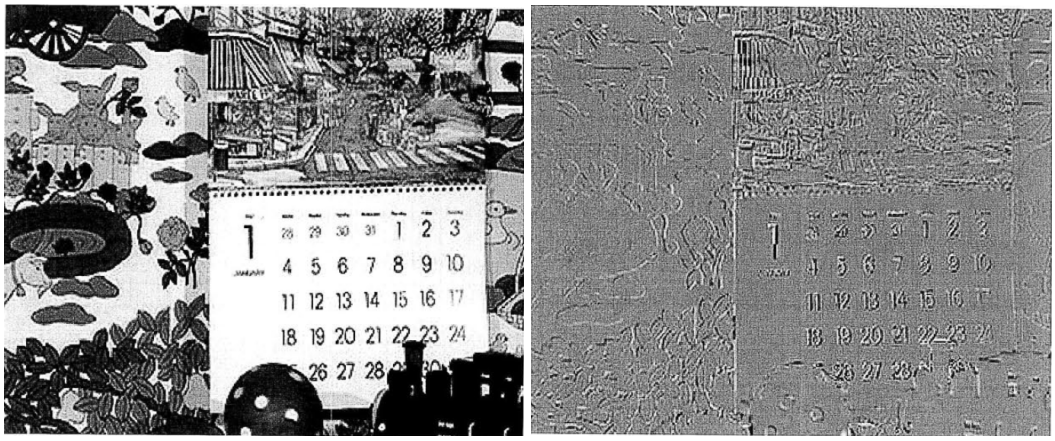

(a) (b)

Figure 3.3: (a) Frame 10 of *mobile* sequence at CIF resolution, (b) Its LDR MC residual predicted from frame 9 using ful-pel motion estimation with 8x8-pixel blocks in [33].

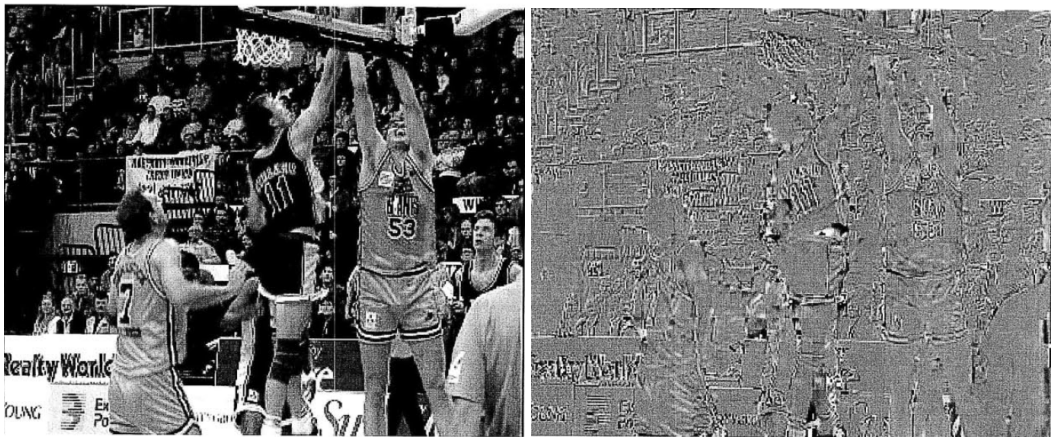

(a) (b)

Figure 3.4: (a) Frame 118 of *basket* sequence at CIF resolution, (b) Its LDR MC residual predicted from frame 117 using ful-pel motion estimation with 8x8-pixel blocks in [33].

3.1.1 AC Models

From the visual inspection of backward compatible high dynamic range (HDR) image coding residues, they have local anisotropic characteristics which differ remarkably

around edges, object boundaries and textured regions as in the case of low dynamic range (LDR) motion-compensated (MC) prediction residuals in [31-33]. A great portion of the signal concentrates along these structures and these structures are 1-D structures and backward compatible HDR image coding residues concentrating on these structures have 1-D characteristics. Therefore, in order to quantify whether backward compatible HDR image coding residues have local anisotropic characteristics or not as in the case of LDR MC prediction residuals in [31-33], auto-covariance (AC) analyses are performed.

With the aim of quantifying results of statistical analyses of backward compatible HDR image coding residues, AC of 8x8-pixel blocks of backward compatible HDR image coding residues are modeled with AC of a 2-D Markov process. Two AC models, which are proposed in [32, 33] for the statistical analyses, are used to analyze AC of local regions. The first AC model is the *separable AC model*, given in Equation 3.1 below:

$$R_s(I, J) = \rho_1^{|I|}\rho_2^{|J|} \tag{3.1}$$

Here, ρ_1 is the correlation parameter along the horizontal direction or the vertical direction, and ρ_2 is the correlation parameter along the other direction, which is perpendicular to the direction of the correlation parameter ρ_1. The larger correlation coefficient is always chosen as ρ_1 for simplicity. This is a separable model, and it can not model well the statistical characteristics of backward compatible HDR image coding residue blocks with strong correlation along diagonal directions. So, this model is global and it is insufficient to capture all local anisotropies in backward compatible HDR image coding residues. For this reason, another AC model given in Equation 3.2 below is also used in the statistical analyses,

$$R_g(\theta, I, J) = \rho_1^{|Icos(\theta)+Jsin(\theta)|}\rho_2^{|-Isin(\theta)+Jcos(\theta)|} \tag{3.2}$$

This model is called the *generalized AC model*, because it generalizes the separable AC model by introducing an additional parameter θ, which allows rotation of the horizontal and vertical axes of the separable AC model and thus can capture more

local anisotropic features. Thus, the generalized AC model is able to adapt and model the statistical characteristics of backward compatible HDR image coding residues which have strong correlation along diagonal directions other than the horizontal and vertical directions better.

Comparison between the separable AC model and the generalized AC model is illustrated in Figure 3.5.

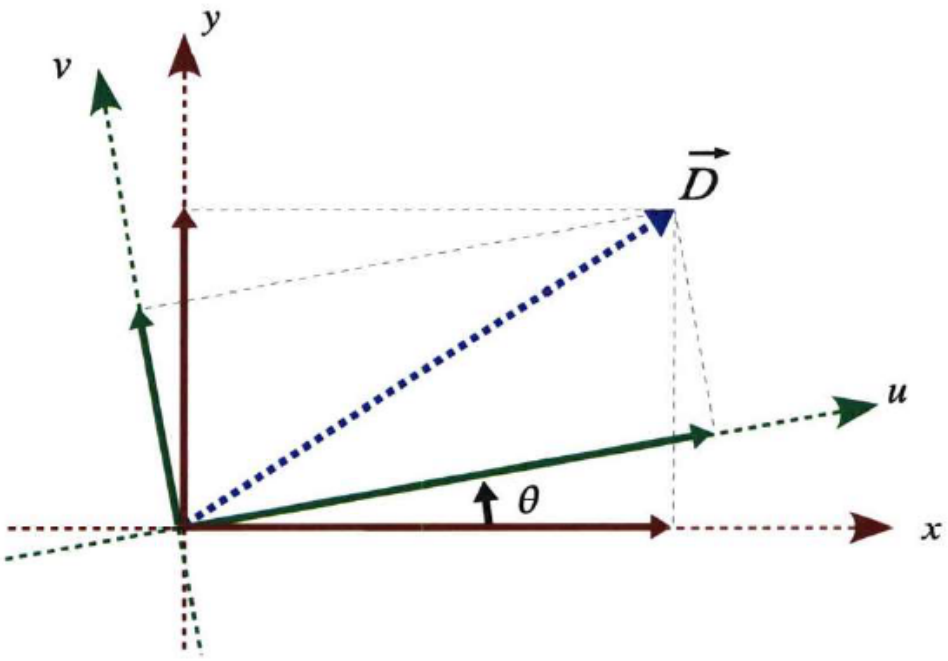

Figure 3.5: Comparison between the separable AC model and the generalized AC model [33].

3.1.2 Estimation of the Parameters of AC Models

Firstly, backward compatible high dynamic range (HDR) image coding residues are partitioned into 8x8-pixel blocks in order to obtain statistics from many local regions of them. After that, the unbiased estimator is utilized to estimate the non-parametric auto-covariance (AC) of each 8x8-pixel block by subtracting the mean of each 8x8-pixel block. Only the blocks, which have enough AC energy, are entered to the statistical analyses by comparing with a threshold. This is because the other blocks will typically be quantized to all-zero-blocks, which are not transformed in the codec and

therefore are ignored in the AC analyses. Finally, each zero mean 8x8-pixel block is correlated with itself, and each element of the correlation sequence is divided by the number of overlapping points used in the computation of that element.

Secondly, after finding the actual AC of each 8x8-pixel block, in order to provide best fit to the actual AC of each 8x8-pixel block, each 8x8-pixel block of backward compatible HDR image coding residues is modeled with both the separable AC model and the generalized AC model, and estimation of the parameters ρ_1 and ρ_2 (and θ for the generalized AC model) are performed by using these models. This is performed by using the optimization toolbox of MATLAB to find the best parameters ρ_1 and ρ_2 (and θ for the generalized AC model) so that the separable and generalized AC models fit the non-parametric estimated unbiased AC in the least square sense (minimum mean square error (MSE)).

Due to the fact that, the number of the overlapping points become less and the estimates become noisy at large lags; in the minimization, only the lags, which are less than four (*i.e.,* $|I|, |J| < 4$), are used. The estimated ρ_1 and ρ_2 parameters from all 8x8-pixel blocks can then be plotted as scatter plots for each backward compatible HDR image coding residue in order to be analyzed by using both the separable AC model and the generalized AC model. Each point in the scatter plots represents the estimated (ρ_1, ρ_2) pair from one 8x8-pixel backward compatible HDR image coding residue block (ρ_1 is the larger correlation coefficient and θ varies between 0° and 180°). By comparing the scatter plots of the ρ_1 and ρ_2 parameters from the separable AC model and ρ_1, ρ_2 and θ from the generalized AC model, statistical characteristics of backward compatible HDR image coding residues can be evaluated as it will be done in the next chapter for several backward compatible HDR image coding residues.

CHAPTER 4

EXPERIMENTAL RESULTS FOR THE AC ANALYSES OF BACKWARD COMPATIBLE HDR IMAGE CODING RESIDUES

In this chapter, experimental results for the auto-covariance (AC) analyses of several backward compatible high dynamic range (HDR) image coding residues, which have different bitrates (different quantization parameters (QPs)), spatial activities and dynamic ranges as the main variables in the HDR image coding, are given and interpreted. By analyzing the behaviours of resulting AC model parameters for a particular image with respect to these main variables, characteristics of the AC of local regions of backward compatible HDR image coding residues are investigated to conclude whether the directional coding methods should be applied for the coding of backward compatible HDR image coding residues or not.

4.1 Experimental Setup

For the experiments, five images are selected from various high dynamic range (HDR) image databases, which exhibit different characteristics in terms of dynamic range and spatial activity [38]. These images are in 32-bit RGBE format as .hdr files. Tone mapped versions of the selected HDR images are shown in Figure 4.1. The dynamic ranges and spatial activities of the selected HDR images are also compared in Figure 4.2. While the dynamic range is defined as the ratio of the maximum luminance to the minimum luminance in an image, the spatial activity is measured as the standard deviation of the output of a Sobel operator applied to an image. The dynamic range of

the selected HDR images varies from 1.5 to 6 and the spatial activity of the selected HDR images is in the range of 0.017 to 0.03. It is assumed that the selected HDR images roughly cover the reasonable dynamic and spatial activity ranges and they are adequately diverse and representative to perform comparisons. The selected HDR images for the experiments are all in high definition (HD) (1920x1080) resolution and specially inspected not to possess any typical HDR acquisition artifact [38].

(a) *AirBellowsGap*

(b) *LasVegasStore*

(c) *MasonLake(1)*

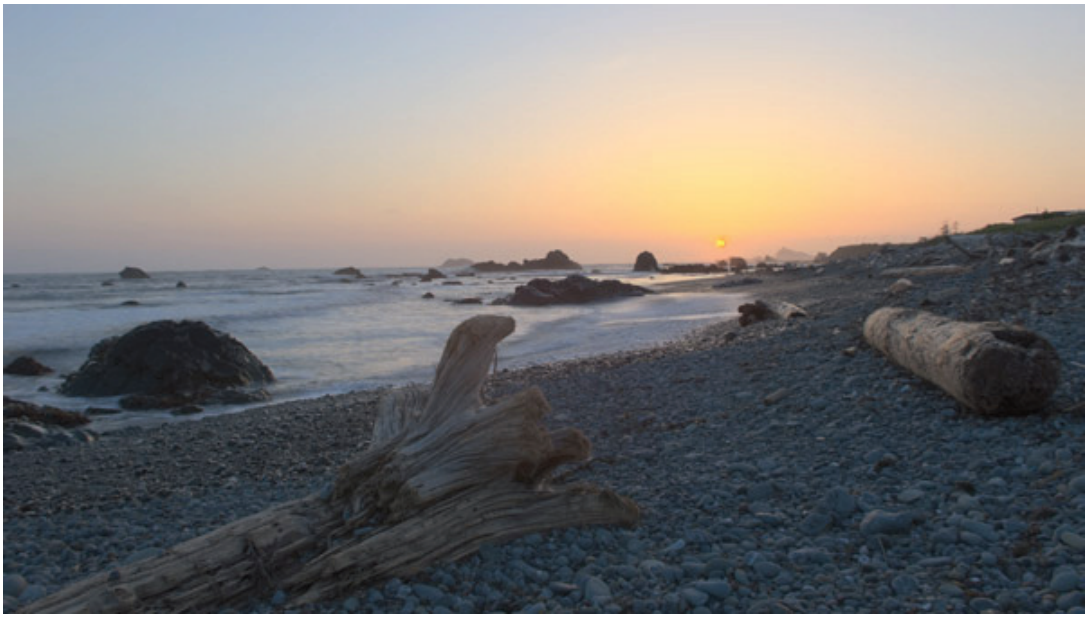

(d) *RedwoodSunset*

(e) *UpheavalDome*

Figure 4.1: The selected HDR images (tone mapped versions) for the experiments.

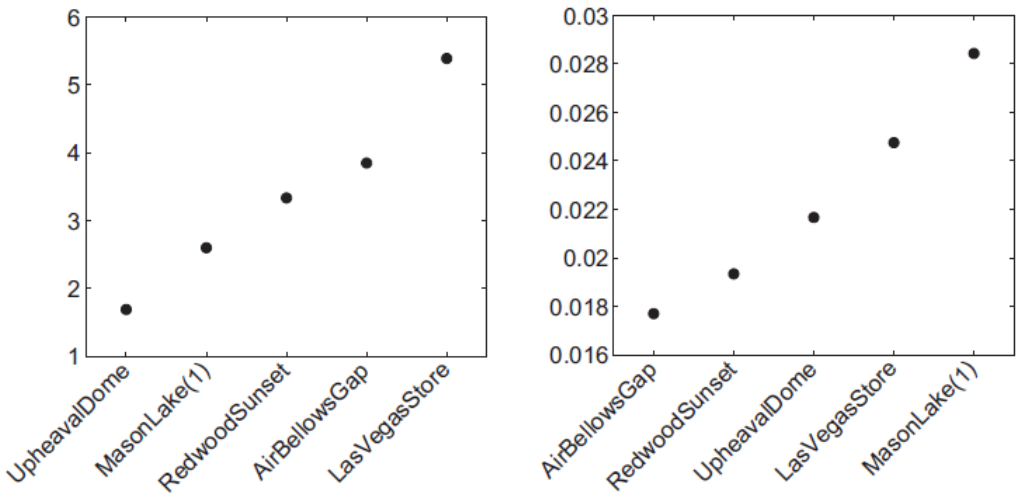

(a) Dynamic Range

(b) Spatial Information

Figure 4.2: Characteristics of the selected HDR images for the experiments [38].

The selected HDR images undergo the color space transformation (CST), tone mapping operation (TMO), encoding, decoding and inverse tone mapping operation (ITMO), and backward compatible HDR image coding residues are obtained as discussed in Chapter 2. As a tone mapping operator (TMO), the optimum tone mapping method

of Mai *et al.* [6] is utilized. However, note that, other TMOs could also be used to understand the statistical behaviour of backward compatible HDR image coding residues. The H.264/AVC JM 10.2 reference software encoder-decoder [8] is utilized in the experiments for the base layer encoding and decoding operations of the low dynamic range (LDR) images, which are found after the CST and the TMO of the selected HDR images, with four different base layer quantization parameters which are selected as QP = 22, 27, 32, 37.

The auto-covariance (AC) analyses, as described in Chapter 3, are performed to analyze backward compatible HDR image coding residues. For the AC analyses, 8x8-pixel blocks are used as a commonly used block size in compression. The DC mean of each 8x8-pixel block is subtracted and only the blocks which have enough AC energy are taken into account for the analyses by comparing with a threshold, which is experimentally chosen as 10^{-4}, as the blocks with lower AC energy are typically not coded in compression.

4.2 AC Analyses Results

Figure 4.3 illustrates the tone mapped (method Mai *et al.* [6]) log luminance (L) images of the selected HDR image set. And Figure 4.4 shows their absolute (each pixel value is equal or greater than zero) backward compatible high dynamic range (HDR) image coding residues as the absolute values of the differences of the original HDR log luminance (L) images and their predictions from the base layer with a fixed base layer quantization parameter, QP = 37. For this figure, base layer quantization parameter is fixed to 37 in order to observe the directional characteristics, or in other words, the 1-D structures in backward compatible HDR image coding residues better. The 1-D structures are quite observable in the backward compatible HDR image coding residues as seen from Figure 4.4.

(a) *AirBellowsGap*

(b) *LasVegasStore*

(c) *MasonLake(1)*

(d) *RedwoodSunset*

(e) *UpheavalDome*

Figure 4.3: The tone mapped (method Mai *et al.*) log luminance (L) images of the selected HDR image set.

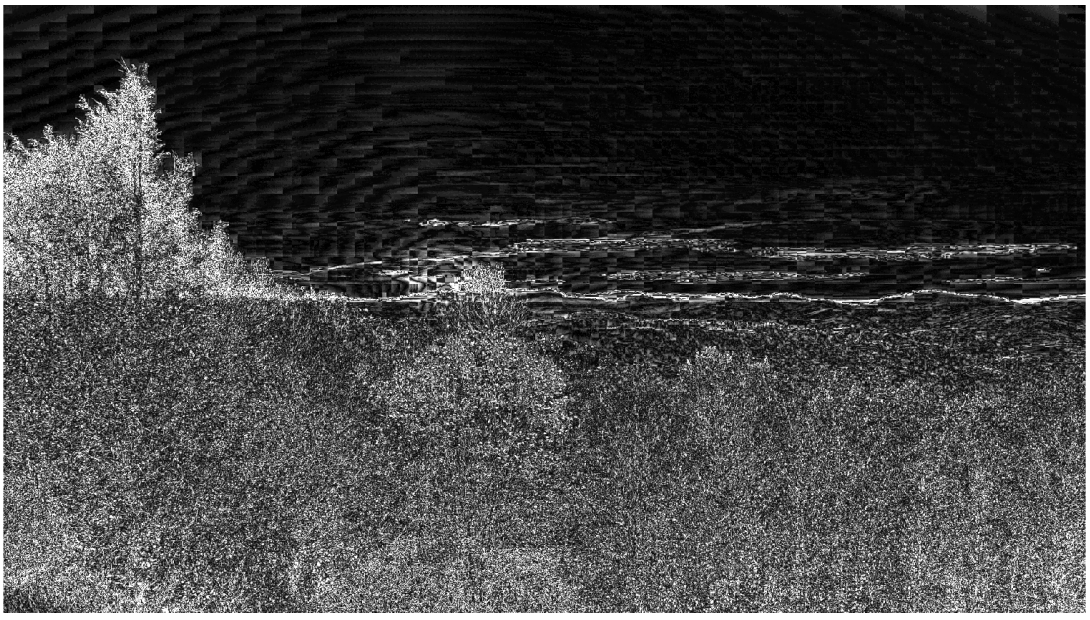

(a) *AirBellowsGap*

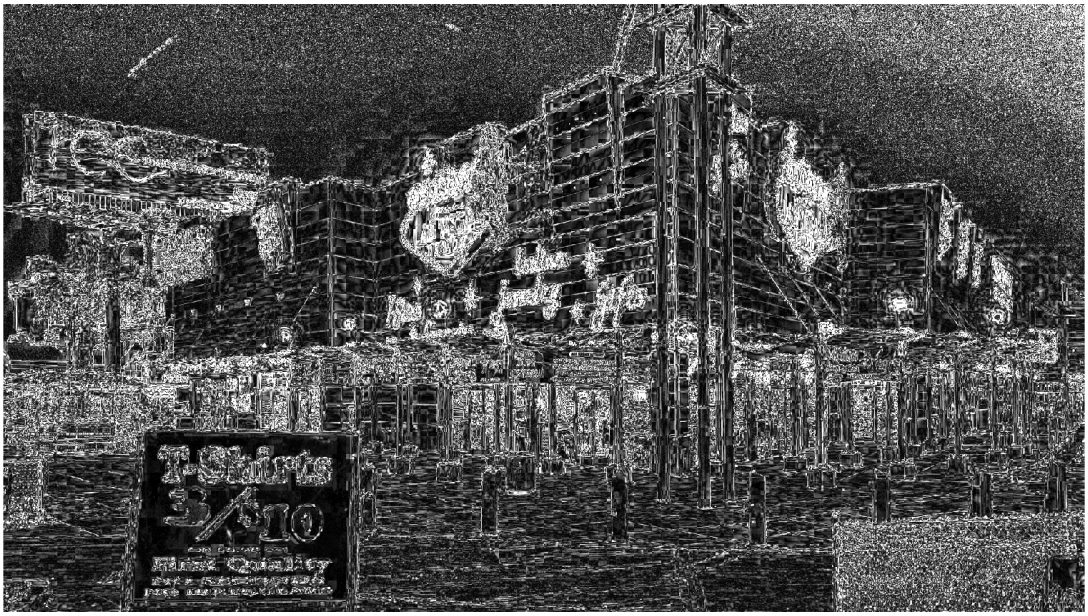

(b) *LasVegasStore*

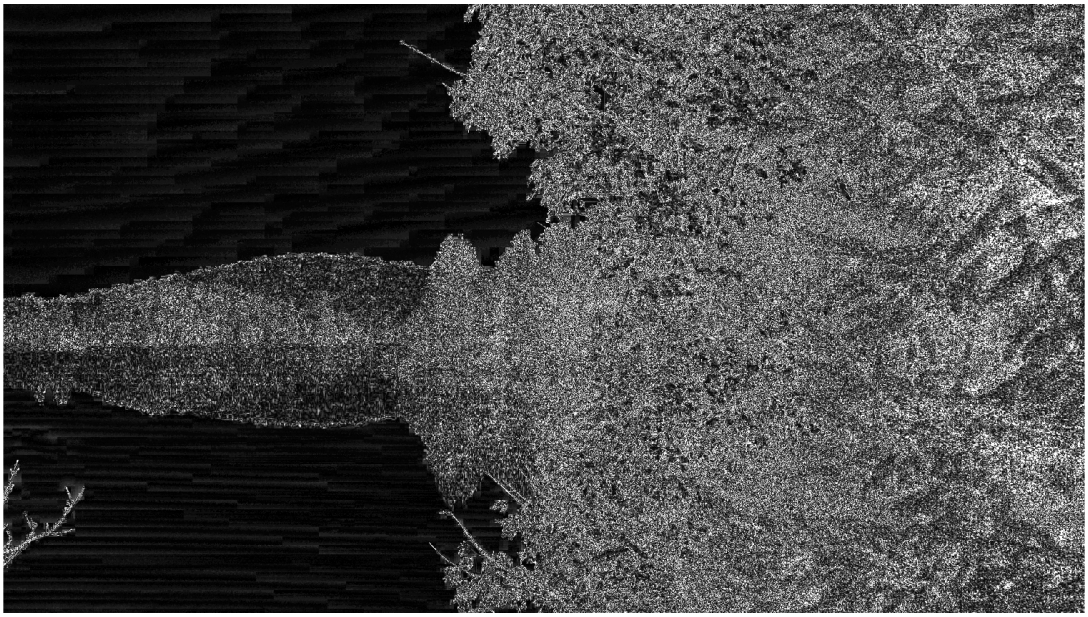

(c) *MasonLake(1)*

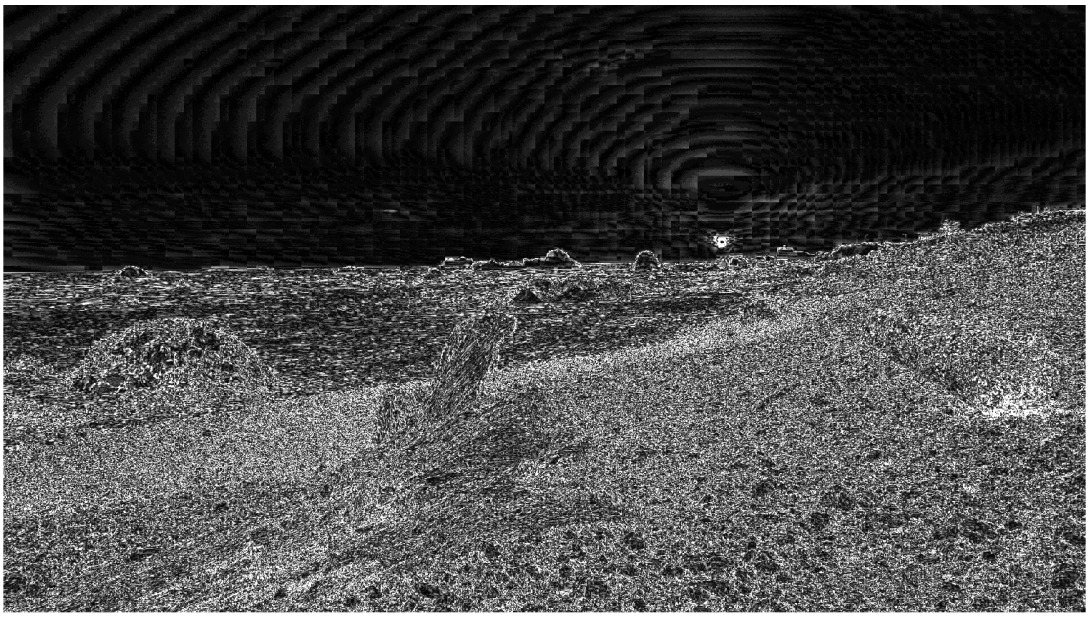

(d) *RedwoodSunset*

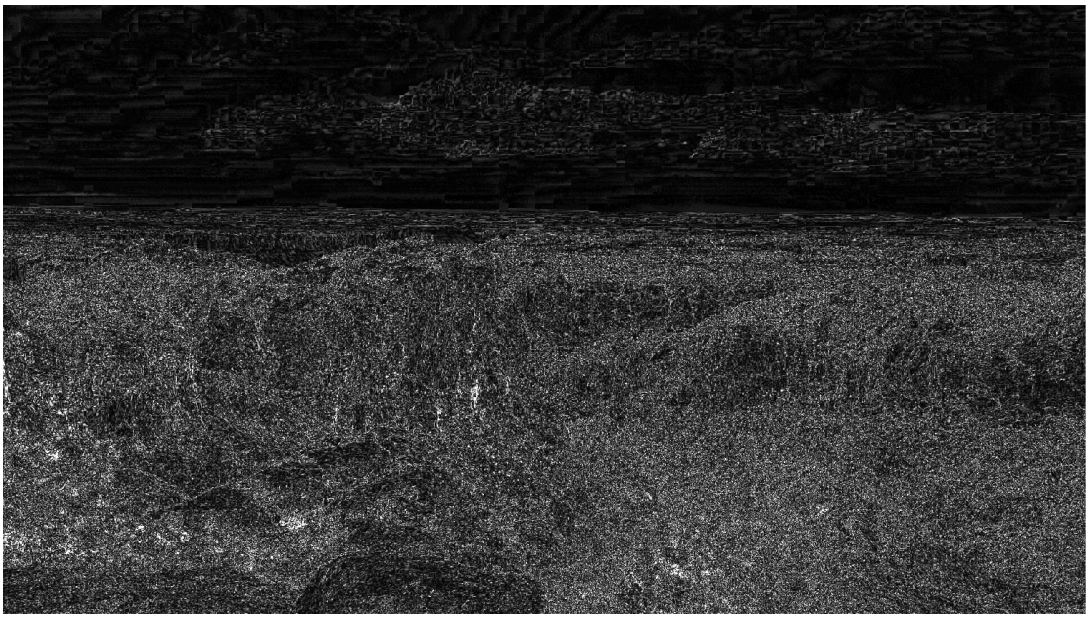

(e) *UpheavalDome*

Figure 4.4: The absolute backward compatible HDR image coding residues for the selected HDR image set with a fixed base layer quantization parameter, QP = 37.

Figure 4.5 gives the auto-covariance (AC) analyses results, which are the separable AC model result (Figure 4.5 (a)), the generalized AC model result (Figure 4.5 (b)) and

the histogram of the estimated angles for the generalized AC model result (Figure 4.5 (c)), for the HDR image *LasVegasStore* with a fixed base layer quantization parameter, QP = 27. Each point in Figures 4.5 (a) and (b) represents the estimated (ρ_1, ρ_2) pair by using the AC models given in Equations 3.1 and 3.2, from one 8x8-pixel backward compatible HDR image coding residue block. Note that ρ_1 is the larger correlation coefficient and θ varies between 0° and 180°. In Figure 4.5 (a), both ρ_1 and ρ_2 are typically smaller than 0.5. However, in Figure 4.5 (b), ρ_2 is mostly smaller than 0.5 but ρ_1 is mostly larger than 0.5. Combination of large ρ_1 and small ρ_2 indicates that a 1-D structure exists along the direction of ρ_1, which indicate 1-D characteristics of the backward compatible HDR image coding residue blocks. The generalized AC model illustrates also the orientation of the 1-D structures with the parameter θ, which allows rotation of the horizontal and vertical axes of the separable AC model, as a main difference with respect to the separable AC model. Thus, the generalized AC model captures more local anisotropic features than the separable AC model and it is capable of adapting and modelling the statistical characteristics of backward compatible HDR image coding residues which have strong correlation along diagonal directions other than the horizontal and vertical directions better. Histograms of the estimated angles (θ) for the generalized AC model is shown in Figure 4.5 (c). In accordance with the dominant vertical and horizontal edges on the given HDR image *LasVegasStore*, the highest peaks in the plot concentrate at around 0°, 90° and 180°, where peaks at 0° and 180° correspond to horizontally aligned features, and a peak at 90° corresponds to vertically aligned features.

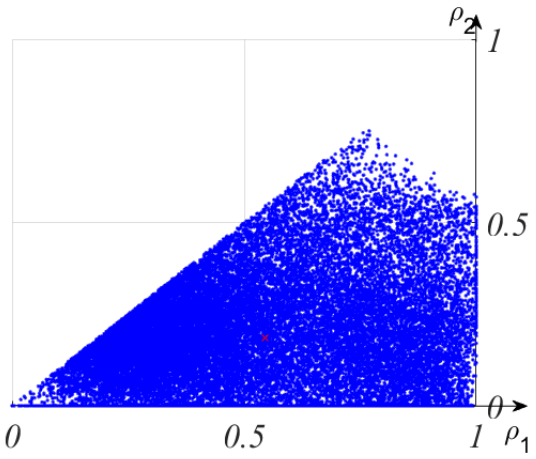

(a) The Separable AC Model Result

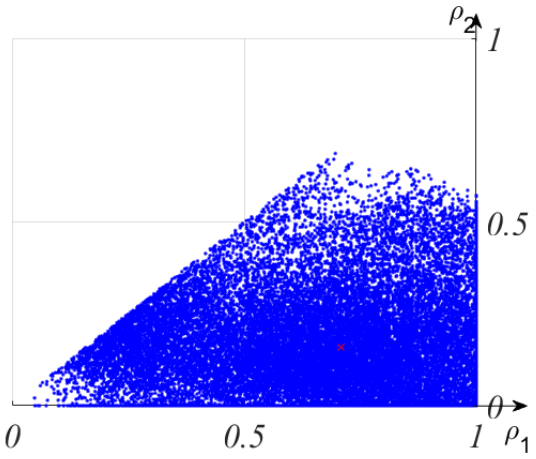

(b) The Generalized AC Model Result

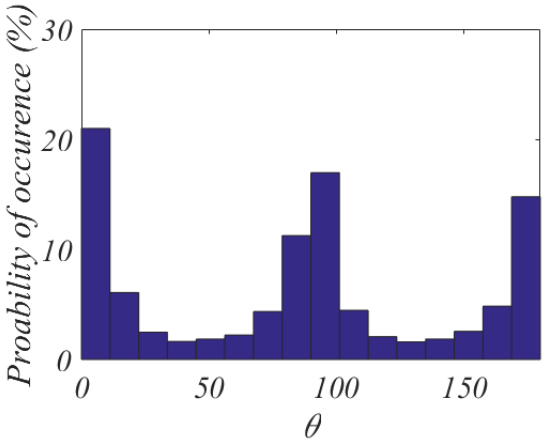

(c) The Histogram of the Estimated Angles for the Generalized AC Model Result

Figure 4.5: The AC analyses results for the HDR image *LasVegasStore* with a fixed base layer quantization parameter, QP = 27.

In the investigation of the behaviour of backward compatible HDR image coding residues with respect to different varibles, the first experiment is performed to reveal the effect of base layer bit-rate (or base layer quantization parameter (QP)). Figures 4.6 and 4.7 illustrate different absolute backward compatible HDR image coding residues, respectively, *LasVegasStore* and *RedwoodSunset* with different base layer quantization parameters, respectively, QP = 22, 27, 32, 37. As can be observed from Figures 4.6 and 4.7, while base layer quantization parameter increases, number of blocks surpassing the AC energy threshold also increases due to the higher coding error. As a corollary of this, the 1-D structures in backward compatible HDR image coding residues are also becoming more salient for higher base layer quantization parameters.

(a)

(b)

(c)

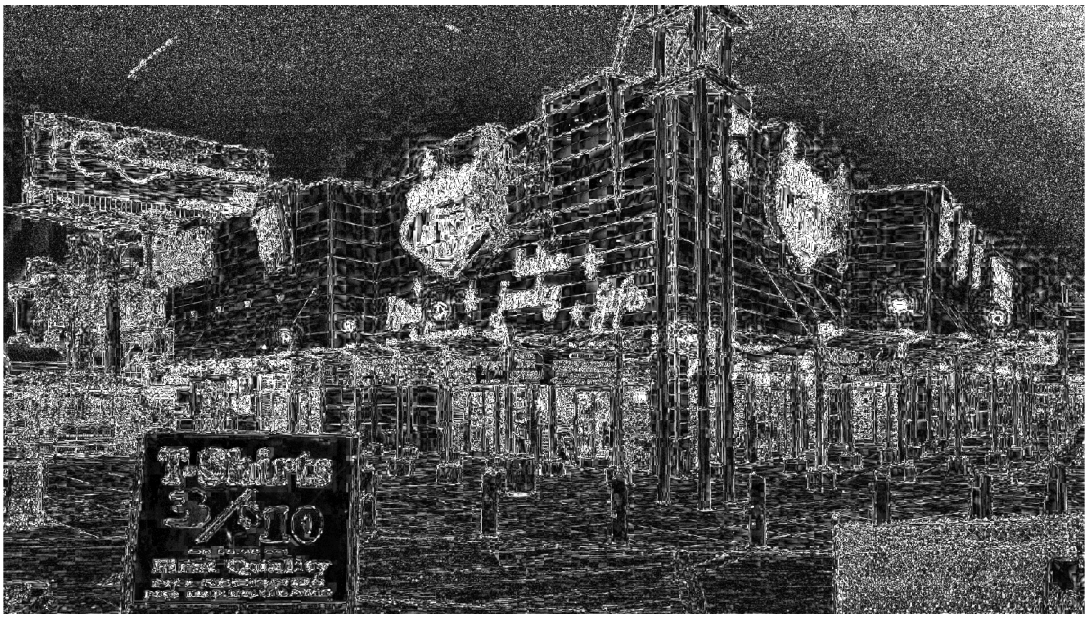

(d)

Figure 4.6: The absolute backward compatible HDR image coding residues for the HDR image *LasVegasStore* with different base layer quantization parameters, respectively, QP = 22, 27, 32, 37.

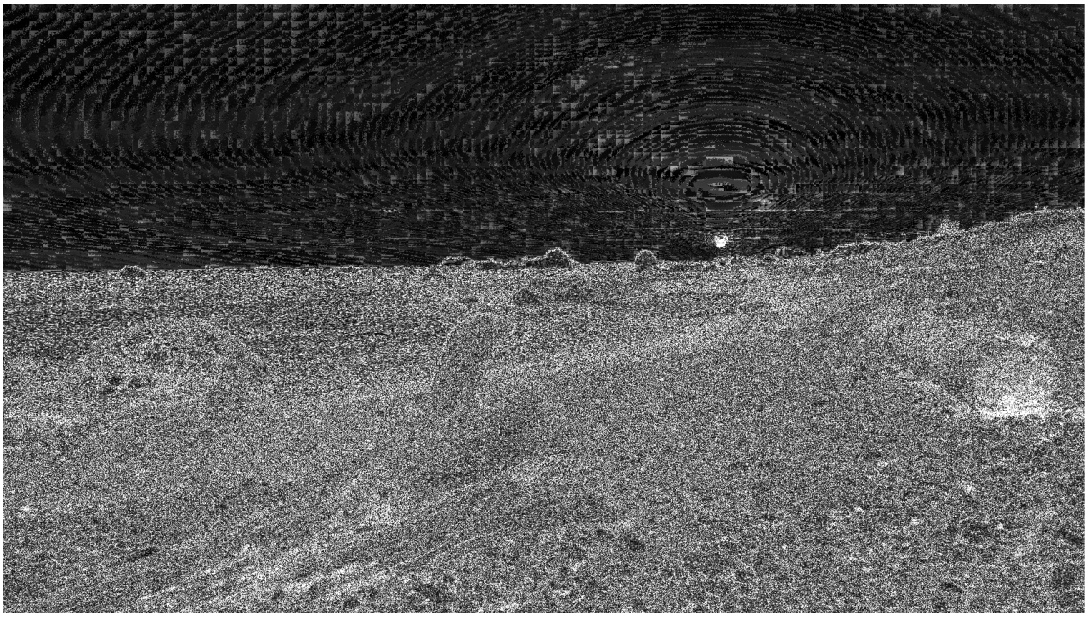

(a)

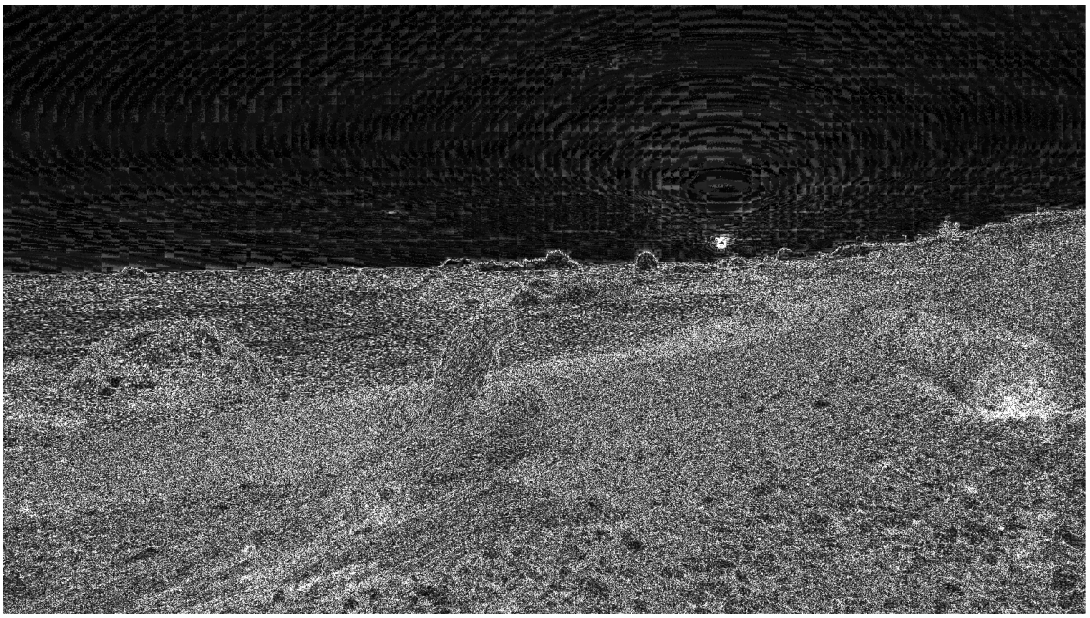

(b)

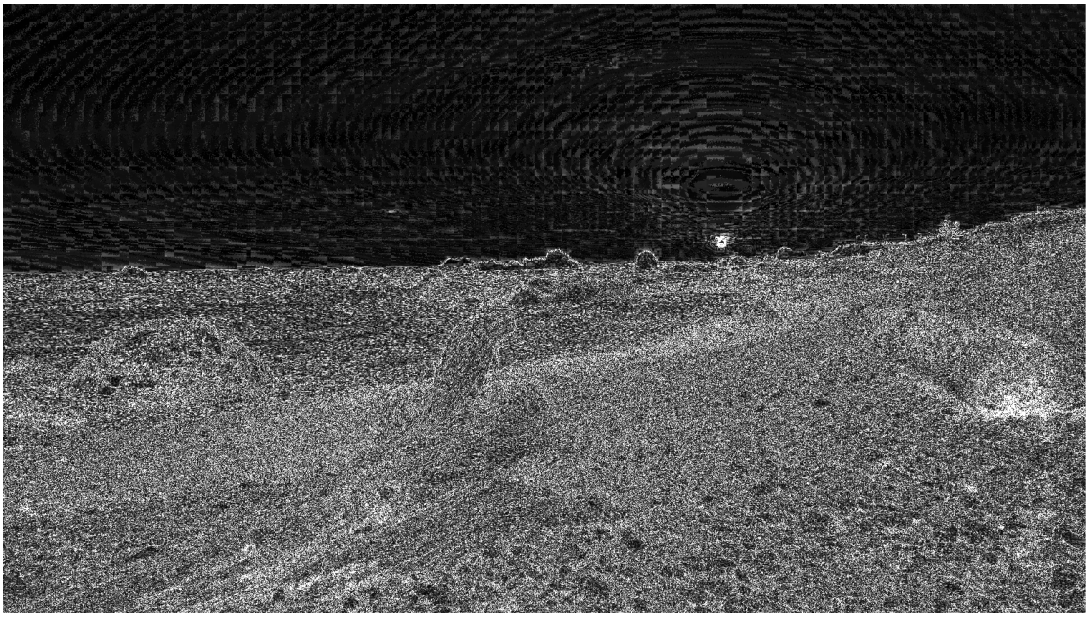

(c)

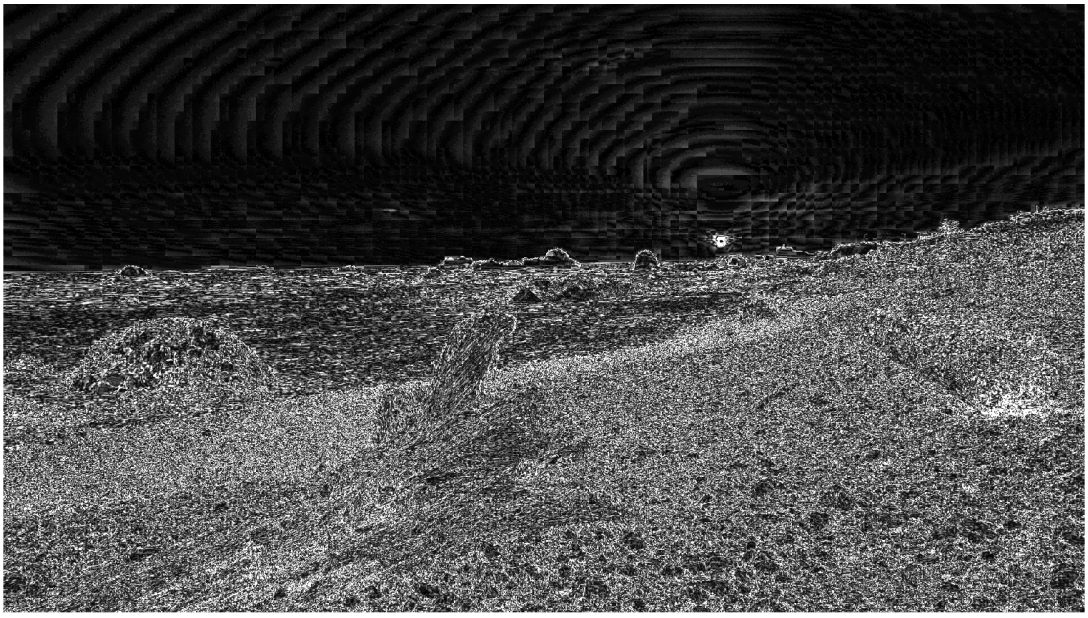

(d)

Figure 4.7: The absolute backward compatible HDR image coding residues for the HDR image *RedwoodSunset* with different base layer quantization parameters, respectively, QP = 22, 27, 32, 37.

Figures 4.8 and 4.9 show the scatter plots of the estimates of the (ρ_1, ρ_2) correlation coefficients pairs with the separable AC model for corresponding selected HDR images as in Figures 4.6 and 4.7 with different base layer quantization parameters, respectively, QP = 22, 27, 32, 37. Figures 4.10 and 4.11 show the scatter plots of the estimates of the (ρ_1, ρ_2) correlation coefficients pairs with the generalized AC model for corresponding selected HDR images as in Figures 4.6 and 4.7 with different base layer quantization parameters, respectively, QP = 22, 27, 32, 37. As base layer quantization parameter increases, the points on the scatter plots show also a scattering behavior towards higher ρ_2 values for both the separable AC model and the generalized AC model. This is because of the fact that, when quantization parameter increases in the base layer, as mentioned before, 1-D structures in backward compatible HDR image coding residues become more salient, or in other words, increase due to the higher coding error. Figures 4.12 and 4.13 show the histograms of the estimated angles (θ) for the generalized AC model with different base layer quantization

parameters, respectively, QP = 22, 27, 32, 37. As seen from Figure 4.12, the histograms of the estimated angles (θ) for *LasVegasStore* concentrates higher at around the angles $0°$, $90°$ and $180°$ as base layer quantization parameter increases. As seen from Figure 4.13, the histograms of the estimated angles (θ) for *RedwoodSunset* concentrates higher at around the angles $0°$ and $180°$ as base layer quantization parameter increases.

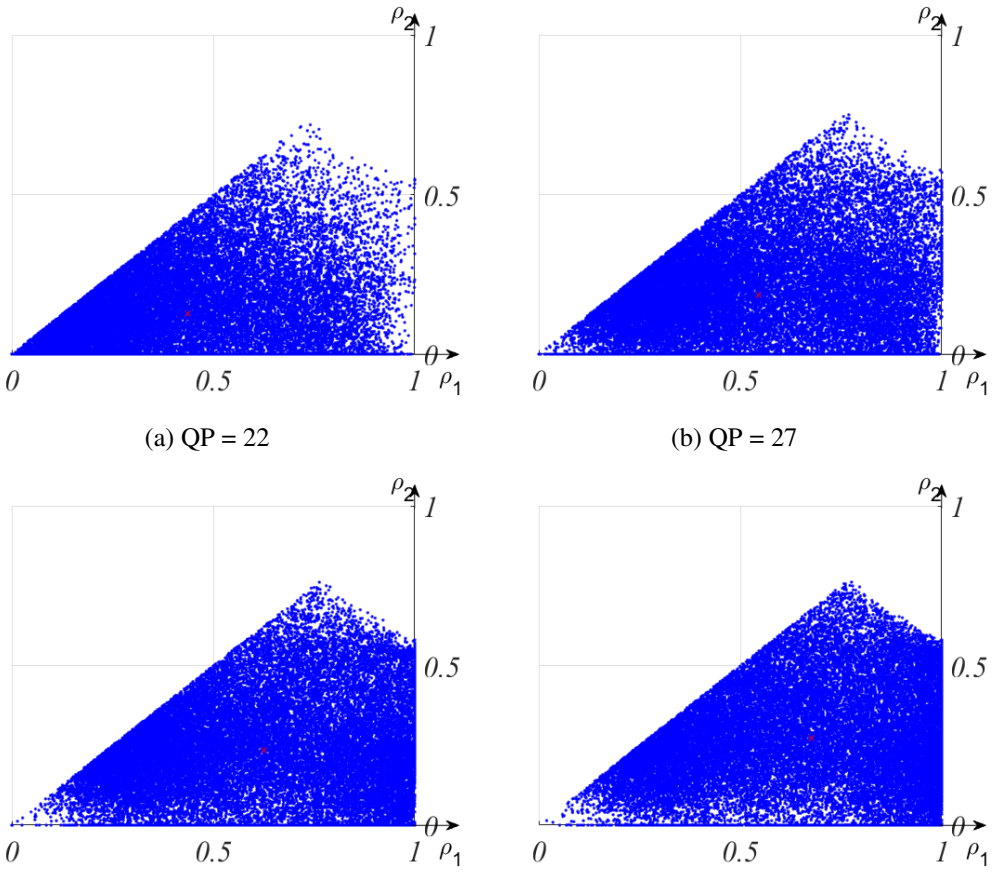

(a) QP = 22

(b) QP = 27

(c) QP = 32

(d) QP = 37

Figure 4.8: The AC analyses results with the separable AC model for the HDR image *LasVegasStore* with different base layer quantization parameters, respectively, QP = 22, 27, 32, 37.

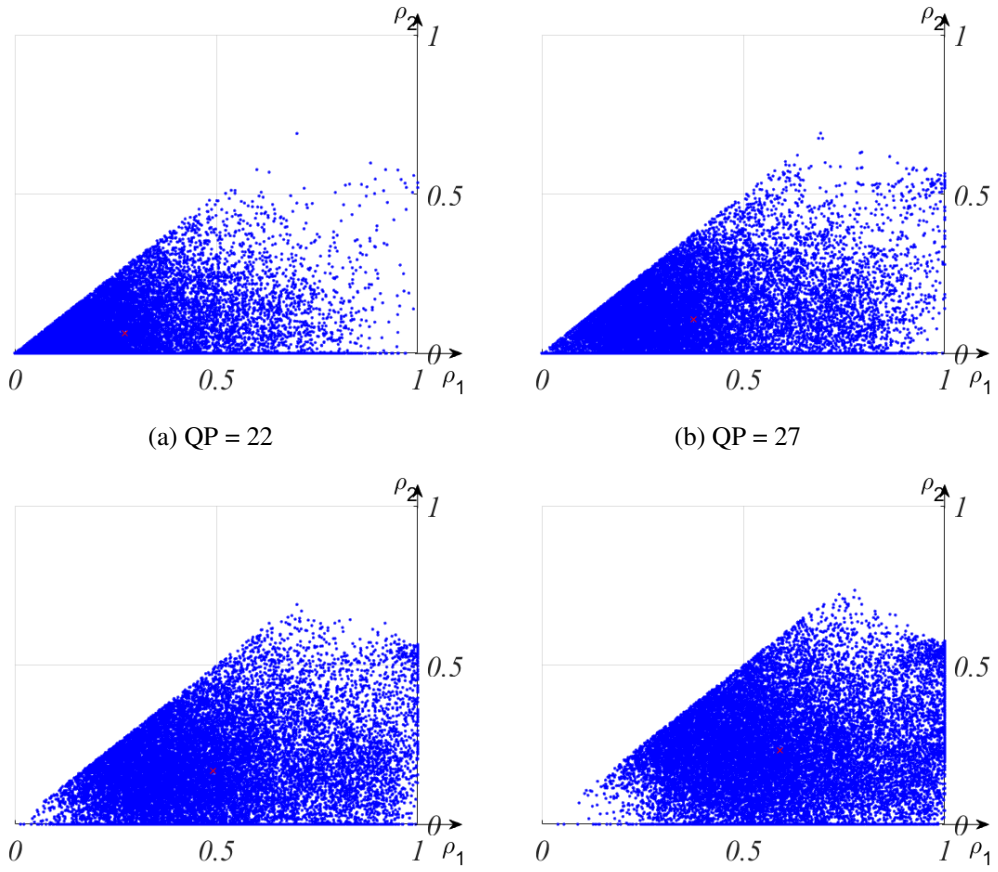

(a) QP = 22

(b) QP = 27

(c) QP = 32

(d) QP = 37

Figure 4.9: The AC analyses results with the separable AC model for the HDR image *RedwoodSunset* with different base layer quantization parameters, respectively, QP = 22, 27, 32, 37.

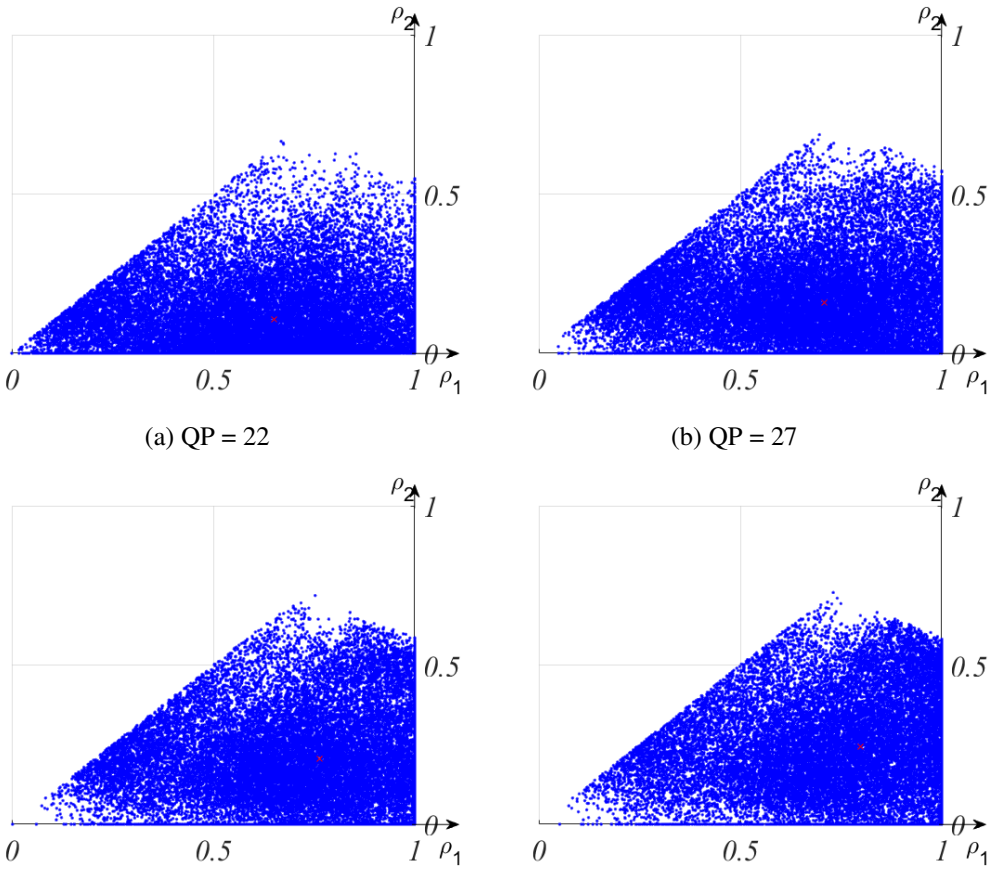

(a) QP = 22

(b) QP = 27

(c) QP = 32

(d) QP = 37

Figure 4.10: The AC analyses results with the generalized AC model for the HDR image *LasVegasStore* with different base layer quantization parameters, respectively, QP = 22, 27, 32, 37.

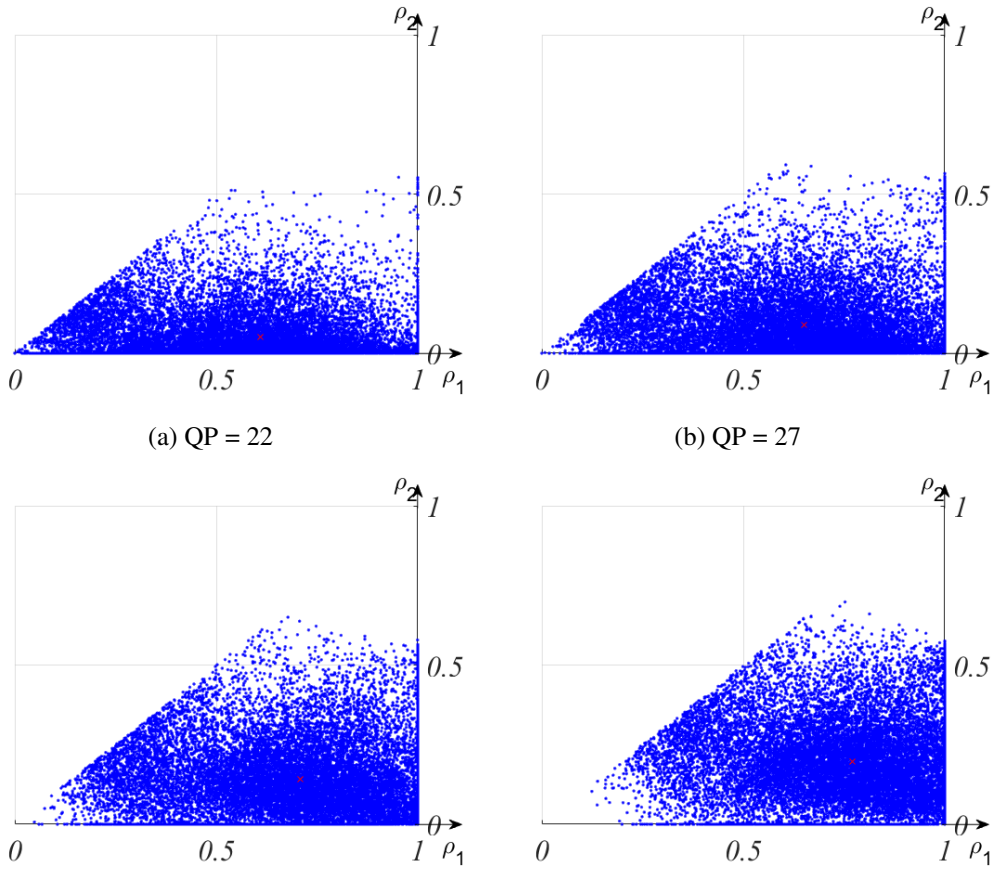

(a) QP = 22

(b) QP = 27

(c) QP = 32

(d) QP = 37

Figure 4.11: The AC analyses results with the generalized AC model for the HDR image *RedwoodSunset* with different base layer quantization parameters, respectively, QP = 22, 27, 32, 37.

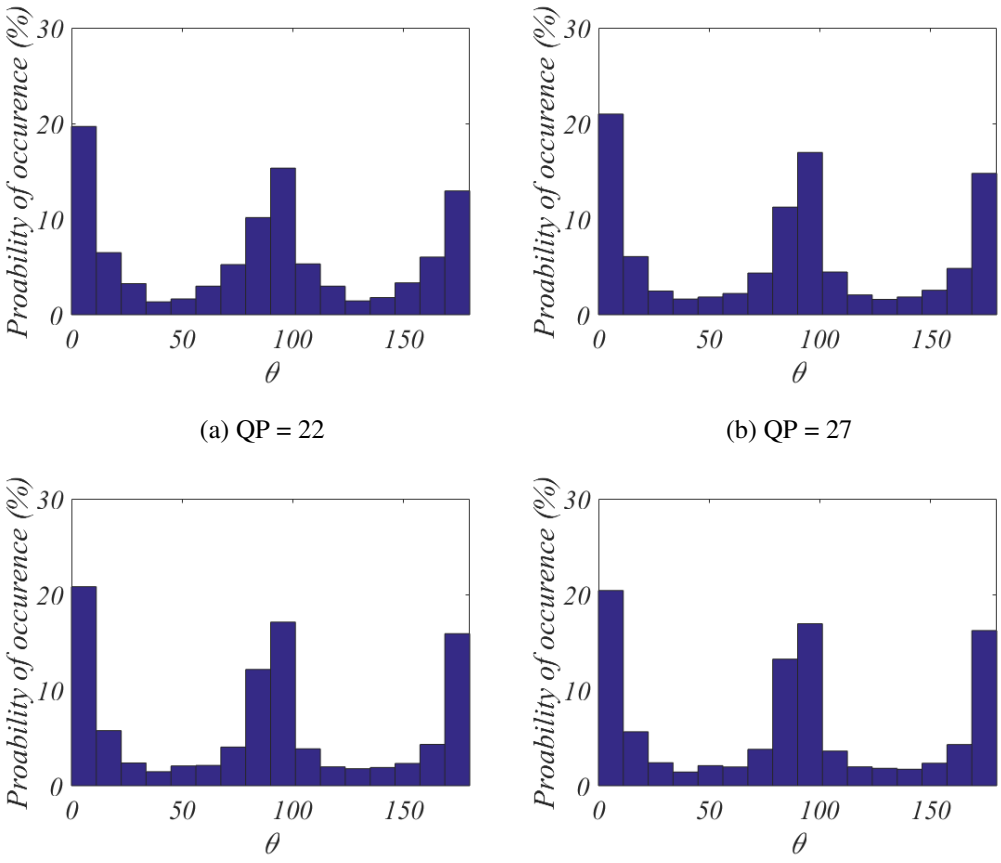

(a) QP = 22

(b) QP = 27

(c) QP = 32

(d) QP = 37

Figure 4.12: The histograms of the estimated angles (θ) with the generalized AC model for the HDR image *LasVegasStore* with different base layer quantization parameters, respectively, QP = 22, 27, 32, 37.

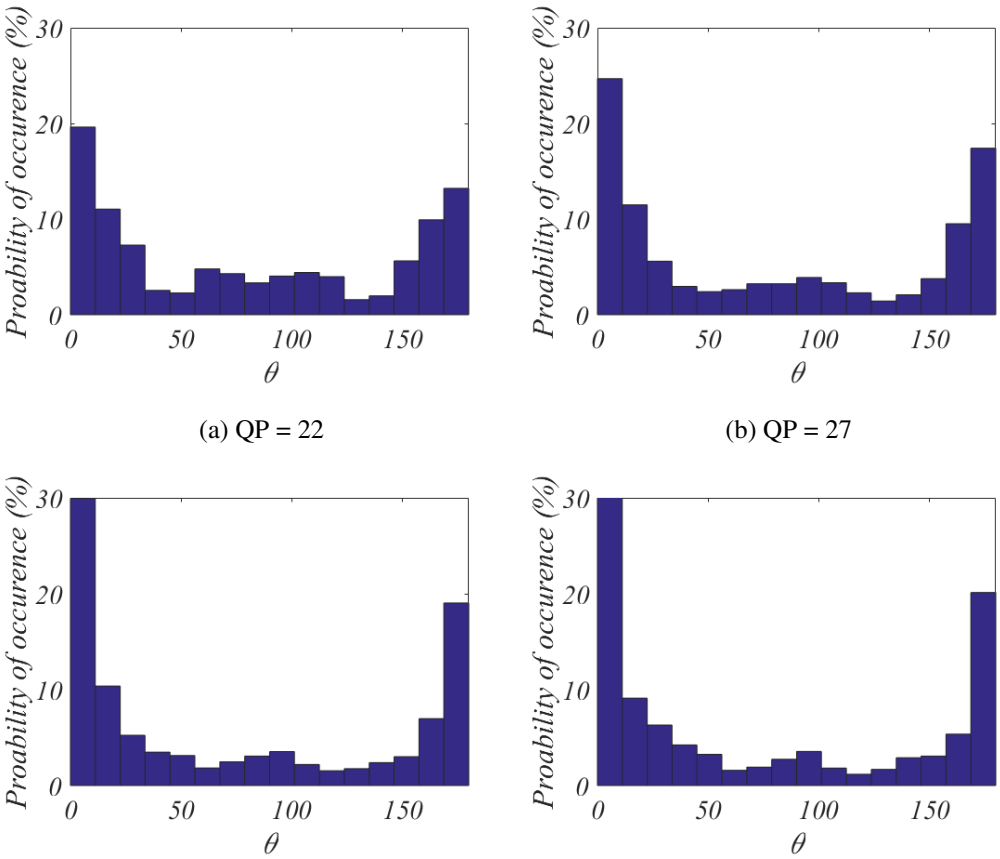

(a) QP = 22

(b) QP = 27

(c) QP = 32

(d) QP = 37

Figure 4.13: The histograms of the estimated angles (θ) with the generalized AC model for the HDR image *RedwoodSunset* with different base layer quantization parameters, respectively, QP = 22, 27, 32, 37.

With the purpose of drawing more generic conclusions regarding the AC analyses results, the AC analyses are performed on all the selected HDR images for varying dynamic range and spatial activity, while keeping base layer quantization parameter fixed at QP = 27. Figure 4.14 illustrates the scatter plots of the estimates of the (ρ_1, ρ_2) correlation coefficients pairs with the separable AC model for different HDR images. Figure 4.15 illustrates the scatter plots of the estimates of the (ρ_1, ρ_2) correlation coefficients pairs with the generalized AC model for different HDR images. As can be observed from all the scatter plots for both Figures 4.14 and 4.15, the points mostly

have a small ρ_2 value and larger ρ_1 value, which indicates 1-D directional characteristics of the backward compatible HDR image coding residue blocks. This can also be observed with very low ρ_2 values for the centroids of the scatter plots, indicated as the red cross on the scatter plots. The scatter plots indicate that both the HDR images having the lowest dynamic range (*UpheavalDome*) and the highest dynamic range (*LasVegasStore*) have enough number of blocks whose structure is dominated in one direction. Similarly, both the HDR images having the lowest spatial activity (AirBellowGap) and the highest spatial activity (MasonLake(1)) exhibit also 1-D structures in their blocks as indicated with the concentration along the ρ_1 axis.

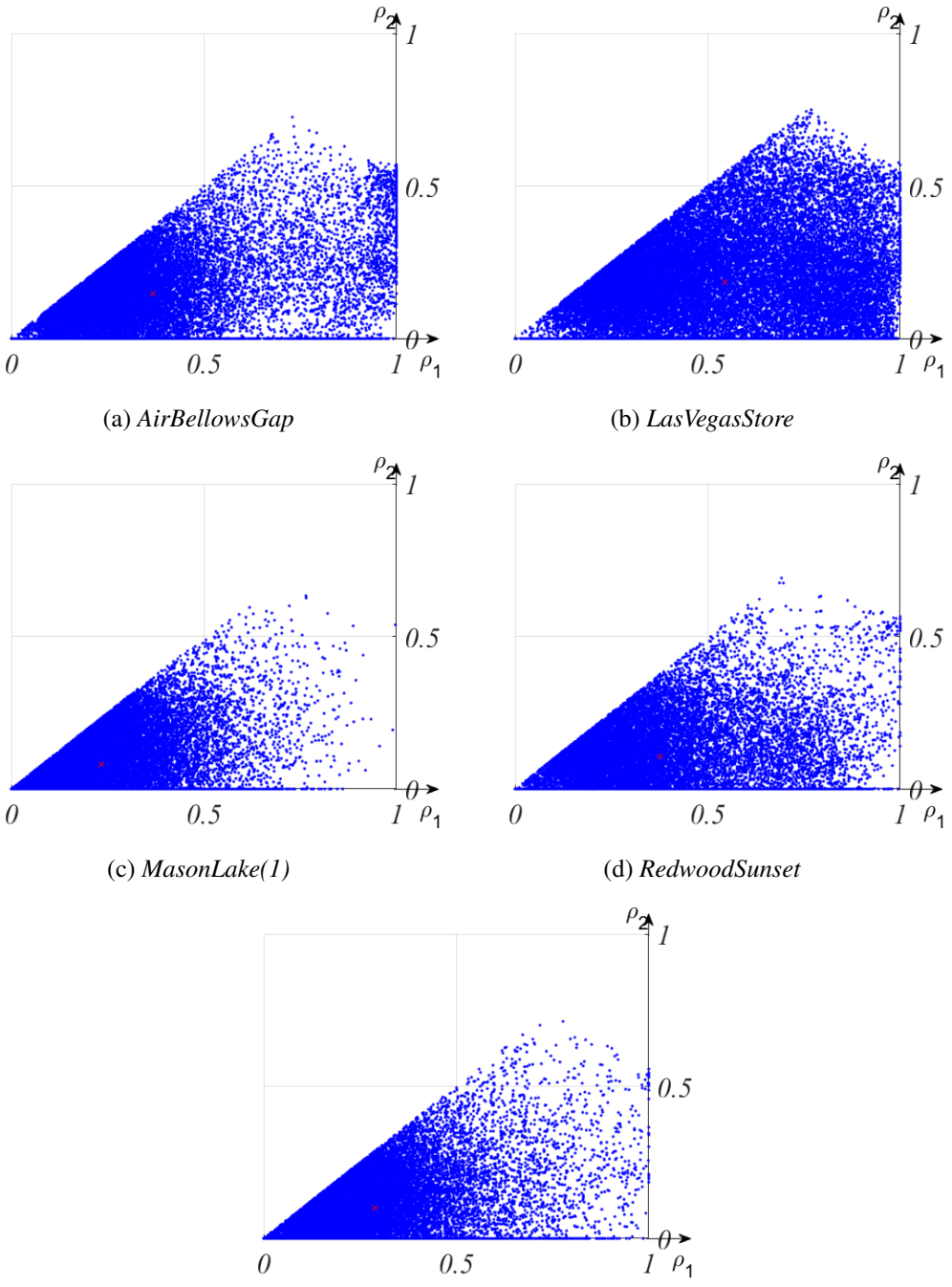

(a) *AirBellowsGap*

(b) *LasVegasStore*

(c) *MasonLake(1)*

(d) *RedwoodSunset*

(e) *UpheavalDome*

Figure 4.14: The AC analyses results with the separable AC model for all the selected HDR images with a fixed base layer quantization parameter, QP = 27.

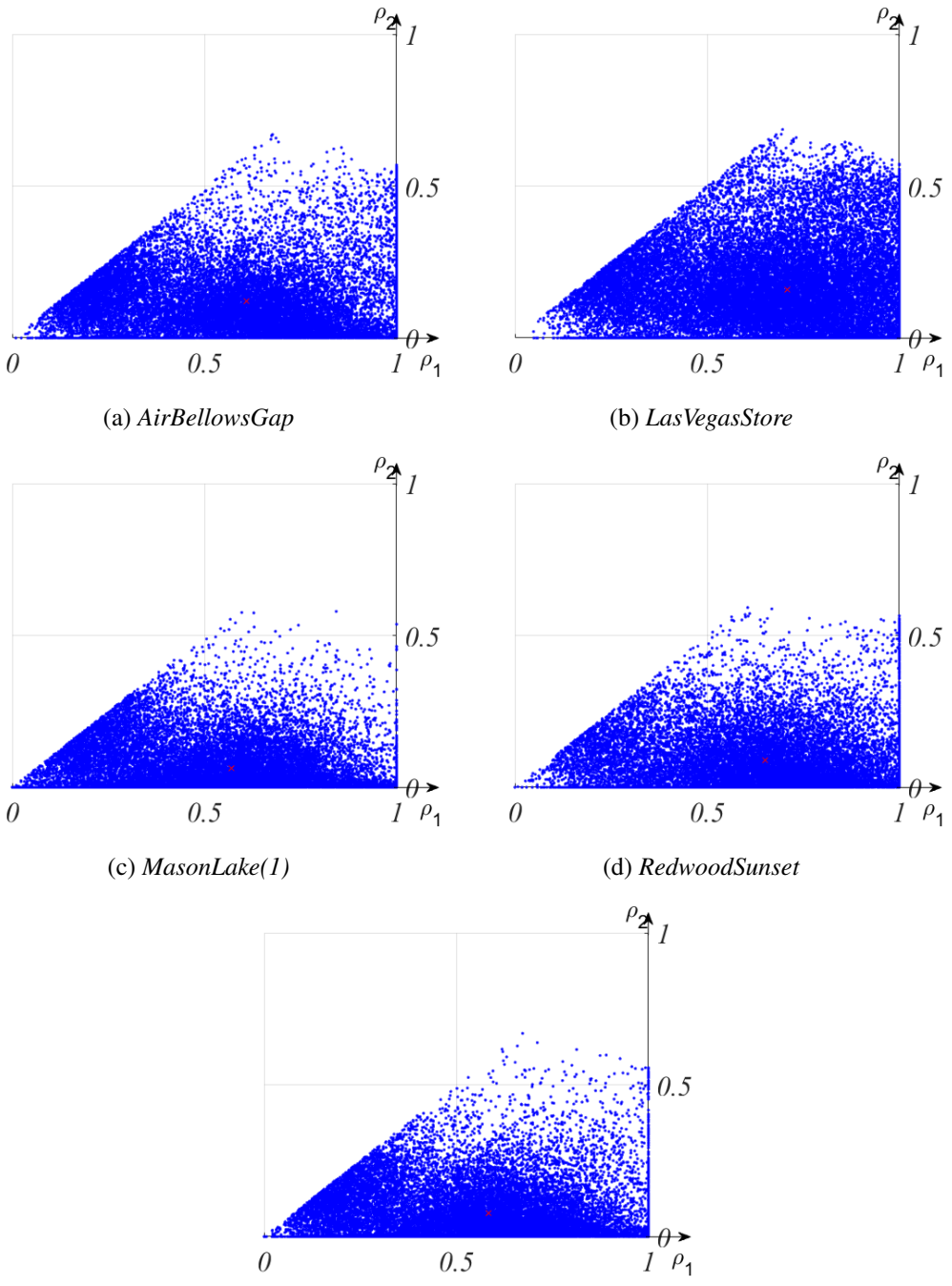

(a) *AirBellowsGap*

(b) *LasVegasStore*

(c) *MasonLake(1)*

(d) *RedwoodSunset*

(e) *UpheavalDome*

Figure 4.15: The AC analyses results with the generalized AC model for all the selected HDR images with a fixed base layer quantization parameter, QP = 27.

The experiments have revealed that backward compatible HDR image coding residues obtained as the differences of original HDR log luminance (L) images and their predictions from the base layer low dynamic range (LDR) images, possess 1-D directional characteristics. The verification of existence of such 1-D structures indicates that the directional coding methods, which are utilized by coding of LDR motion-compensated (MC) prediction residuals with 1-D directional transforms in addition to the conventional 2-D transforms [35, 36], can also be a good candidate solution for the encoding and decoding of backward compatible HDR image coding residues.

CHAPTER 5

PROPOSED CODING METHOD FOR BACKWARD COMPATIBLE HDR IMAGE CODING RESIDUES

In this chapter, proposed coding method for backward compatible high dynamic range (HDR) image coding residues are presented and explained in detail. Details of the codec, which is utilized for this proposed coding method, are also discussed. Proposed coding method for HDR image coding residues comprises two stages, which are firstly 8-bit conversion of backward compatible HDR image coding residues and secondly directional coding of these 8-bit backward compatible HDR image coding residues, as shown in Figure 2.1.

5.1 8-bit Conversion of Backward Compatible HDR Image Coding Residues

As mentioned in Chapter 2, owing to the fact that high dynamic range (HDR) image coding residues are represented in floating point real numbers, 8-bit conversion should be applied to them in order to provide the 8-bit input requirement of the utilized codecs which are responsible for the encoding-decoding operations in the residue layer. 8-bit conversion of backward compatible HDR image coding residues consists of two stages which are firstly normalization (Norm) of backward compatible HDR image coding residues and secondly their conversion to 8-bit. For the conversion of backward compatible HDR image coding residues to 8-bit, two 8-bit conversion methods are used and it is investigated which method performs better as an 8-bit conversion. As the first method, the adaptive residual mapping method including the *Sigmoid function* and the *Logit function* proposed by Mir *et al.* [22] is used. As

the second method, the optimum tone mapping method which is proposed by Mai *et al.* [6] is adapted to the characteristics of backward compatible HDR image coding residues as an 8-bit conversion.

5.1.1 The Sigmoid Function of the Adaptive Residual Mapping Method for Backward Compatible HDR Image Coding Residues

The Sigmoid function of the adaptive residual mapping method, which is proposed by Mir *et al.* [22], for backward compatible high dynamic range (HDR) image coding residues involves the following steps.

Backward compatible HDR image coding residue in the matrix form is firstly converted to the vector form. The vector of backward compatible HDR image coding residue values, which is denoted as *r*, is normalized to [0, 1] range with respect to its maximum and minimum values as given in Equation 5.1:

$$r_n = \frac{r - min(r)}{max(r) - min(r)} \tag{5.1}$$

The vector of normalized backward compatible HDR image coding residue values, which is denoted as r_n, is passed through the Sigmoid function:

$$R_n = \frac{1}{1 + e^{-s(r_n - m)}} \tag{5.2}$$

The resulting values in the vector form R_n are multiplied with 255 and rounded. Afterwards, the rounded values in the vector form are converted to the matrix form again in order to obtain the 8-bit backward compatible HDR image coding residue.

The algorithm [24] defines the *m* value as a parameter which is similar to the geometric mean definition:

$$m = e^{\frac{1}{N}\sum log(r_n + e)} \tag{5.3}$$

However, after all experiments which are performed, it is observed that the arithmetic

mean gives better and more accurate results. Therefore, the *m* value is selected as the arithmetic mean of the vector of normalized backward compatible HDR image coding residue values (r_n):

$$m = \frac{1}{N} \sum r_n \tag{5.4}$$

In given Equation 5.2, the *s* parameter, which is defined as the steepness of the Sigmoid function, is selected as the value which minimizes the mean square error (MSE) between the original backward compatible HDR image coding residue and the reconstructed version of it after the 8-bit conversion by iterating the *s* parameter recursively. For the experiments, the *s* parameter is iterated between values 5 and 20 with step size value 1 recursively. This iteration interval [5, 20] and the step size value 1 is selected experimentally.

In Figure 5.1, an illustration of the optimum *s* parameter value selection in the Sigmoid function of the adaptive residual mapping method for the each selected five HDR images is given. As seen from Figure 5.1, for each of the selected five HDR images, change of MSE value with respect to the *s* parameter values, which are selected experimentally, is convex shaped. The optimum *s* parameter values are the ones giving minimum MSE values.

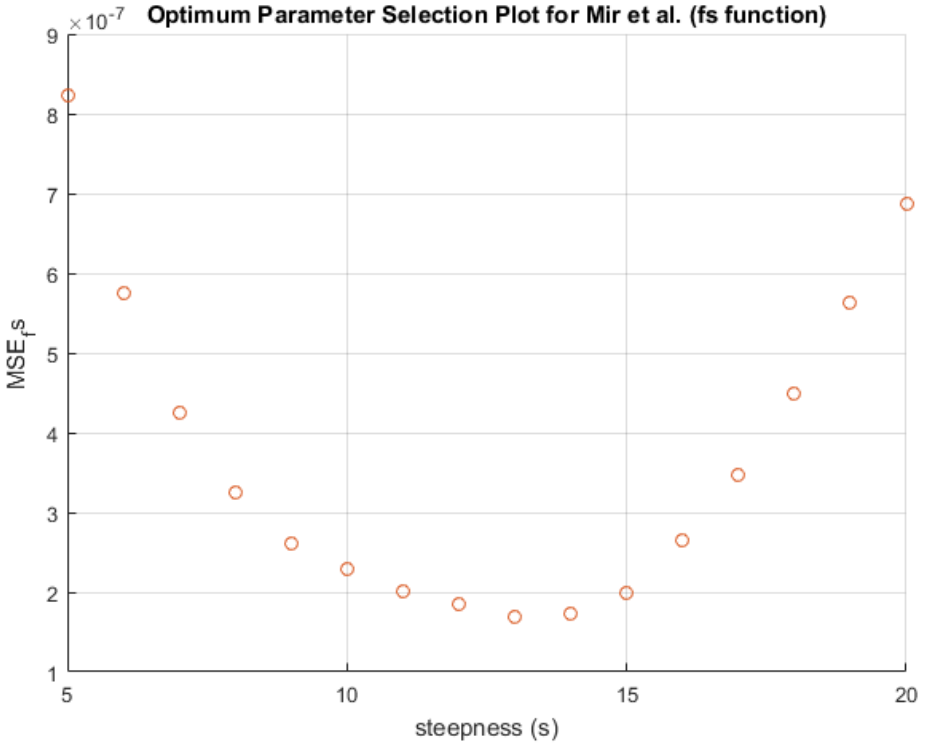

(a) *AirBellowsGap*

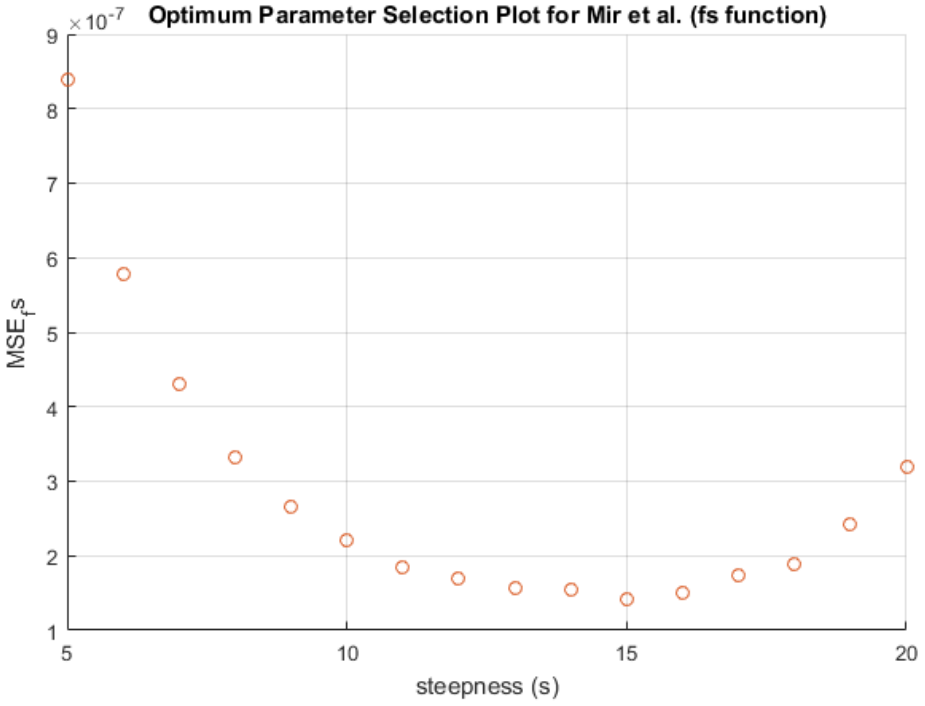

(b) *LasVegasStore*

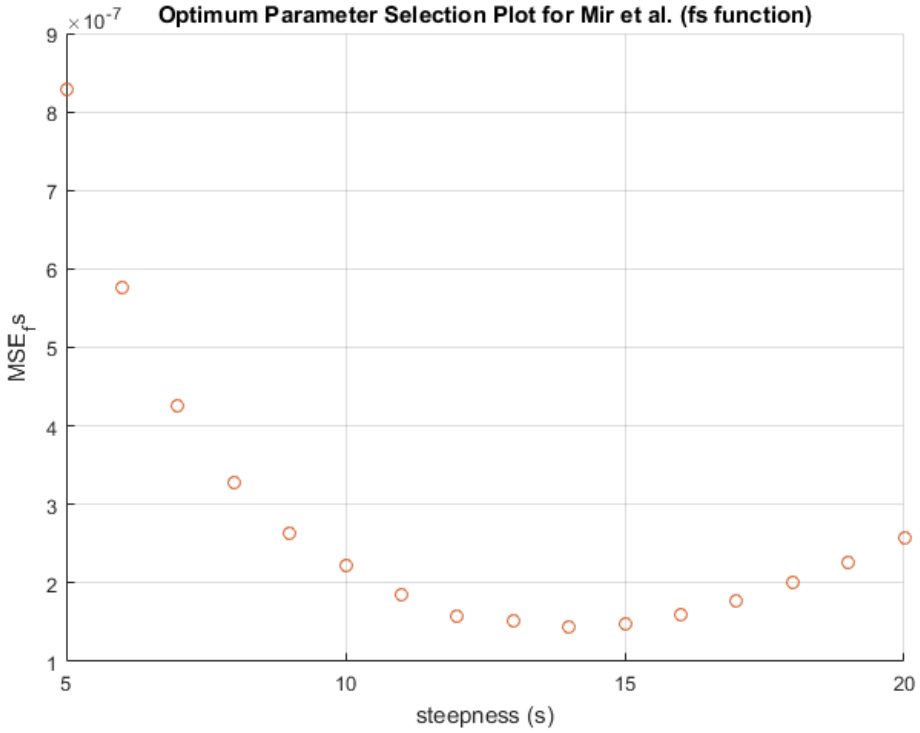

(c) *MasonLake(1)*

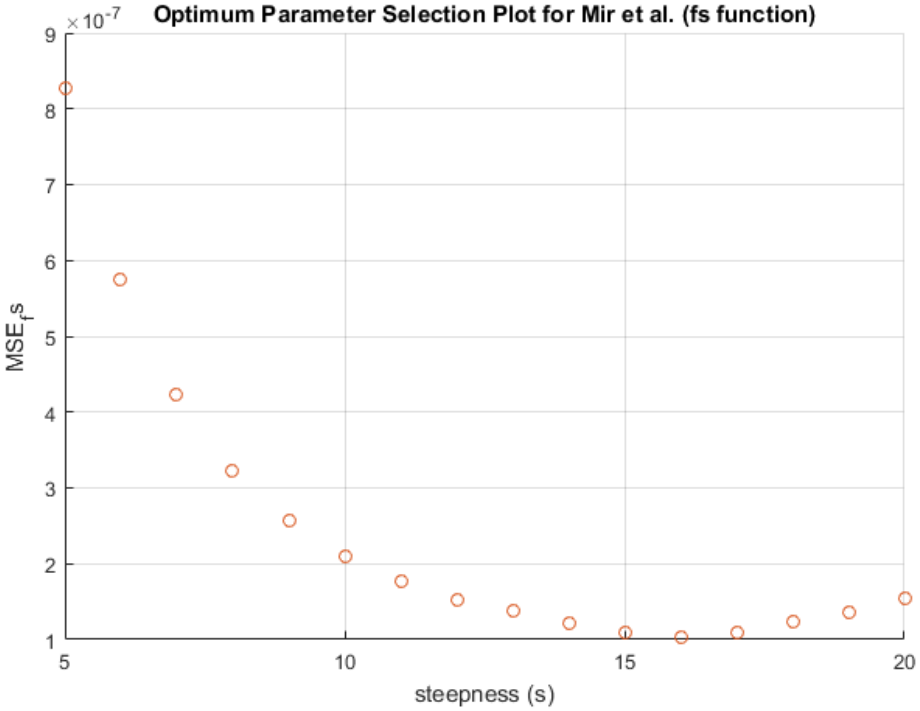

(d) *RedwoodSunset*

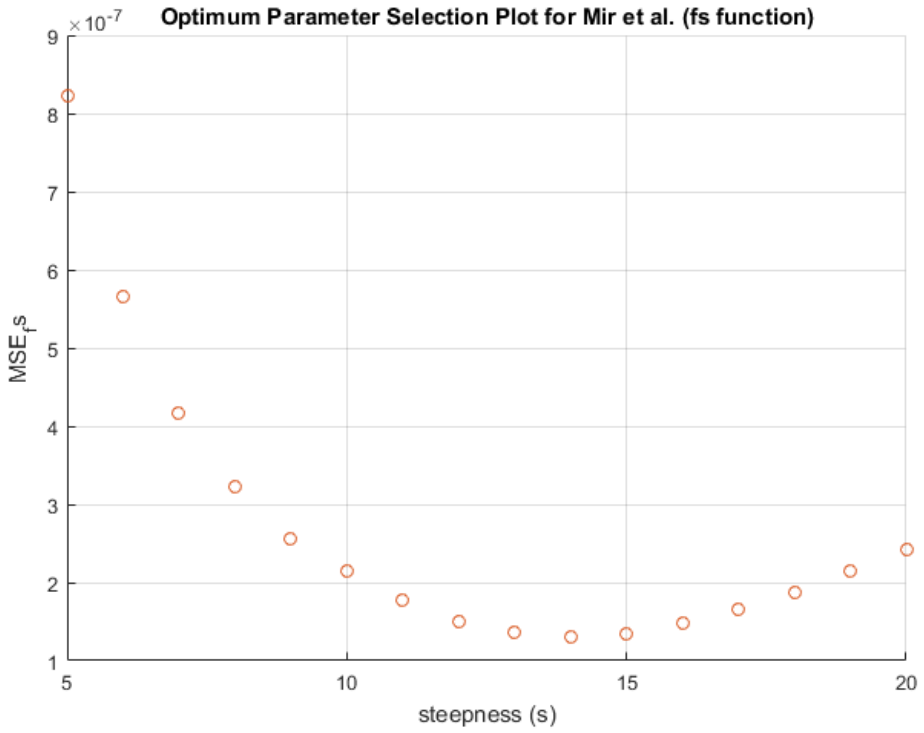

(e) *UpheavalDome*

Figure 5.1: An illustration of the optimum s parameter value selection in the Sigmoid function of the adaptive residual mapping method for each of the selected five HDR images.

In Figure 5.2, 8-bit backward compatible HDR image coding residues, which are obtained with the Sigmoid function of the adaptive residual mapping method that uses the optimum s parameter values, are given for the selected five HDR images with a fixed base layer quantization parameter, QP = 27.

(a) *AirBellowsGap*

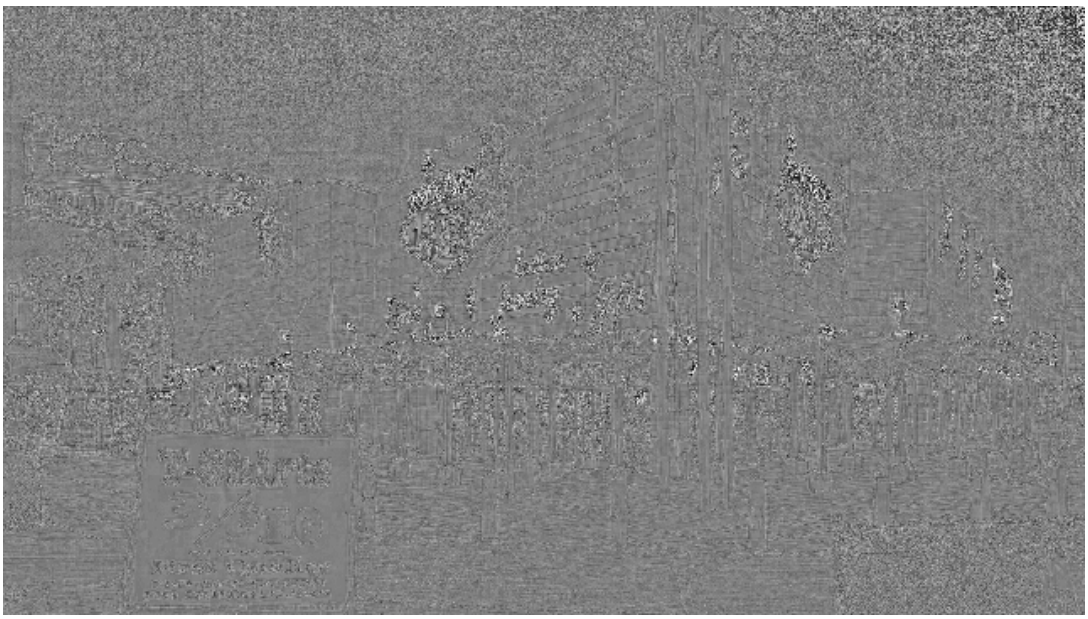

(b) *LasVegasStore*

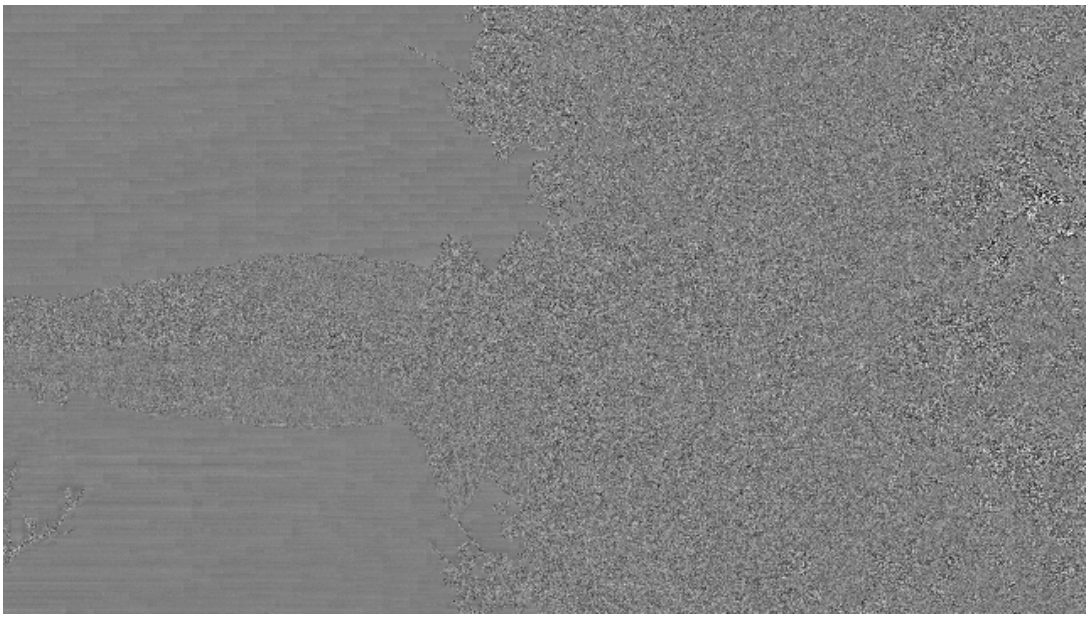

(c) *MasonLake(1)*

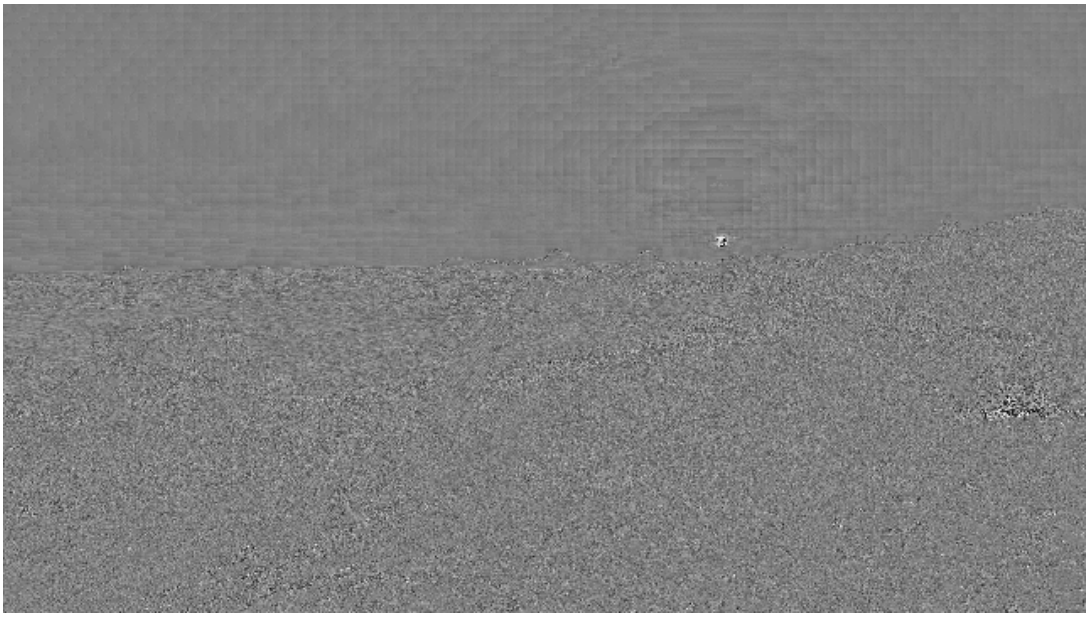

(d) *RedwoodSunset*

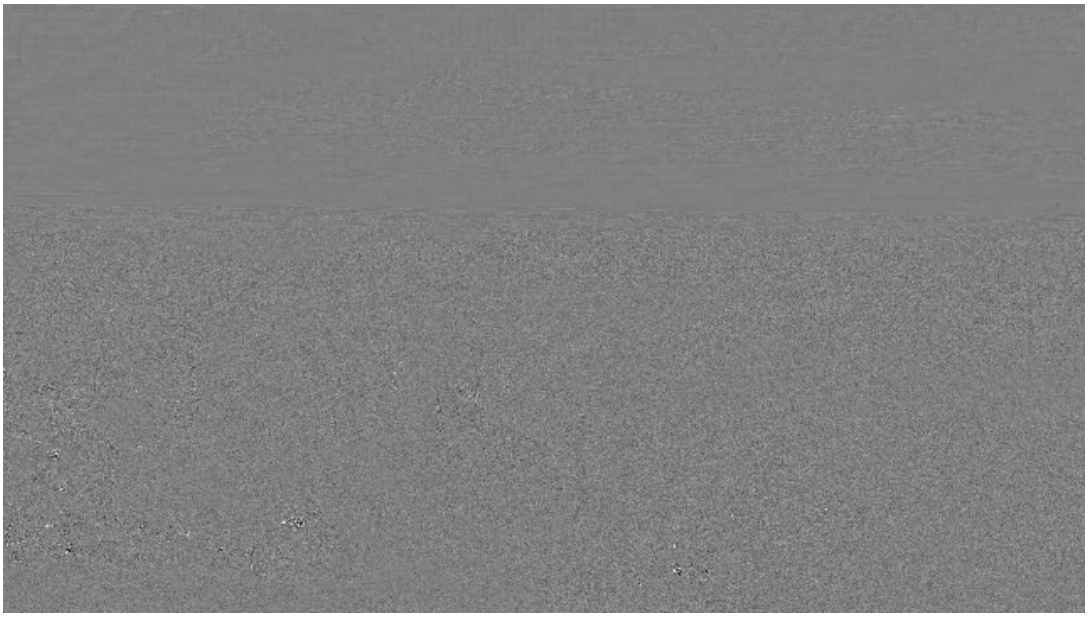

(e) *UpheavalDome*

Figure 5.2: 8-bit backward compatible HDR image coding residues obtained with the Sigmoid function of the adaptive residual mapping method using the optimum *s* parameter values with a fixed base layer quantization parameter, QP = 27.

5.1.2 The Logit Function of the Adaptive Residual Mapping Method for Backward Compatible HDR Image Coding Residues

The Logit function of the adaptive residual mapping method, which is proposed by Mir *et al.* [22], for backward compatible high dynamic range (HDR) image coding residues involves the following steps.

Backward compatible HDR image coding residue in the matrix form is firstly converted to the vector form. After that, the vector of backward compatible HDR image coding residue values, which is denoted as *r*, is normalized to [0, 1] range with respect to its maximum and minimum values as given in Equation 5.5:

$$r_n = \frac{r - min(r)}{max(r) - min(r)} \tag{5.5}$$

The vector of normalized HDR image coding residue values, which is denoted as r_n,

is passed through the Logit function:

$$R_n = \frac{1}{s} ln(\frac{r_n}{1 - r_n}) + m \tag{5.6}$$

The resulting values in the vector form R_n are multiplied with 255 and rounded. The rounded values in the vector form which are bigger than 255 and smaller than 0 are cropped to 255 and 0, respectively. Afterwards, the cropped values in the vector form are converted to the matrix form again in order to obtain the 8-bit backward compatible HDR image coding residue.

The *m* value in given Equation 5.6, is selected as the arithmetic mean as in the case of the Sigmoid function for the same reasons:

$$m = \frac{1}{N} \sum r_n \tag{5.7}$$

In given Equation 5.6, the *s* parameter, which is defined as the steepness of the Logit function, is selected as the value which minimizes the mean square error (MSE) between the original backward compatible HDR image coding residue and the reconstructed version of it after the 8-bit conversion by iterating the *s* parameter recursively as in the case of the Sigmoid function. For the experiments, the *s* parameter is iterated between values -5 and 5 with step size value 0.25 recursively. This iteration interval [-5, 5] and the step size value 0.25 is selected experimentally.

In Figure 5.3, an illustration of the optimum *s* parameter selection in the Logit function of the adaptive residual mapping method for each of the selected five HDR images is given. As seen from Figure 5.3, for each of the selected five HDR images, change of MSE value with respect to the *s* parameter values, which are selected experimentally, is convex shaped. The optimum *s* parameter values are the ones giving minimum MSE values.

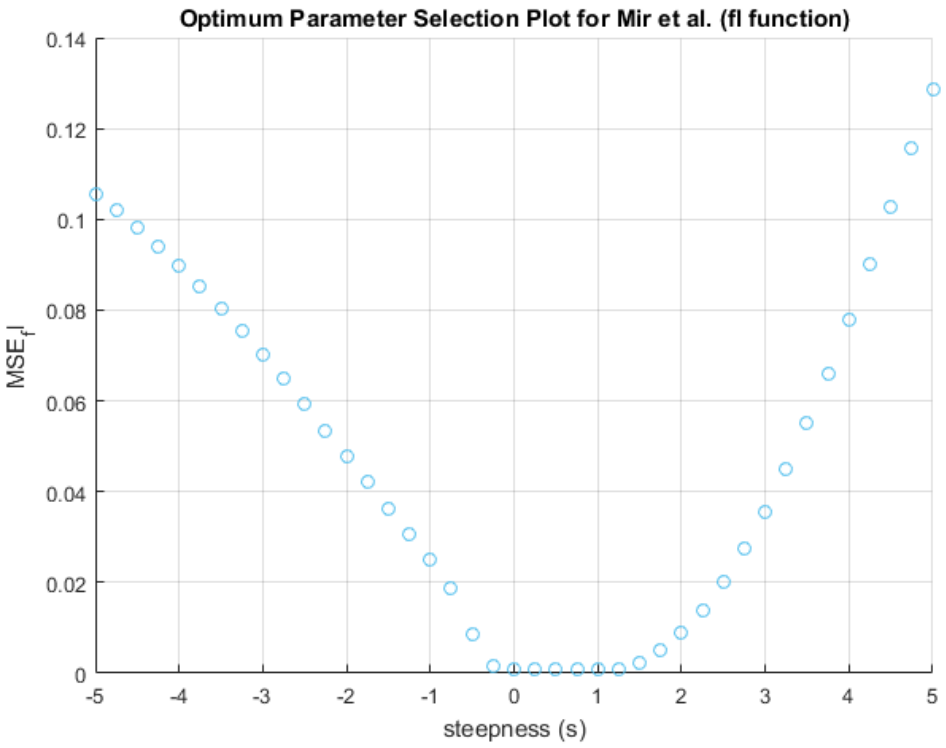

(a) *AirBellowsGap*

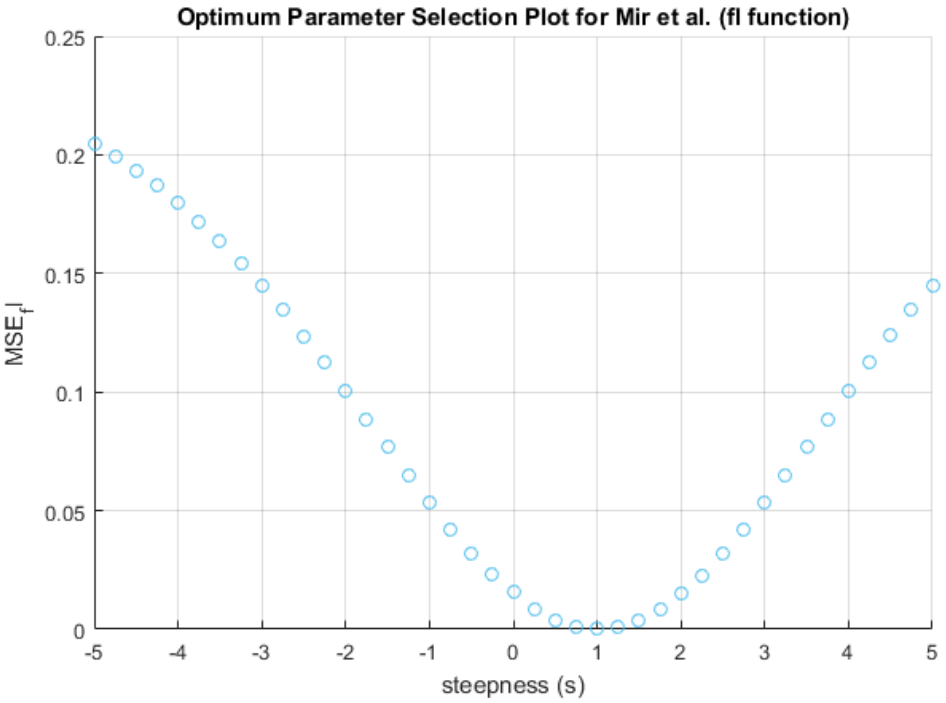

(b) *LasVegasStore*

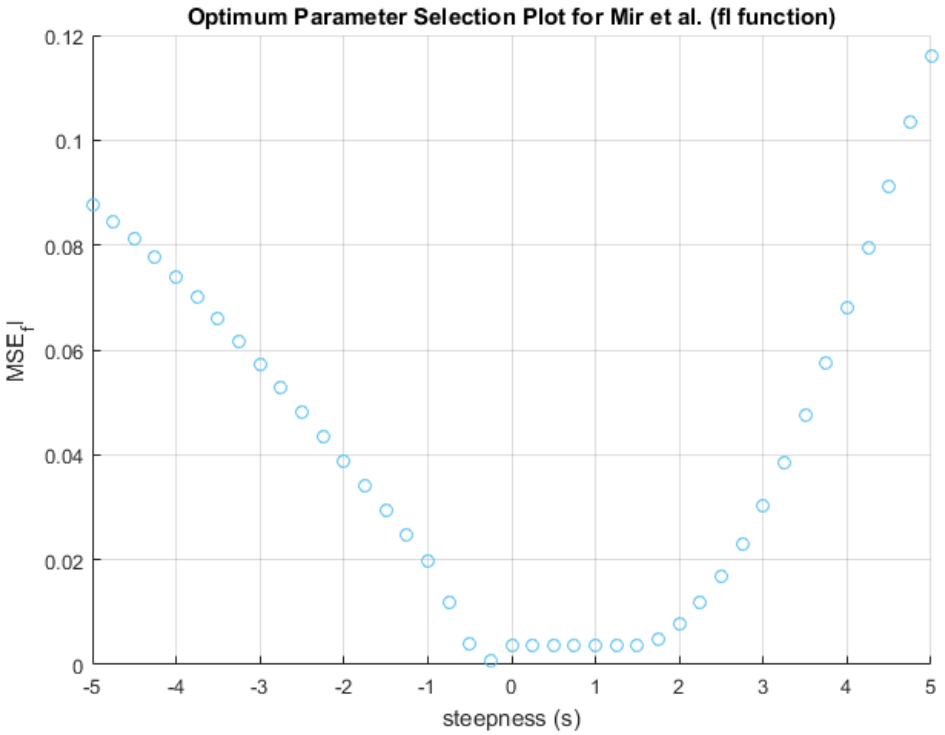

(c) *MasonLake(1)*

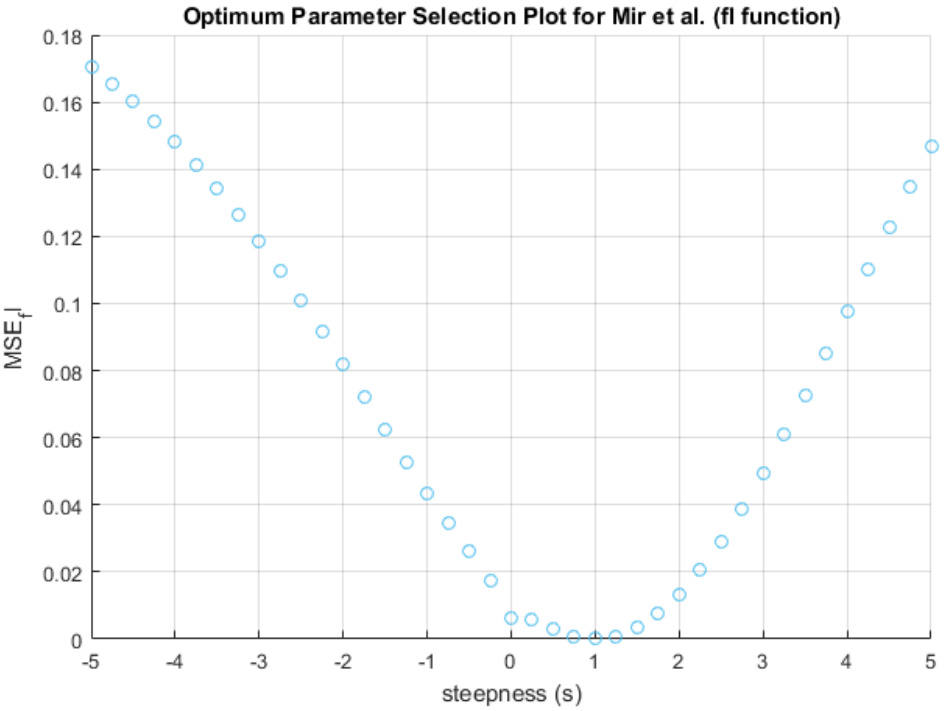

(d) *RedwoodSunset*

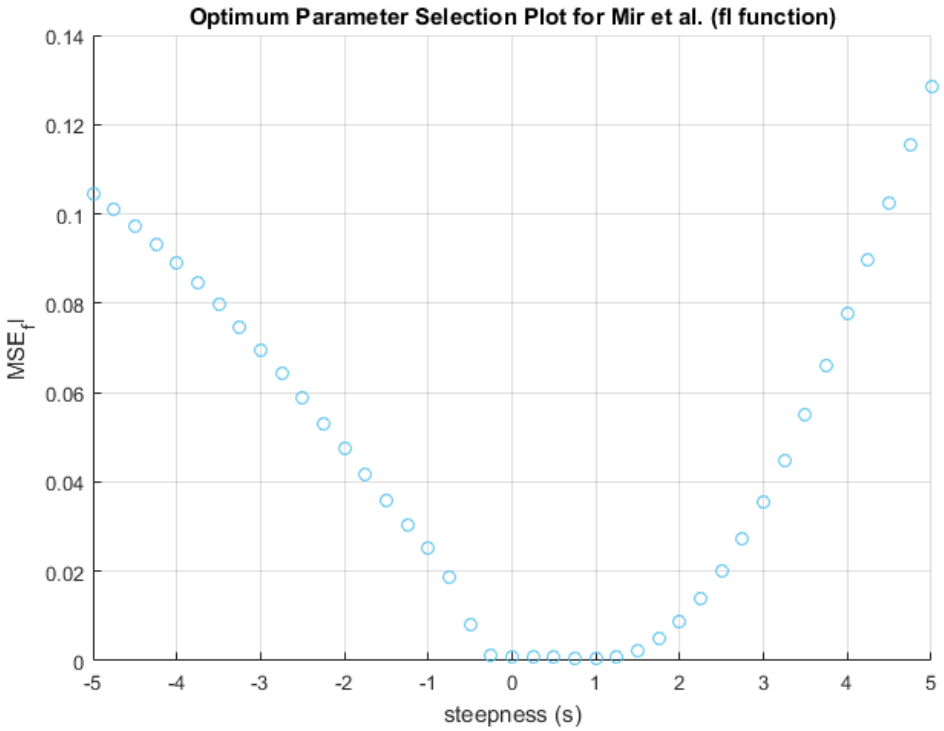

(e) *UpheavalDome*

Figure 5.3: An illustration of the optimum s parameter value selection in the Logit function of the adaptive residual mapping method for each of the selected five HDR images.

In Figure 5.4, an illustration of 8-bit conversion curves, which are obtained with the optimum s parameter values, and the histogram of the normalized backward compatible HDR image coding residue in the Sigmoid and the Logit functions of the adaptive residual mapping method for each of the selected five HDR images are given.

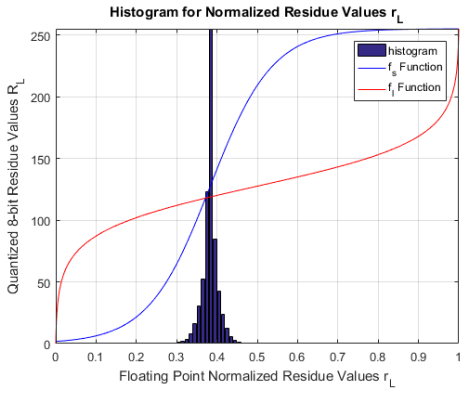

(a) *AirBellowsGap*

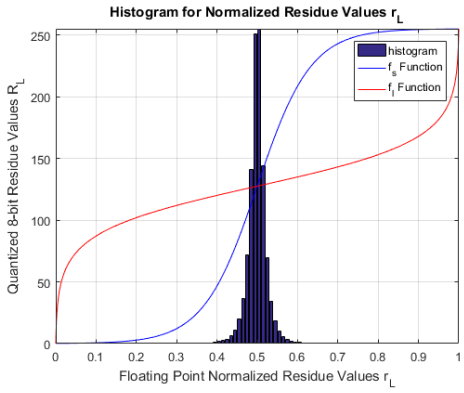

(b) *LasVegasStore*

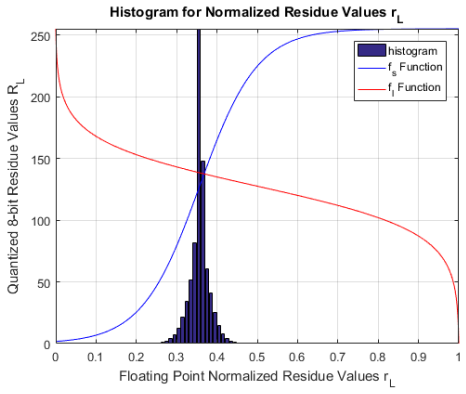

(c) *MasonLake(1)*

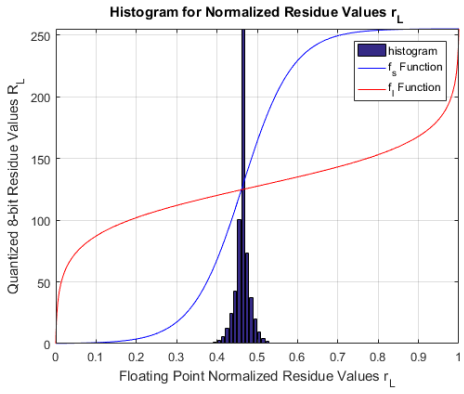

(d) *RedwoodSunset*

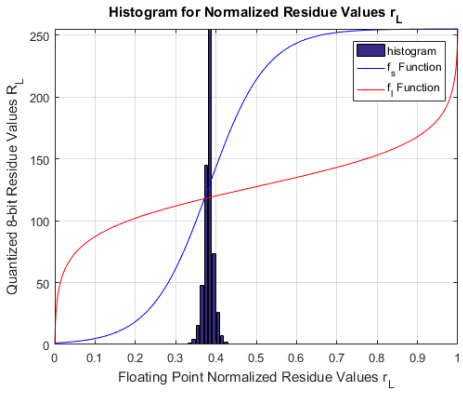

(e) *UpheavalDome*

Figure 5.4: An illustration of 8-bit conversion curves obtained with the optimum s parameter values and the histogram of the normalized backward compatible HDR image coding residue in the Sigmoid (blue) and the Logit (red) functions of the adaptive residual mapping method for each of the selected five HDR images.

In Figure 5.5, 8-bit backward compatible HDR image coding residues, which are obtained with the Logit function of the adaptive residual mapping method that uses the optimum s parameter values, are given for the selected five HDR images with a fixed base layer quantization parameter, QP = 27.

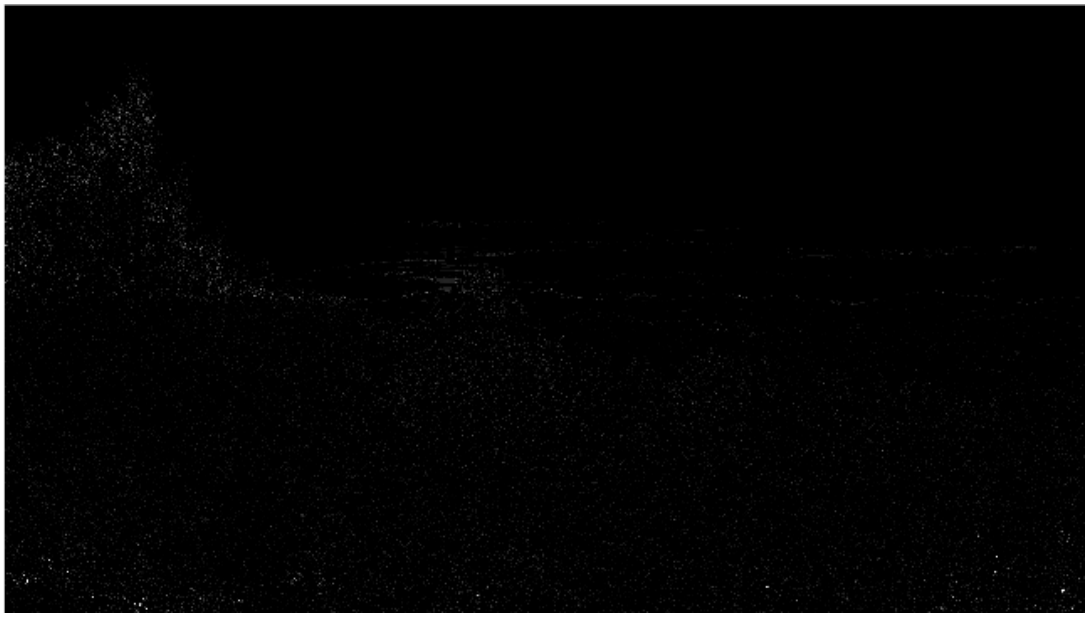

(a) *AirBellowsGap*

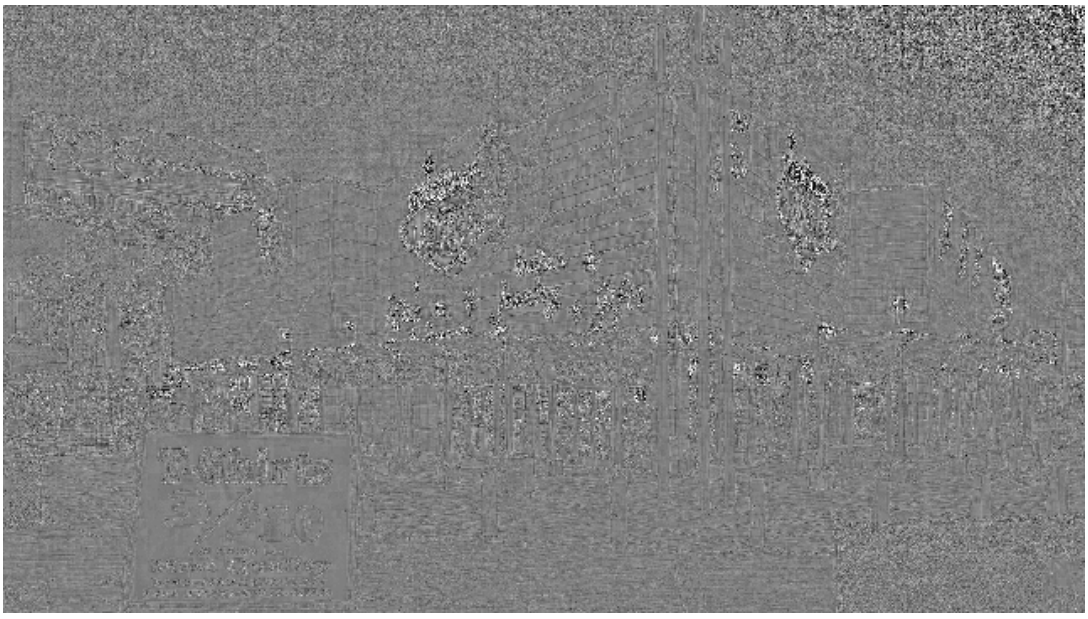

(b) *LasVegasStore*

(c) *MasonLake(1)*

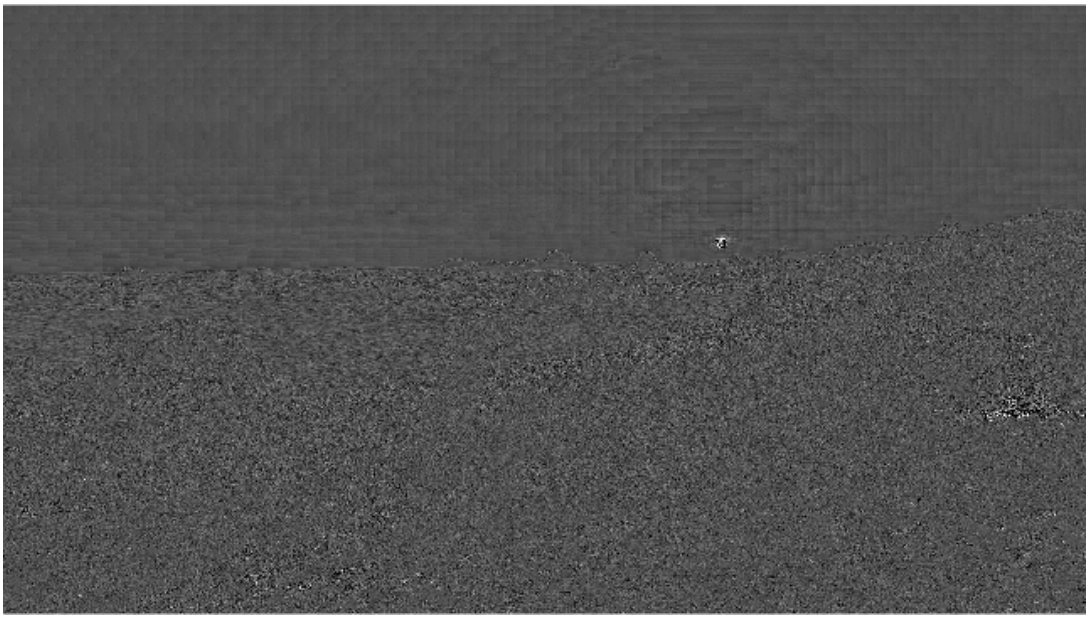

(d) *RedwoodSunset*

(e) *UpheavalDome*

Figure 5.5: 8-bit backward compatible HDR image coding residues obtained with the Logit function of the adaptive residual mapping method using the optimum s parameter values with a fixed base layer quantization parameter, QP = 27.

5.1.3 Adaptation of the Optimum Tone Mapping Method to Backward Compatible HDR Image Coding Residues

The optimum tone mapping method, which is proposed by Mai *et al.* [6], for high luminance values of an high dynamic range (HDR) image is adapted to the characteristics of backward compatible HDR image coding residues as an 8-bit conversion method, in addition to the adaptive residual mapping method of Mir *et al.* [22], in order to investigate which method performs better as an 8-bit conversion. The optimum tone mapping method will not be described step by step in this section entirely as in the case of the Sigmoid function and the Logit function, since essential detailed description of the optimum tone mapping method is given in Chapter 2 in the base layer operations. Further detailed description of the optimum tone mapping method can be found in [6]. Only the adapted parts of the optimum tone mapping method to the characteristics of backward compatible HDR image coding residues will be explained in this section.

Backward compatible HDR image coding residue in the matrix form is firstly converted to the vector form as in the case of the Sigmoid function and the Logit function. The vector of backward compatible HDR image coding residue values, which is denoted as *r*, is normalized to [0, 1] range with respect to its maximum and minimum values as given in Equation 5.8. r_n is the vector of normalized backward compatible HDR image coding residue values.

$$r_n = \frac{r - min(r)}{max(r) - min(r)} \tag{5.8}$$

After the normalization operation of the vector of backward compatible HDR image coding residue values, the optimum tone mapping method operations are performed on the vector of normalized backward compatible HDR image coding residue values in the same way as in the base layer operations which are explained in Chapter 2.

δ parameter is proposed to be selected as 0.1 by Mai *et al.* [6] for the optimum tone mapping of high luminance values of an HDR image, considering the luminance sensitivity of human visual system (HVS). However, since floating point real valued backward compatible HDR image coding residues are hardly outside the range of [-0.1 0.1], the proposed step size δ value of 0.1 for the tone mapping operation (TMO) of an HDR image is not an appropriate solution for backward compatible HDR image coding residues. Hence, the step size δ is considered as a design parameter and it is determined by iteratively changing it, and selecting the value which minimizes the mean square error (MSE) between the original backward compatible HDR image coding residue and the reconstructed version of it after the 8-bit conversion. For the experiments, the iteratively changed δ values are experimentally selected as 0.001, 0.002, 0.004, 0.005, 0.008, 0.01, 0.0125, 0.02, 0.025, 0.04, 0.05, 0.1, 0.2, 0.25, 0.5.

In Figure 5.6, an illustration of the optimum δ parameter value selection in the adaptation of the optimum tone mapping method for the selected five HDR images is given. As seen from Figure 5.6, in the adaptation of the optimum tone mapping method, as expected, MSE value which is obtained for piecewise linear function is saturated as the δ parameter value, which is selected experimentally, decreases. The optimum δ parameter value is the value at the level of this saturation.

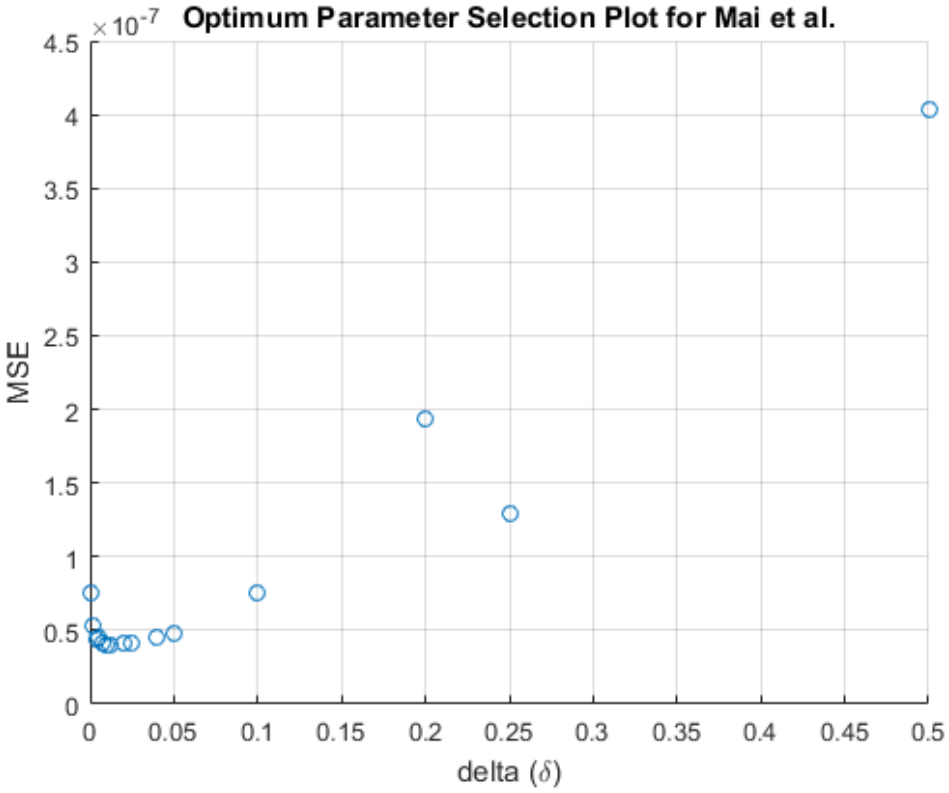

(a) *AirBellowsGap*

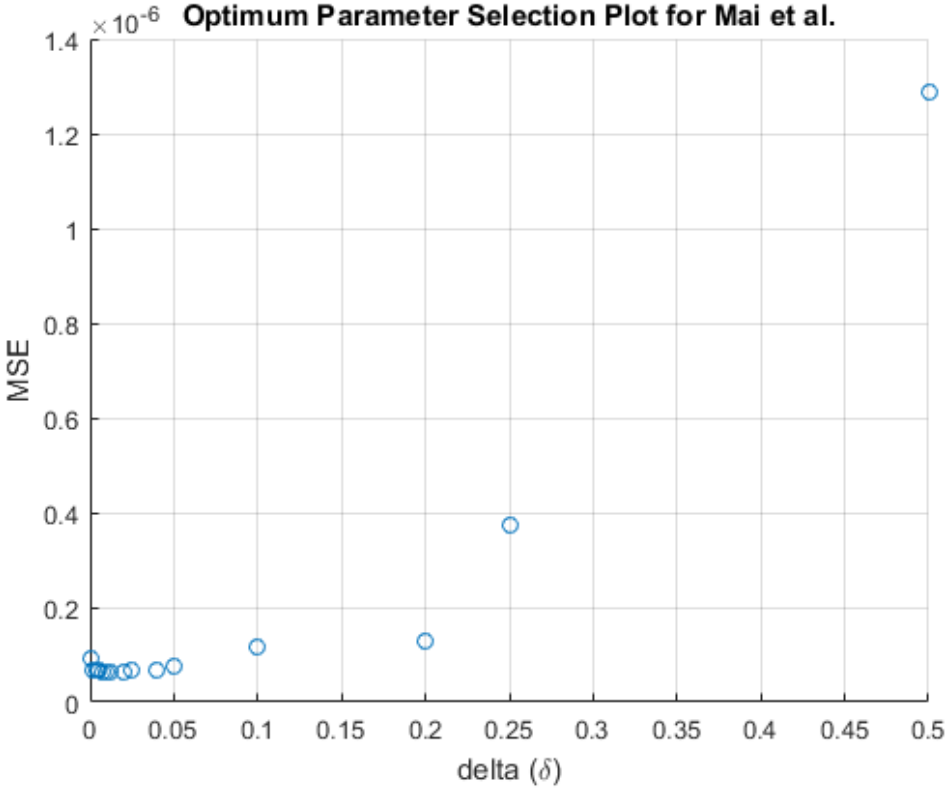

(b) *LasVegasStore*

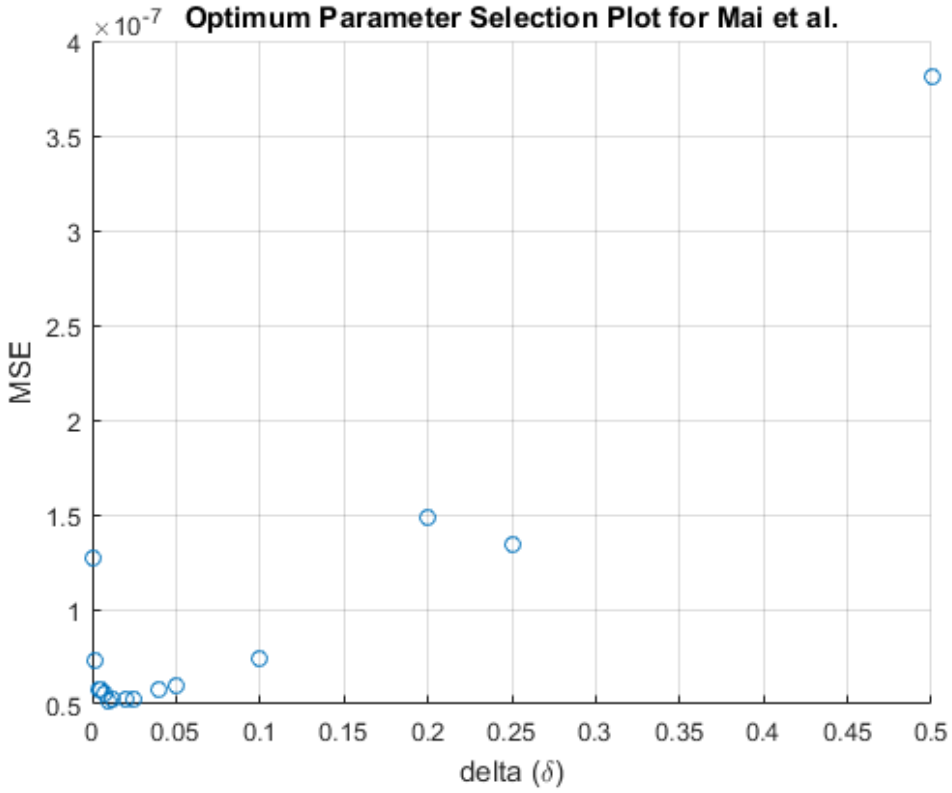

(c) *MasonLake(1)*

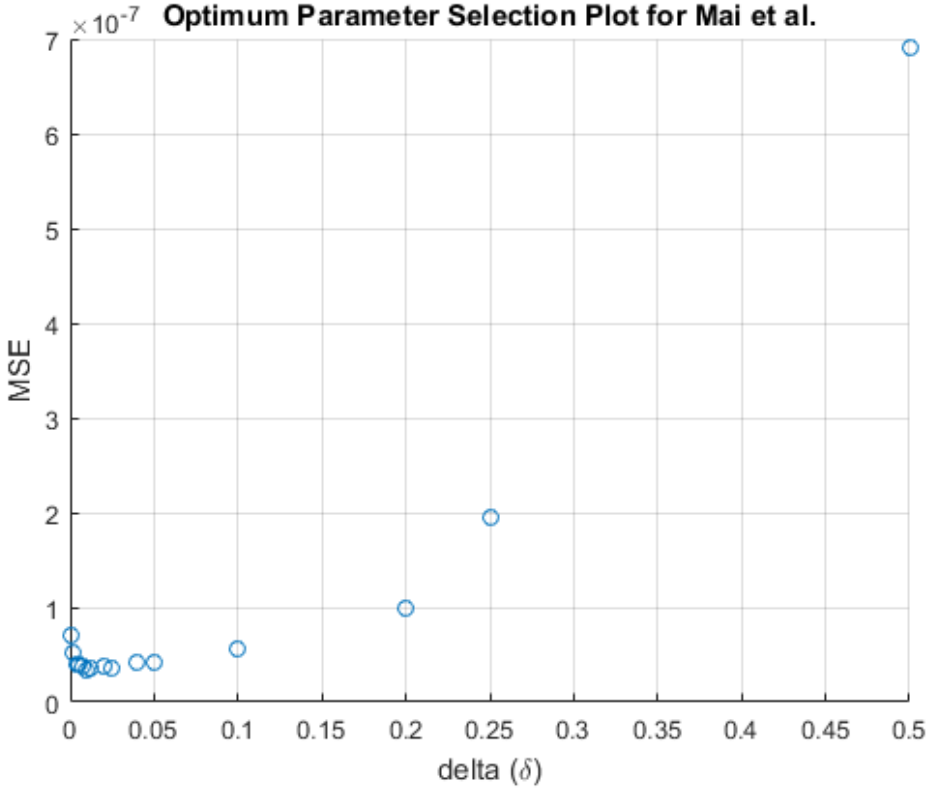

(d) *RedwoodSunset*

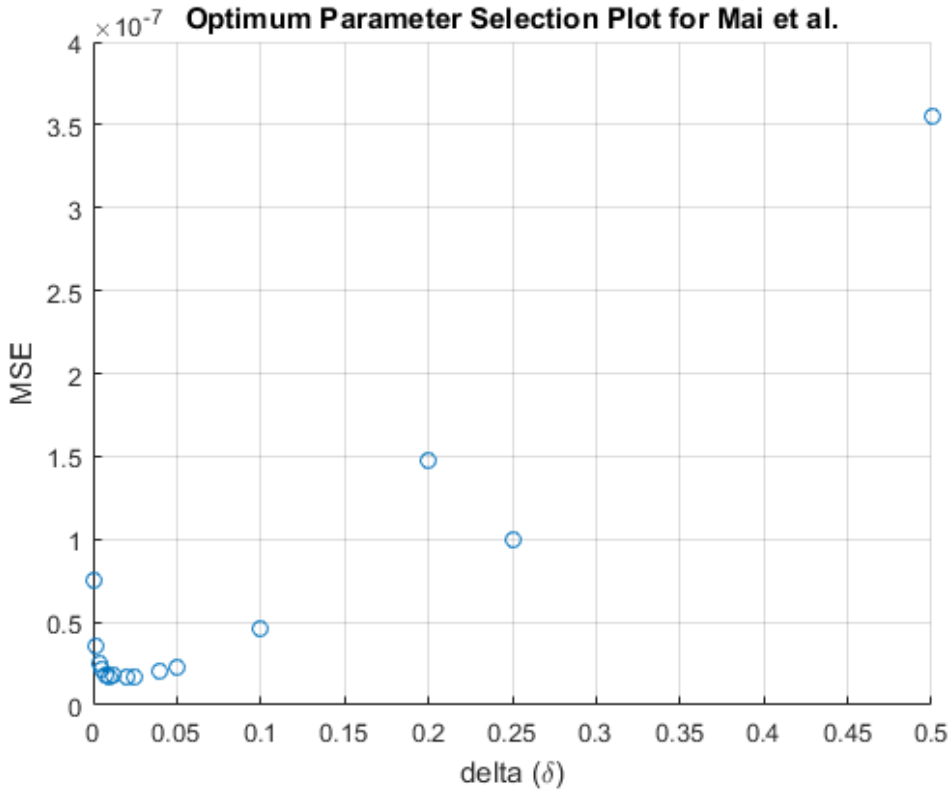

(e) *UpheavalDome*

Figure 5.6: An illustration of the optimum δ parameter value selection in the adaptation of the optimum tone mapping method for the selected five HDR images.

In Figure 5.7, an illustration of 8-bit conversion curve, which is obtained with the optimum δ parameter value, and the histogram of the normalized backward compatible HDR image coding residue in the adaptation of the optimum tone mapping method for the each selected five HDR images are given.

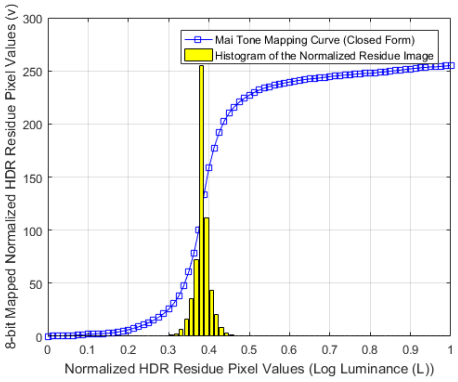

(a) *AirBellowsGap*

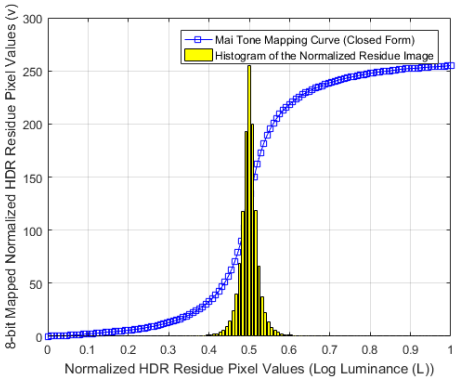

(b) *LasVegasStore*

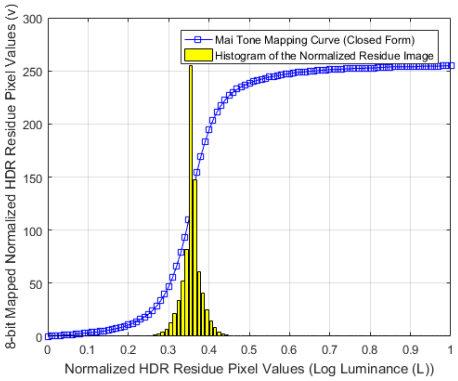

(c) *MasonLake(1)*

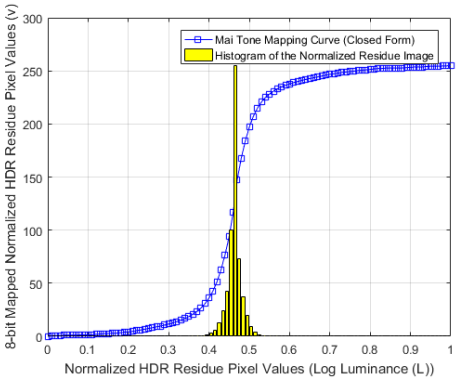

(d) *RedwoodSunset*

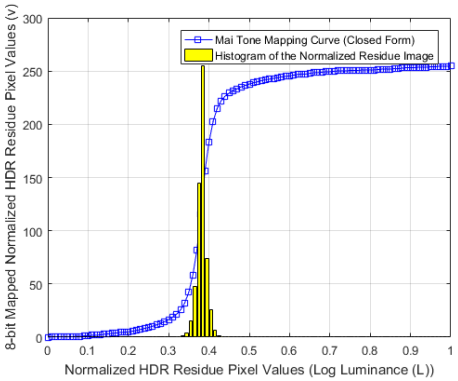

(e) *UpheavalDome*

Figure 5.7: An illustration of 8-bit conversion curve obtained with the optimum δ parameter value and the histogram of the normalized backward compatible HDR image coding residue in the adaptation of the optimum tone mapping method for each of the selected five HDR images.

In Figure 5.8, 8-bit backward compatible HDR image coding residues, which are obtained with the adaptation of the optimum tone mapping method that uses the optimum δ parameter values, are given for the selected five HDR images with a fixed base layer quantization parameter, QP = 27.

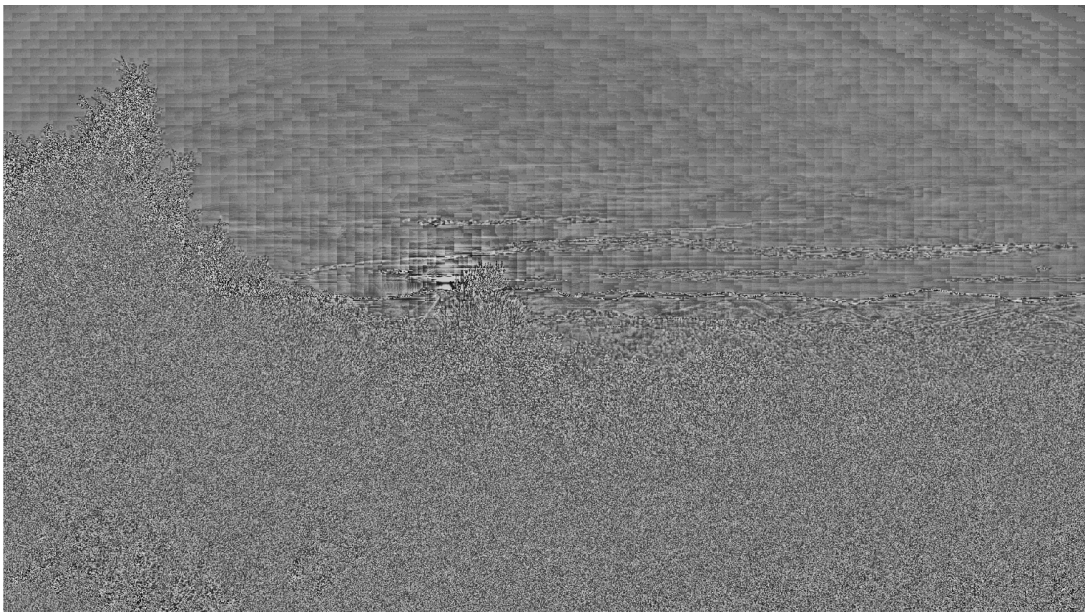

(a) *AirBellowsGap*

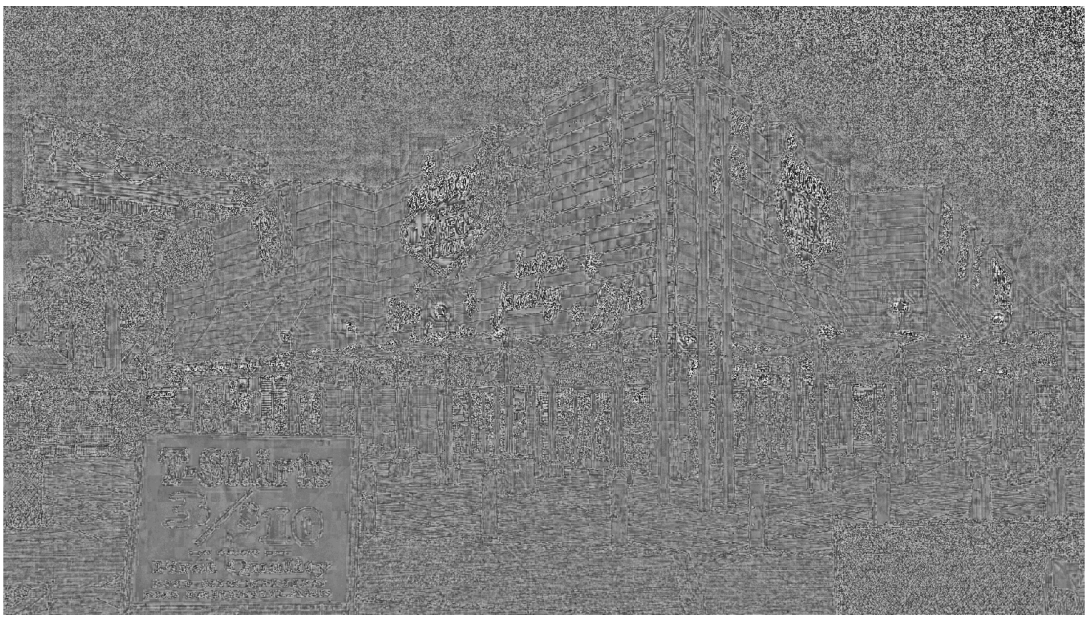

(b) *LasVegasStore*

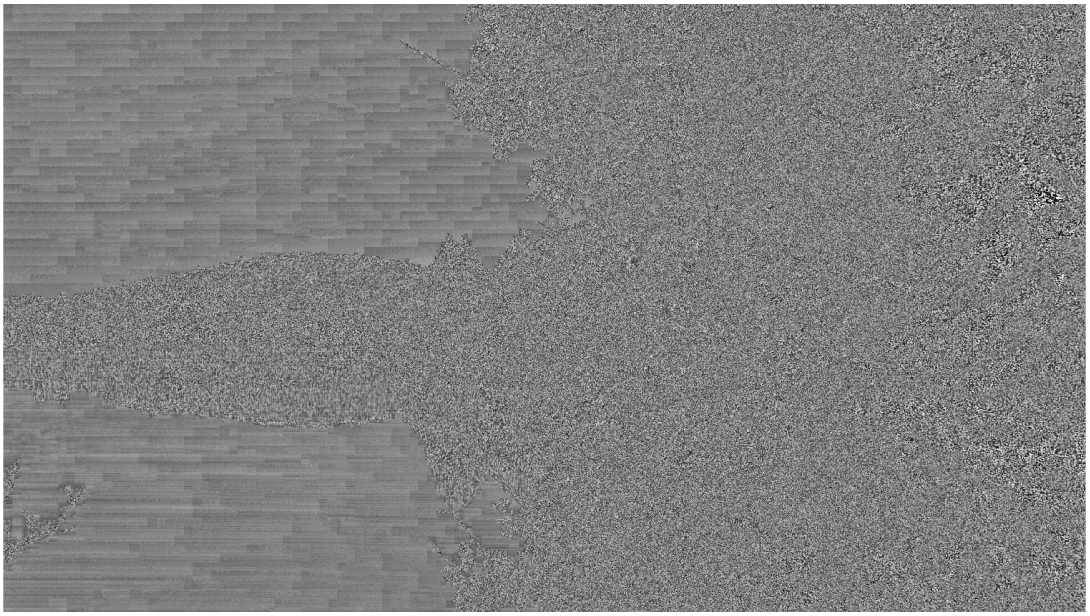

(c) *MasonLake(1)*

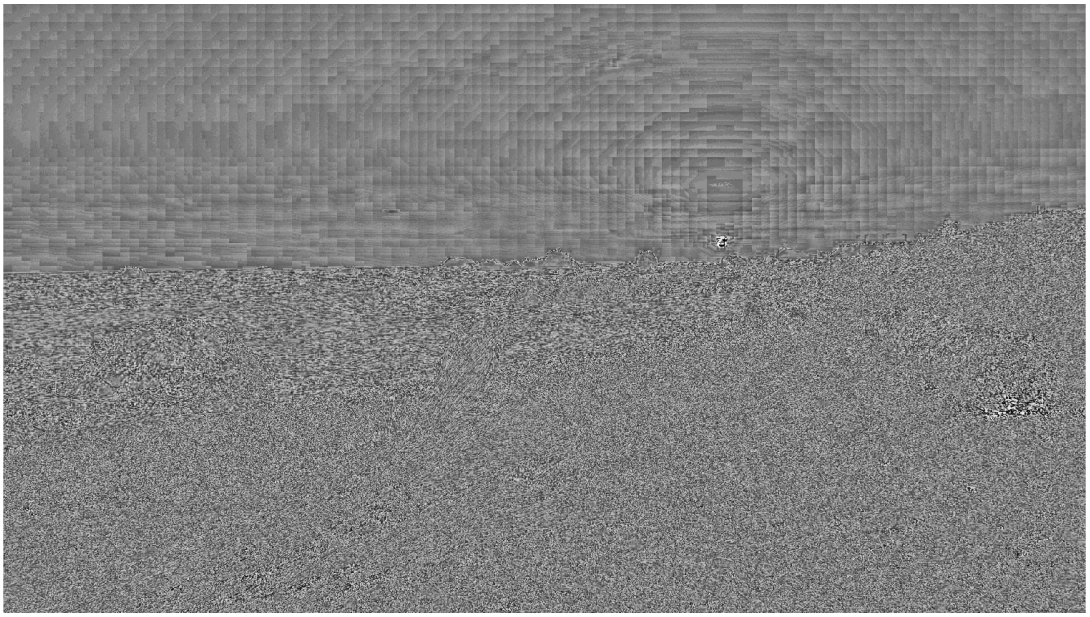

(d) *RedwoodSunset*

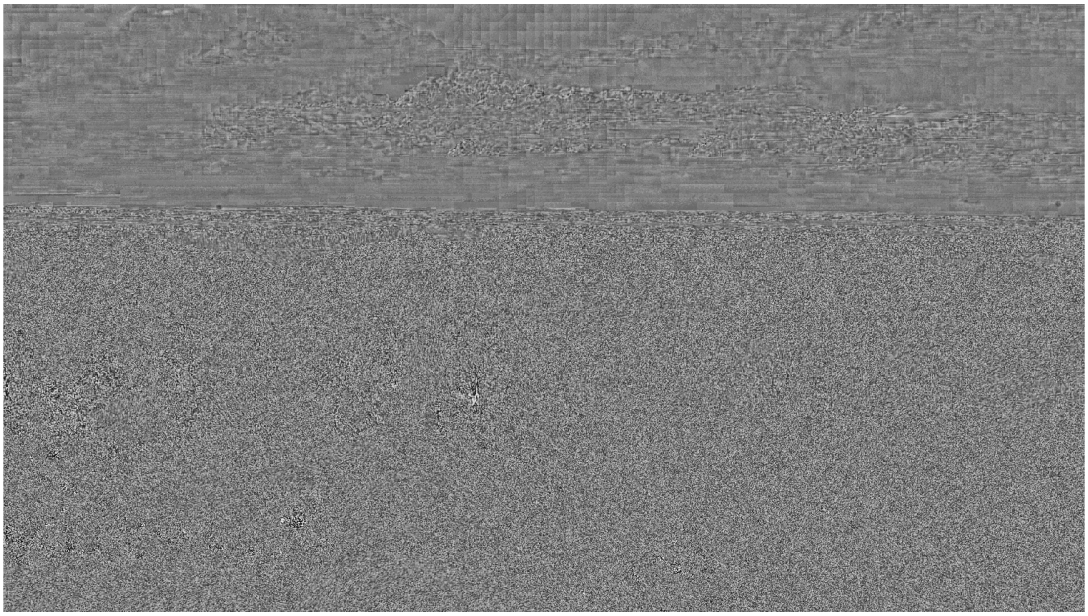

(e) *UpheavalDome*

Figure 5.8: 8-bit backward compatible HDR image coding residues obtained with the adaptation of the optimum tone mapping method using the optimum δ parameter values with a fixed base layer quantization parameter, QP = 27.

As a conclusion, as seen from Figures 5.2, 5.5 and 5.8, while the Sigmoid function of the adaptive residual mapping method and the adaptation of the optimum tone mapping method give good results, the Logit function of the adaptive residual mapping method gives poor results that can not be used for comparisons. Therefore, only the results of the Sigmoid function of the adaptive residual mapping method and the adaptation of the optimum tone mapping method will be used for comparisons as an 8-bit conversion in the next chapter.

5.2 Directional Coding of 8-bit Backward Compatible HDR Image Coding Residues and Details of the Utilized Directional Codec

From the visual inspection results in Chapter 3 and the experimental results in Chapter 4, it is observed and verified that backward compatible high dynamic range (HDR) image coding residues have local anisotropic characteristics which differ around edges, object boundaries and textured regions significantly and most of the information con-

centrates along these structures and these structures are 1-D structures. So, in order to code these 1-D structures more efficiently as in the case of low dynamic range (LDR) motion-compensated (MC) prediction residuals, the directional coding [32, 33], which refers to a modified H.264/AVC JM reference software encoder-decoder that uses diverse 1-D directional transforms in addition to the conventional 2-D transforms of the codec, is utilized. The goal is to see whether the directional coding is a better candidate solution or not for the coding of 8-bit backward compatible HDR image coding residues, compared to the standard coding, which refers to a standard H.264/AVC JM reference software encoder-decoder [8].

The directional codec which is utilized for the experiments is the modified H.264/AVC JM 10.2 codec same as in [32, 33] and it contains 8 1-D directional transforms for 4x4-pixel 8-bit backward compatible HDR image coding residue blocks and 16 1-D directional transforms for 8x8-pixel 8-bit backward compatible HDR image coding residue blocks. Figure 5.9 shows the 8 1-D directional transforms which are used for 4x4-pixel 8-bit backward compatible HDR image coding residue blocks, and Figure 5.10 shows the 16 1-D directional transforms which are used for 8x8-pixel 8-bit backward compatible HDR image coding residue blocks.

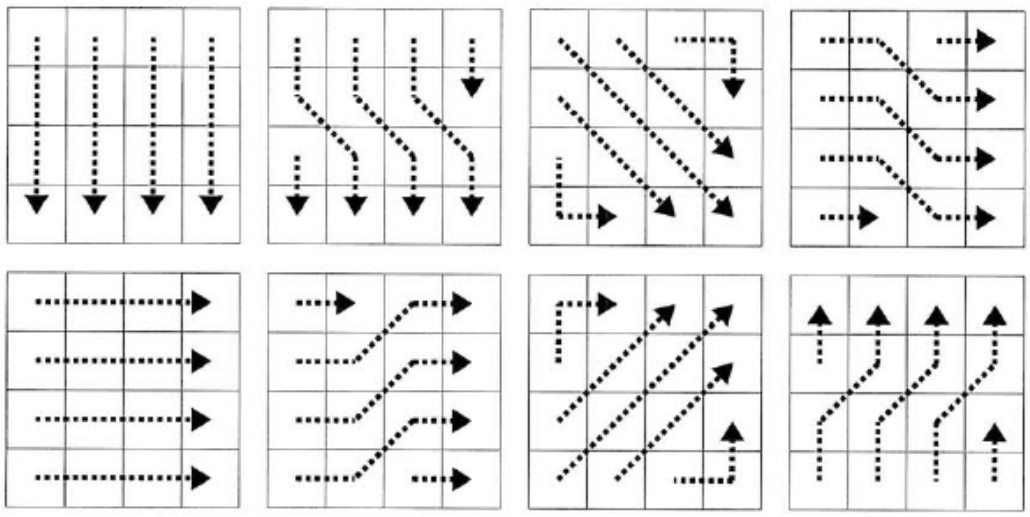

Figure 5.9: The 8 1-D directional transforms defined on the 4x4-pixel 8-bit backward compatible HDR image coding residue blocks [33].

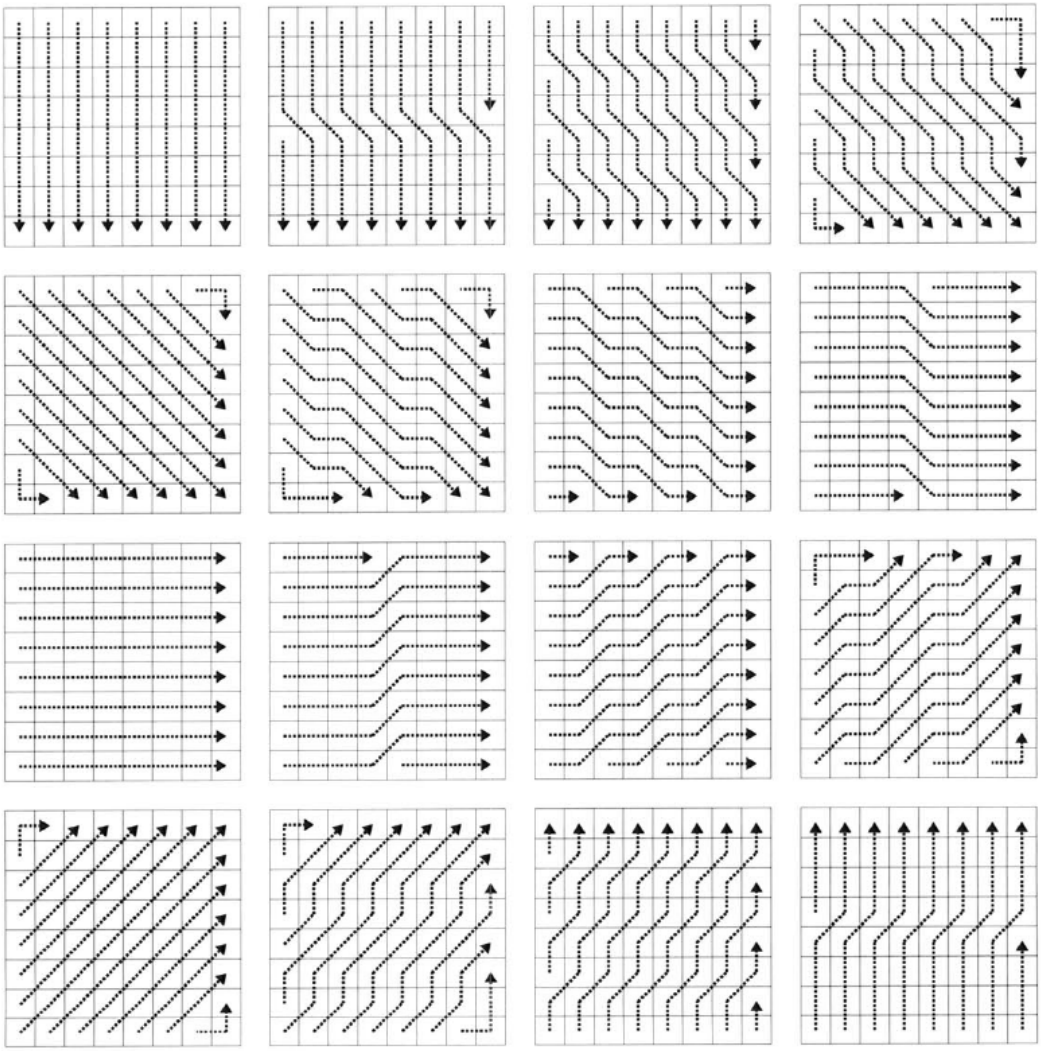

Figure 5.10: The 16 1-D directional transforms defined on the 8x8-pixel 8-bit backward compatible HDR image coding residue blocks [33].

Each arrow in Figures 5.9 and 5.10 indicates a different 1-D structure in either a 4x4-pixel 8-bit backward compatible HDR image coding residue block or an 8x8-pixel 8-bit backward compatible HDR image coding residue block on which the 1-D DCT is applied. All the 1-D structures, which are shown through these arrows, are directed at the same angle that corresponds to the direction of the large correlation coefficient roughly. The directions of all the 4x4-pixel 8-bit backward compatible HDR image coding residue blocks and 8x8-pixel 8-bit backward compatible HDR image coding residue blocks roughly cover $180°$. Lengths of the 1-D structures are different and the

1-D structures do not extend to neighbouring blocks. In addition to the 1-D directional transforms, the conventional 2-D discrete cosine transform (DCT) is used in the codec since there exists still regions in the 8-bit backward compatible HDR image coding residue blocks which can be better approximated with the 2-D transforms.

There are also other encoding-decoding modifications in the utilized directional codec and these are all performed likewise as in [32, 33]. These encoding-decoding modifications are entropy coding of the quantized 1-D directional transform coefficients with the alternative scans designed in [33] defined on both the 4x4-pixel and 8x8-pixel 8-bit backward compatible HDR image coding residue blocks, selection of the best block size for coding 8-bit backward compatible HDR image coding residues and selection of the best 1-D directional transform or the conventional 2-D DCT, and transmission of this selected best transform to the decoder so that the decoder can use the correct inverse transform for the each 8-bit backward compatible HDR image coding residue block.

The H.264/AVC JM reference software encoder-decoder offers two entropy coding methods which are the universal variable length coding (UVLC) [39] and the context adaptive binary arithmetic coding (CABAC) [40]. The transform coefficients can be coded using either the UVLC mode or the CABAC mode with the utilized directional codec. Since the statistics of the transform coefficients obtained with 1-D directional transforms and conventional 2-D DCT can be different, a redesigned entropy coder adapted to the statistics of 1-D transform coefficients may improve the entropy coding performance with the 1-D transforms. However, since such redesign requires significant modifications, a simpler alternative, modification of only the scanning patterns of the 1-D transform coefficients, is preferred in the H.264/AVC JM reference software encoder-decoder in the UVLC mode [33]. In particular, for each 1-D transform, a particular alternative scan is designed and used in [33].

The designed alternative scans [33], which are used in entropy coding of the quantized 1-D directional transform coefficients for the 4x4-pixel 8-bit backward compatible HDR image coding residue blocks and the 8x8-pixel 8-bit backward compatible HDR image coding residue blocks, are showed in Figures 5.11 and 5.12, respectively. The designed alternative scans in the each 4x4-pixel 8-bit backward compatible HDR

image coding residue block belongs to the corresponding 1-D directional transforms in Figure 5.9, and the designed alternative scans in the each 8x8-pixel 8-bit backward compatible HDR image coding residue block belongs to the corresponding 1-D directional transforms in Figure 5.10. Further details on the design of these alternative scans and the design considerations can be found in [33].

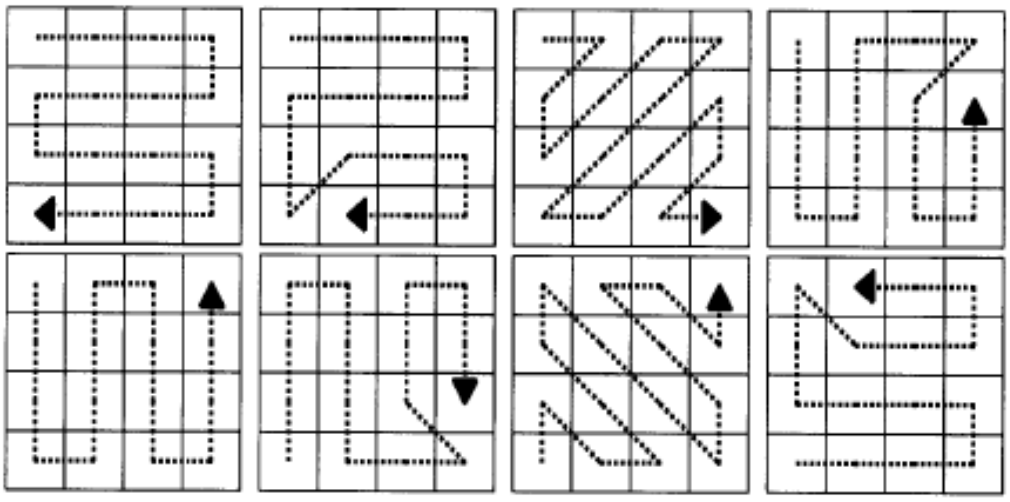

Figure 5.11: The designed alternative scans used in entropy coding of the quantized 1-D directional transform coefficients defined on the 4x4-pixel 8-bit backward compatible HDR image coding residue blocks [33].

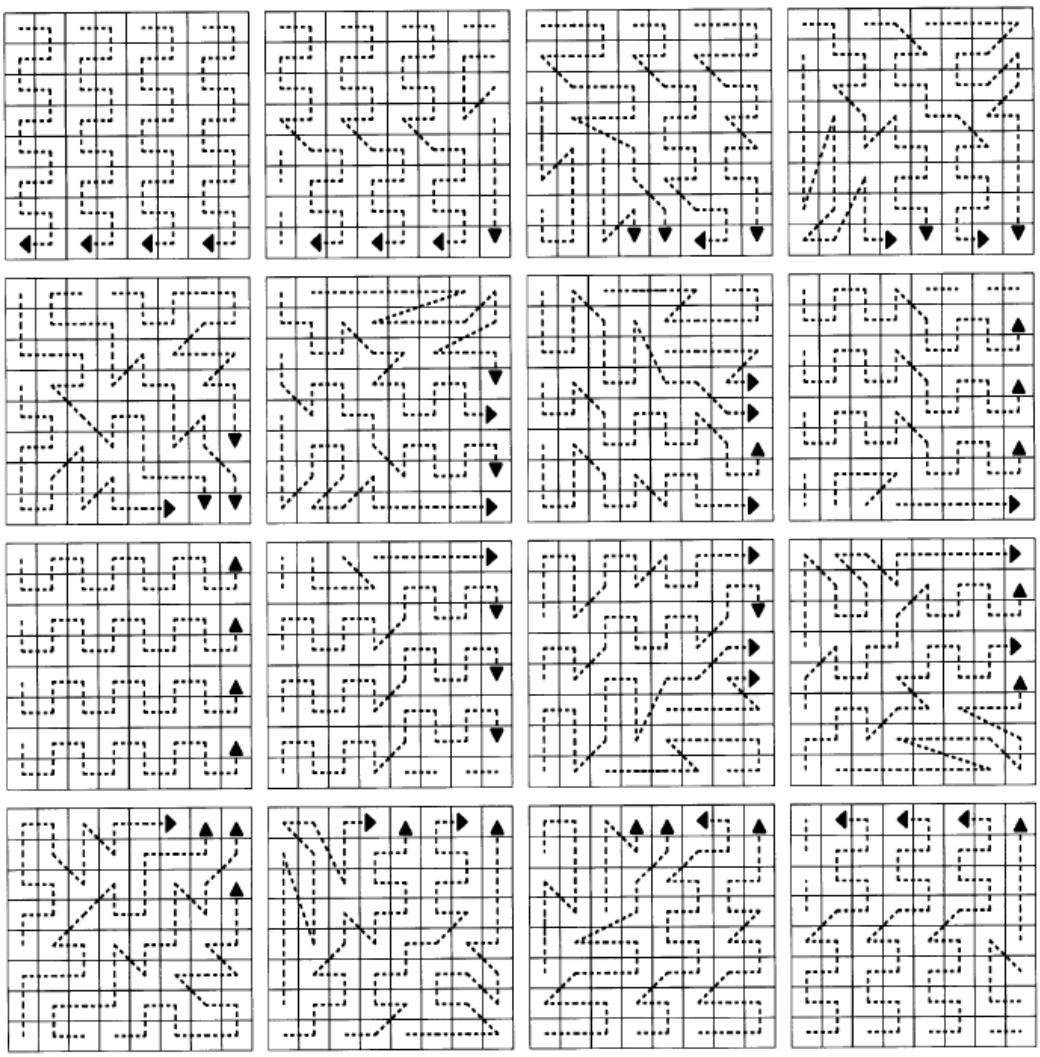

Figure 5.12: The designed alternative scans used in entropy coding of the quantized 1-D directional transform coefficients defined on the 8x8-pixel 8-bit backward compatible HDR image coding residue blocks [33].

The another important issue is how to select the best block size for 8-bit backward compatible HDR image coding residues and how to select the best 1-D directional transform or the conventional 2-D DCT for the each 8-bit backward compatible HDR image coding residue block. The solution of these two selection problems will not be described in detail in this section, further details on this can be found in [33]. However, briefly, these two selection problems are solved jointly. Firstly, for the each possible block size (4x4-pixel or 8x8-pixel) the best 1-D directional transform or the

conventional 2-D DCT for the each 8-bit backward compatible HDR image coding residue block is selected then the best block size for 8-bit backward compatible HDR image coding residue is selected given the best 1-D directional transforms. Thus, the best block size-transform combination is obtained [33].

The selected best transform for the each 8-bit backward compatible HDR image coding residue block needs to be transmitted to the decoder so that the decoder can use the correct inverse transform for the each 8-bit backward compatible HDR image coding residue block. This transmitted information is called as the *side information* [33]. The codewords in order to represent the selected transforms for both the 4x4-pixel 8-bit backward compatible HDR image coding residue blocks and the 8x8-pixel 8-bit backward compatible HDR image coding residue blocks are shown in Table 5.1. Further details can be found in [33].

Table 5.1: The codewords in order to represent the selected transforms for both the 4x4-pixel 8-bit backward compatible HDR image coding residue blocks and the 8x8-pixel 8-bit backward compatible HDR image coding residue blocks [33]

Selected Transforms	Codewords
2-D DCT	1
1-D Transform #1-8	0XXX

(a) For the 4x4-pixel 8-bit backward compatible HDR image coding residue block transforms

Selected Transforms	Codewords
2-D DCT	1
1-D Transform #1-16	0XXXX

(b) For the 8x8-pixel 8-bit backward compatible HDR image coding residue block transforms

In this thesis, the 1-D directional transforms are not integrated and the mentioned modifications are not performed in the state-of-the-art codec, which is the high efficiency video coding (HEVC) standard at the time this research was conducted. There are several reasons for this, such as mainly despite the H.264/AVC JM reference software encoder-decoder uses the 4x4 and 8x8 block sizes, the HEVC standard uses the

16x16 and 32x32 block sizes in addition to them, hence the 1-D directional transforms and the related modifications should be expanded to these block sizes too if the HEVC standard is utilized. Therefore, instead of any integration or modification, proof of the concept of whether the directional coding is a good candidate solution or not for the coding of backward compatible HDR image coding residues as well besides the standard coding is aimed mainly by utilizing the same directional codec, which is the modified H.264/AVC JM 10.2 reference software encoder-decoder in [32, 33] for the directional coding in the experiments, and the standard H.264/AVC JM 10.2 reference software encoder-decoder [8] for the standard coding in the experiments.

Eventually, it should be noted that 8-bit backward compatible HDR image coding residues are coded as intra-frames with both the directional codec and the standard codec. The coding procedure, nevertheless, remains the same. A block from the 8-bit backward compatible HDR image coding residue is intra predicted, and this intra predicted 8-bit backward compatible HDR image coding residue block is coded with either a 1-D directional transform or the conventional 2-D DCT, which is determined by the codec with rate-distortion optimized transform selection.

CHAPTER 6

EXPERIMENTAL RESULTS FOR THE PROPOSED CODING METHOD FOR BACKWARD COMPATIBLE HDR IMAGE CODING RESIDUES

In this chapter, experimental results for the proposed coding method for several backward compatible high dynamic range (HDR) image coding residues, which have different bitrates (different quantization parameters (QPs)), spatial activities and dynamic ranges as the main variables in the HDR image coding, are given, compared and interpreted.

6.1 Experimental Setup

The experimental setup for the proposed coding method for backward compatible high dynamic range (HDR) image coding residues is likewise the experimental setup for the auto-covariance (AC) analyses of backward compatible HDR image coding residues. Further details on the experimental setup can be found in Chapter 4. Only the additions in the experimental setup will be explained in this chapter.

As mentioned before in Chapter 4, the selected HDR images undergo the color space transformation (CST), tone mapping operation (TMO), encoding, decoding and inverse tone mapping operation (ITMO) in the base layer and backward compatible HDR image coding residues are obtained by taking difference between the log luminances of original HDR images and predicted versions of them. As a tone mapping operator (TMO), only the optimum tone mapping method of Mai *et al.* [6] is utilized

in the base layer. However, note that, other TMOs could also be used to understand the rate-distortion performances of proposed coding method for backward compatible HDR image coding residues. For the base layer encoding and decoding operations, the H.264/AVC JM 10.2 reference software encoder-decoder [8] is used. Four different base layer quantization parameters, which are selected as QP = 22, 27, 32, 37, are used in order to perform the encoding and decoding operations.

In the residue layer, after finding backward compatible HDR image coding residues, the residues undergo the normalization (Norm), 8-bit conversion, encoding, decoding, inverse 8-bit conversion and inverse normalization (Inv Norm). As an 8-bit conversion, two 8-bit conversion methods as explained in detail in Chapter 5, the adaptive residual mapping method of Mir *et al.* [22], which consists of the Sigmoid function and the Logit function, and the adaptation of the optimum tone mapping method of Mai *et al.* [6] to backward compatible HDR image coding residues are used. Because of the fact that, the Logit function of the adaptive residual mapping method gives poor results that can not be used for comparisons, only the rate-distortion performance results of the Sigmoid function of the adaptive residual mapping method and the adaptation of the optimum tone mapping method of Mai *et al.* [6] to backward compatible HDR image coding residues will be given, compared and interpreted. For the residue layer encoding and decoding operations, two codecs, as explained in detail in Chapter 5, the directional codec, which is the modified H.264/AVC JM 10.2 codec likewise in [32, 33], and the standard codec or in other words the typical codec, which is the standard H.264/AVC JM 10.2 codec [8], are used. Four different residue layer quantization parameters, which are selected as QP = 22, 27, 32, 37 for the both codecs, are used in order to perform the encoding and decoding operations.

6.2 Rate-Distortion Performance Results

In order to compare the rate-distortion performance results of the 8-bit conversion and the coding of backward compatible high dynamic range (HDR) image coding residues, base layer quantization parameter is fixed to QP = 27 for avoiding complexity. In the computation of distortion between the original and reconstructed HDR images, two objective quality metrics, namely the high dynamic range-minimum

square error (HDR-MSE), and the perceptually uniform-peak signal to noise ratio (PU-PSNR) [41], are utilized. In addition to the objective quality metrics, subjective quality metrics, the high dynamic range visible differences predictor (HDR-VDP) [42], and the high dynamic range video quality measure (HDR-VQM) [43] are also used for the computation of the distortions. The HDR-MSE is computed as the logarithm (log_{10}) of the mean square error (MSE) between the log luminances of original and reconstructed HDR images. The PU-PSNR metric is similar to the PSNR metric but extended version of it to wider luminance gamut considering the sensitivity of the human visual system (HVS). Therefore the PU-PSNR is assumed more convenient to HDR content as an objective quality metric. The HDR-VDP is the extended version of the visible differences predictor (VDP) [44] to the HDR content. It briefly simulates the human eye for light scattering, and performs modifications in order to accord with the wider luminance range of HDR. The HDR-VDP is computed between the original and reconstructed HDR images by using its quality (Q) option. Note that, the implementation of HDR-VDP is available publicly. The HDR-VQM is originally used for quality assessment of HDR video sequences, however, it can also be utilized for quality assessment of HDR images as it is done in this thesis. Again, note that, likewise the HDR-VDP, the implementation of HDR-VQM is also available publicly. Finally, the bitrate is taken as the total bitrate of the base layer and the residue layer to draw the rate-distortion curves.

6.2.1 Rate-Distortion Performance Results for the 8-bit Conversion of Backward Compatible HDR Image Coding Residues

As mentioned before in Chapter 5, for the 8-bit conversion of backward compatible high dynamic range (HDR) image coding residues, two methods are used and it is investigated which method performs better as an 8-bit conversion. As the first method, the adaptive residual mapping method, which is proposed by Mir *et al.* [22] and includes the Sigmoid function and the Logit function, is used. Since, the Logit function of the adaptive residual mapping method gives poor results that can not be used for comparisons, only the results of the Sigmoid function of the adaptive residual mapping method is used for comparisons. As the second method, the optimum tone mapping method which is proposed by Mai *et al.* [6] is adapted to the characteristics

of backward compatible HDR image coding residues as an 8-bit conversion.

Figures 6.1 and 6.2 give the rate-distortion performance plot results for the two compared 8-bit conversion methods, the Sigmoid function of the adaptive residual mapping method which is proposed by Mir *et al.* [22] and the optimum tone mapping method which is proposed by Mai *et al.* [6], of backward compatible HDR image coding residues for the selected five HDR images coded with the standard and the directional or in other words 1-D codec, respectively, in the residue layer and with a fixed base layer quantization parameter, QP = 27.

As seen from the figures, the adaptation of the optimum tone mapping method to backward compatible HDR image coding residues outperforms the Sigmoid function of the adaptive residual mapping method appreciably in the meaning of rate-distortion performances for both the standard and the directional coding. The gain in the HDR-MSE (log_{10}) for the adaptation of the optimum tone mapping method to backward compatible HDR image coding residues for the same bitrate is about 0.3 to 0.9 dB for both the standard and directional coding.

Finally, because of the fact that the adaptation of the optimum tone mapping method to backward compatible HDR image coding residues surpasses remarkably the Sigmoid function of the adaptive residual mapping method in the meaning of rate-distortion performances for both the standard and the directional coding, in the remaining rate-distortion performance results, which are on the coding of 8-bit backward compatible HDR image coding residues, the adaptation of the optimum tone mapping method is used for the 8-bit conversion of backward compatible HDR image coding residues owing to its better rate-distortion performance.

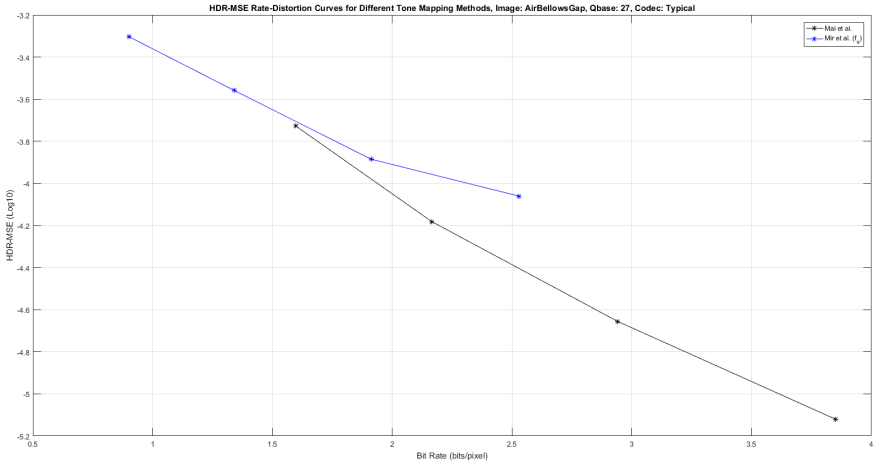

(a) *AirBellowsGap*

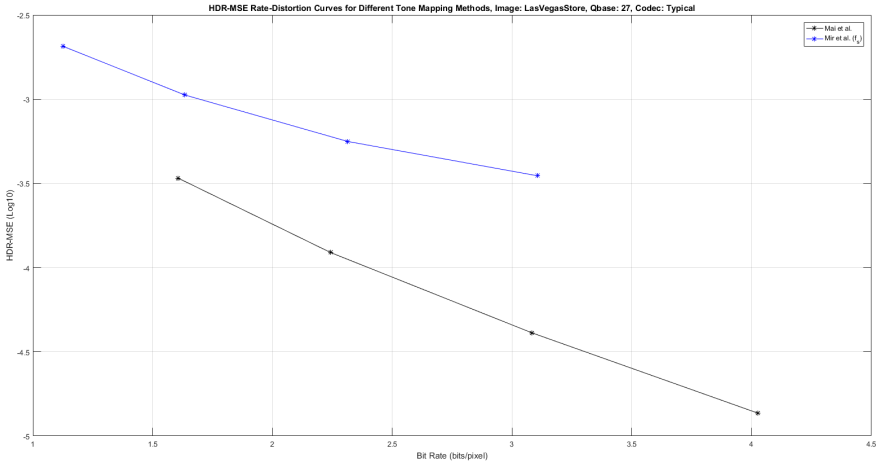

(b) *LasVegasStore*

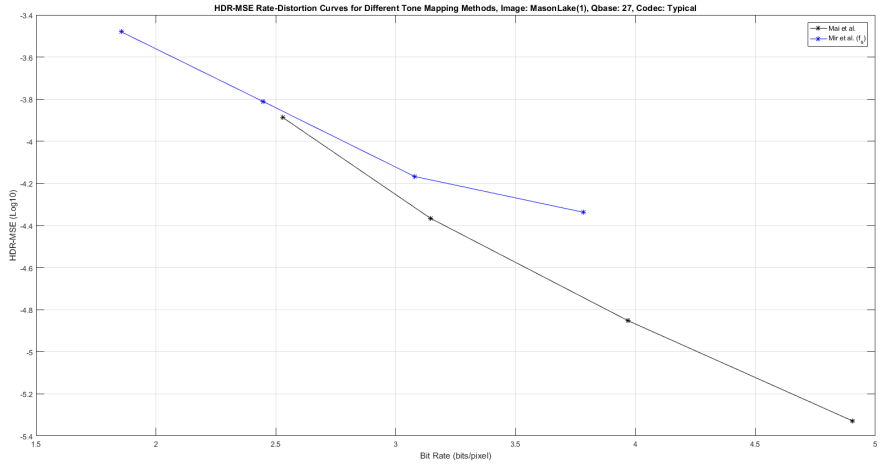

(c) *MasonLake(1)*

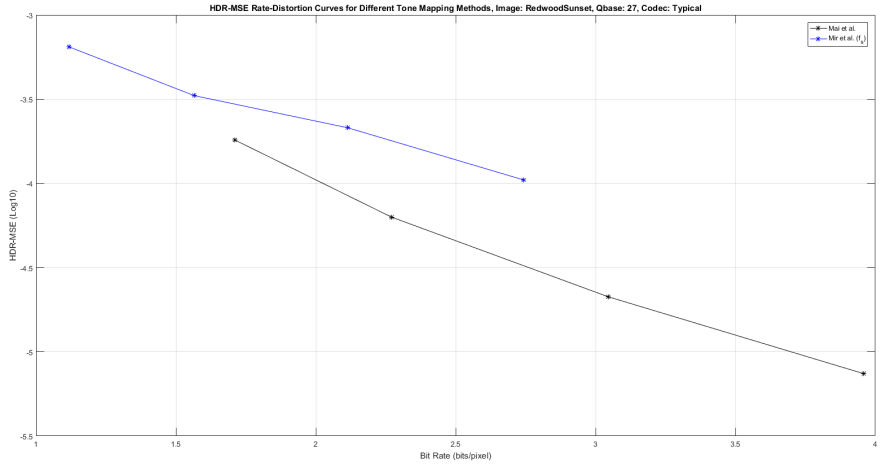

(d) *RedwoodSunset*

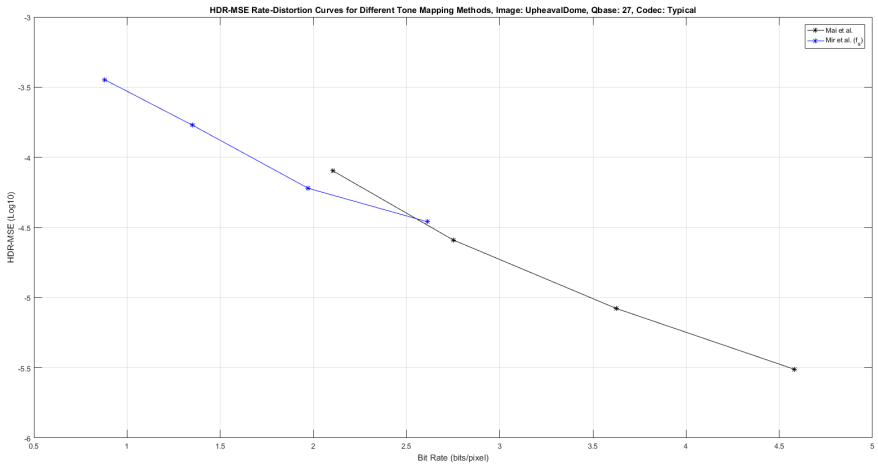

(e) *UpheavalDome*

Figure 6.1: HDR-MSE (log_{10}) vs. bitrate (bits/pixel) rate-distortion performance plot results for the different 8-bit conversions (Mai *et al.* (black) and Mir *et al.* (f_s) (blue)) of backward compatible HDR image coding residues for the selected five HDR images coded with the standard codec in the residue layer and with a fixed base layer quantization parameter, QP = 27.

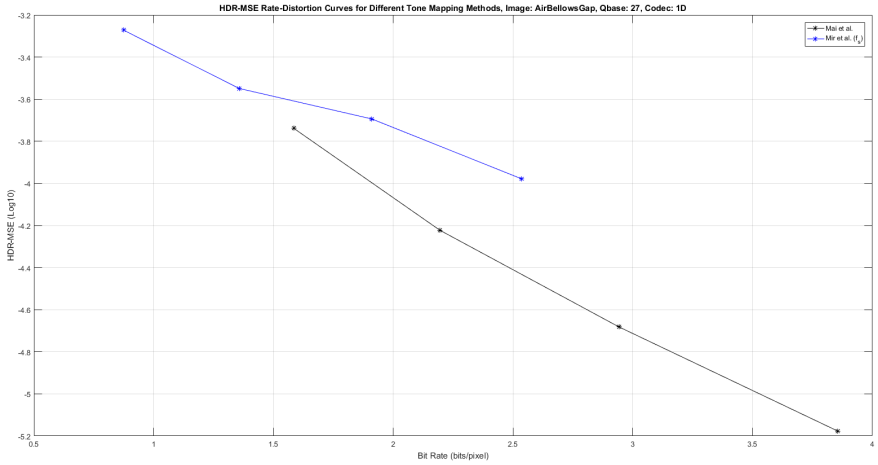

(a) *AirBellowsGap*

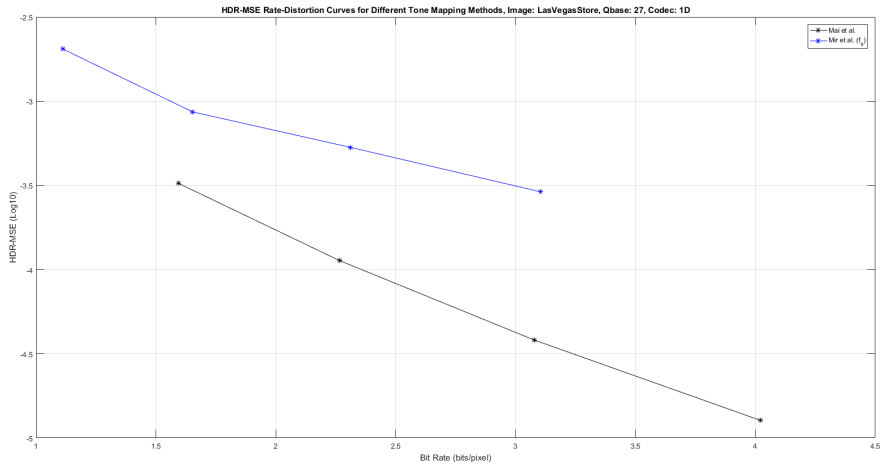

(b) *LasVegasStore*

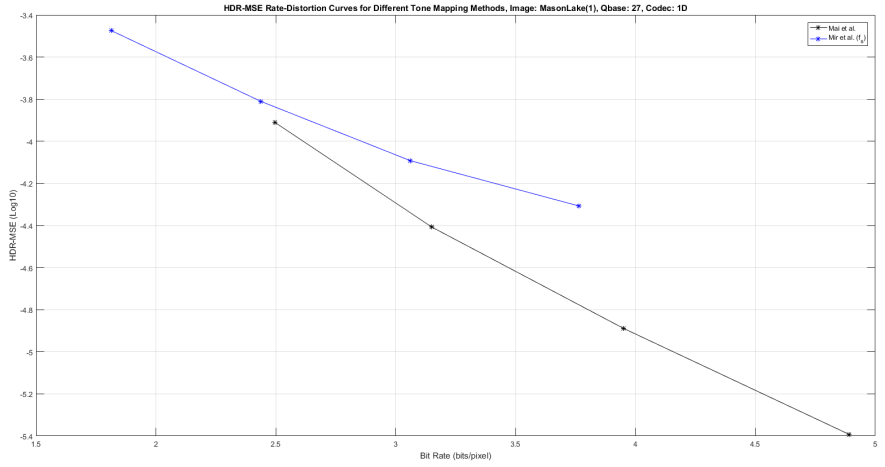

(c) *MasonLake(1)*

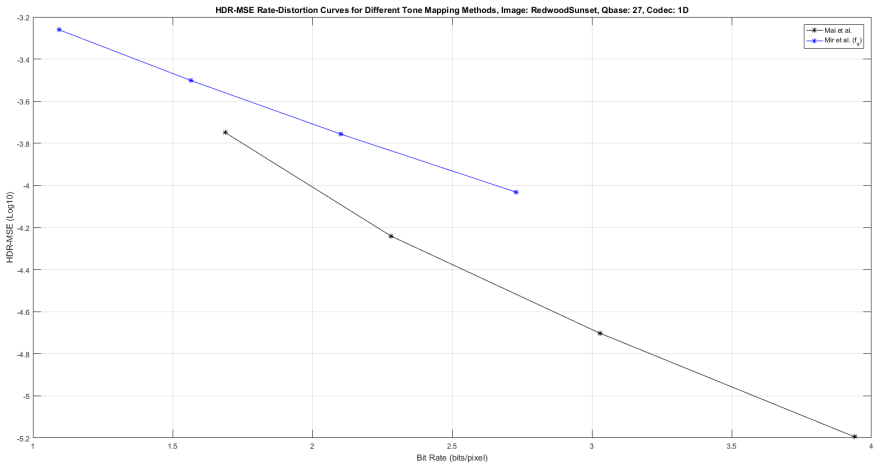

(d) *RedwoodSunset*

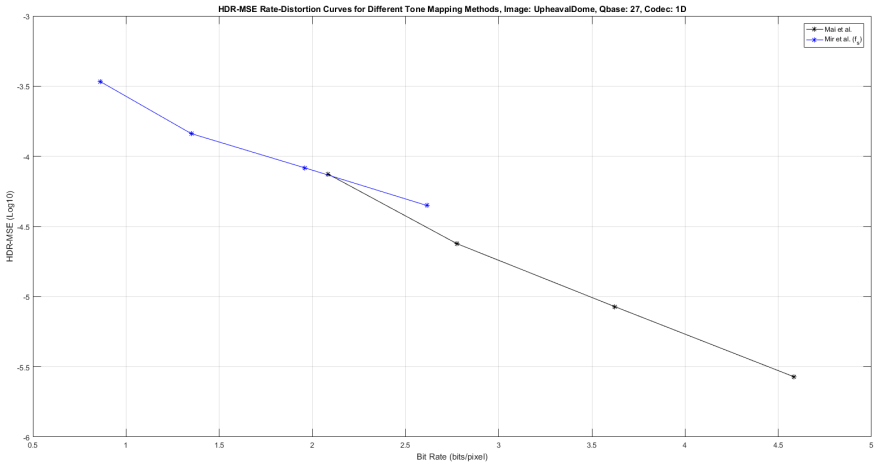

(e) *UpheavalDome*

Figure 6.2: HDR-MSE (log_{10}) vs. bitrate (bits/pixel) rate-distortion performance plot results for the different 8-bit conversions (Mai *et al.* (black) and Mir *et al.* (f_s) (blue)) of backward compatible HDR image coding residues for the selected five HDR images coded with the directional or in other words the 1-D codec in the residue layer and with a fixed base layer quantization parameter, QP = 27.

6.2.2 Rate-Distortion Performance Results for the Coding of 8-bit Backward Compatible HDR Image Coding Residues

As mentioned before in Chapter 5, after the verification of local anisotropic characteristics of high dynamic range (HDR) image coding residues for the coding of backward compatible HDR image coding residues after the 8-bit conversion, two coding methods, which are the directional coding [31-33] that refers to coding with the modified H.264/AVC JM 10.2 reference software encoder-decoder in [32, 33] and the standard coding that refers to coding with the standard H.264/AVC JM 10.2 reference software encoder-decoder [8], are utilized to see whether the directional coding is a good candidate solution or not besides the standard coding. In addition, as mentioned before in the previous section, after the verification of better rate-distortion performance of the adaptation of the optimum tone mapping method to backward compatible HDR image coding residues against the Sigmoid function of the adaptive residual mapping method, the adaptation of the optimum tone mapping method is used in the experiments on the coding of 8-bit backward compatible HDR image coding residues.

Figures 6.3, 6.4, 6.5 and 6.6 show the rate-distortion performance plot results for the coding of 8-bit backward compatible HDR image coding residues in terms of high dynamic range-minimum square error (HDR-MSE), perceptually uniform-peak signal to noise ratio (PU-PSNR), high dynamic range-visible differences predictor quality metric (HDR-VDP) (Q) and high dynamic range-video quality measure (HDR-VQM), respectively. From Figures 6.3 and 6.4, the superiority of the directional coding against the standard coding in the meaning of rate-distortion performances is quite observable for all the selected five HDR images, which are adequately diverse, roughly cover the reasonable dynamic and spatial activity ranges and representative to perform comparisons as mentioned before in Chapter 4. The gains in the HDR-MSE and the PU-PSNR metrics are almost similar with each other and are about 0.2 to 0.6 dB depending on the bitrate and the image. This corresponds to gains in the bitrate of about 2 to 6 % for a fixed HDR-MSE value and a fixed PU-PSNR value. These obtained gains are parallel with the gains that have been obtained for low dynamic range (LDR) motion-compensated (MC) prediction residuals in [32, 33].

In Figures 6.5 and 6.6, the rate-distortion performance plot results are given in terms

of perceptual quality metrics the HDR-VDP (Q), which is known as the HDR visible differences predictor quality metric, and the HDR-VQM, which is known as the HDR video quality measure metric. With these metrics, it can be observed that, the rate-distortion performance plot results obtained with the directional codec are not consistently better than the rate-distortion performance plot results obtained with the standard codec. According to the rate-distortion performance plot results in terms of these perceptual quality metrics, it can be inferred that, even though the directional coding is a good candidate solution for the coding of 8-bit backward compatible HDR image coding residues, this does not always mean that these perceptual quality metrics, which can better model the human visual system (HVS) perception, give better results.

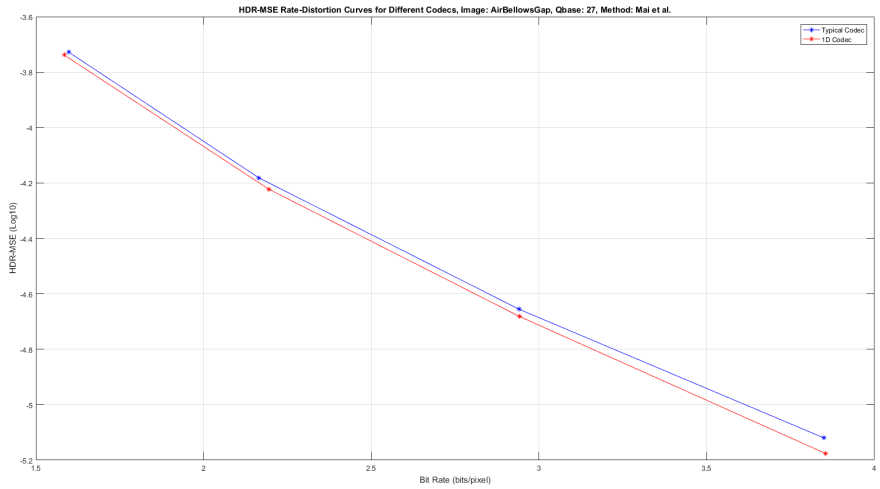

(a) *AirBellowsGap*

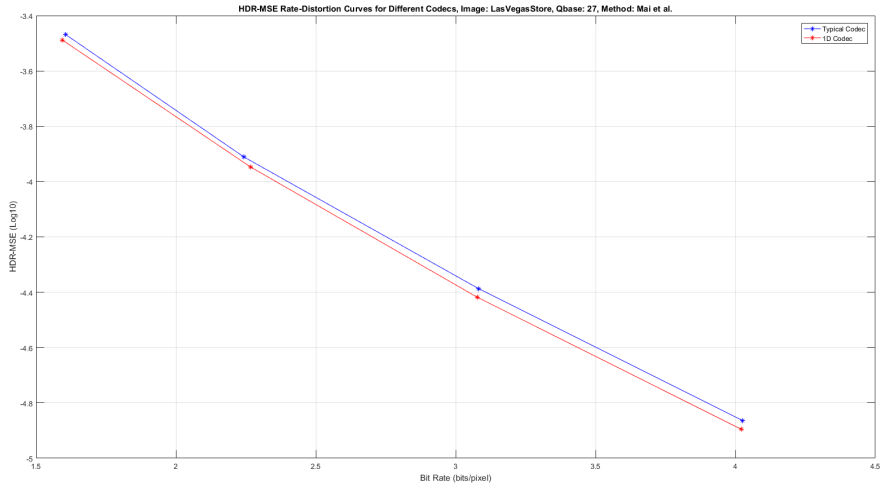

(b) *LasVegasStore*

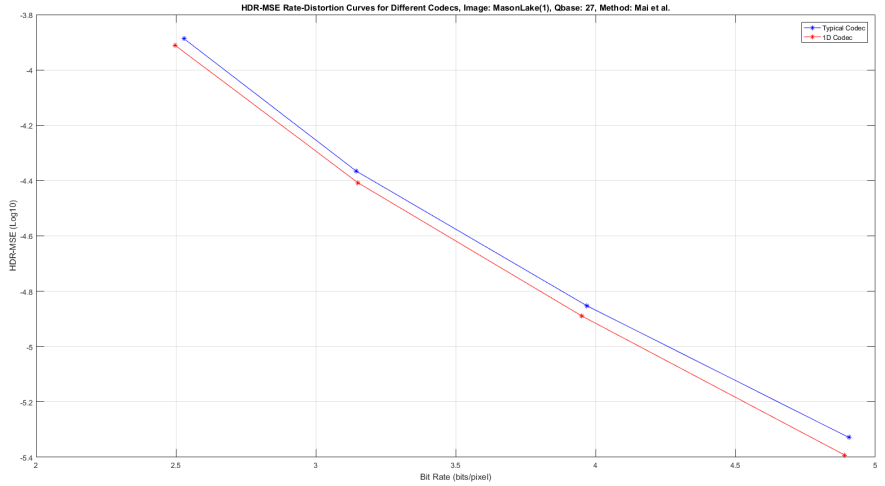

(c) *MasonLake(1)*

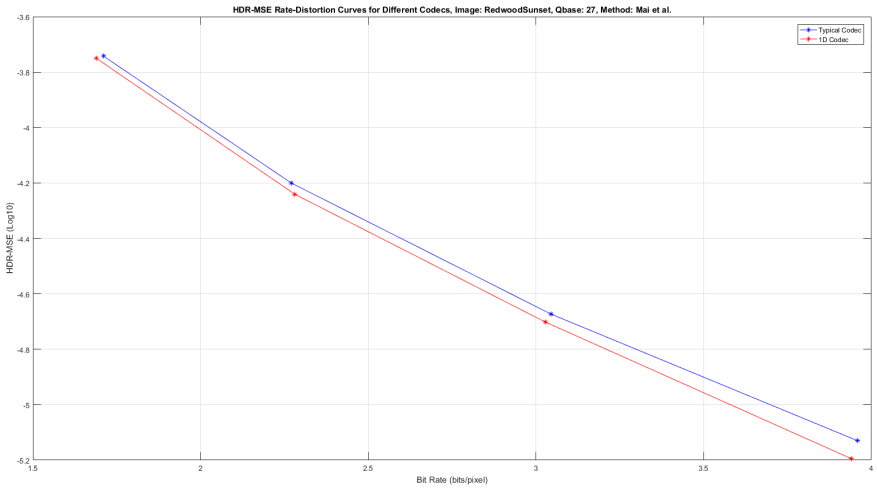

(d) *RedwoodSunset*

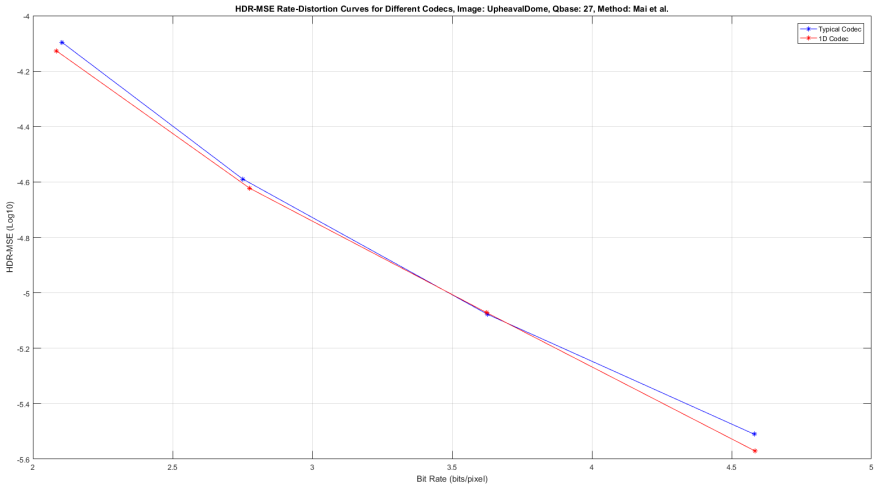

(e) *UpheavalDome*

Figure 6.3: HDR-MSE (log_{10}) vs. bitrate (bits/pixel) rate-distortion performance plot results for the coding (the standard coding (blue) and the directional coding (red)) of 8-bit backward compatible HDR image coding residues for the selected five HDR images coded with the 8-bit conversion method of Mai *et al.* in the residue layer and a fixed base layer quantization parameter, QP = 27.

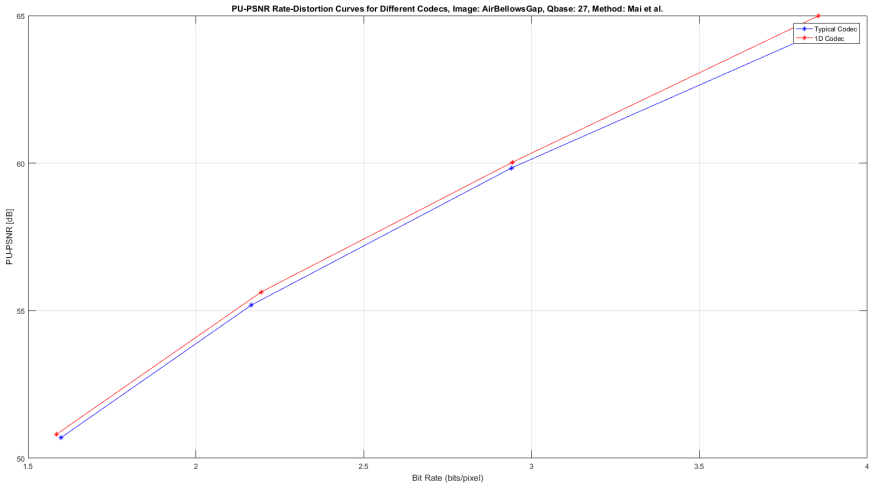

(a) *AirBellowsGap*

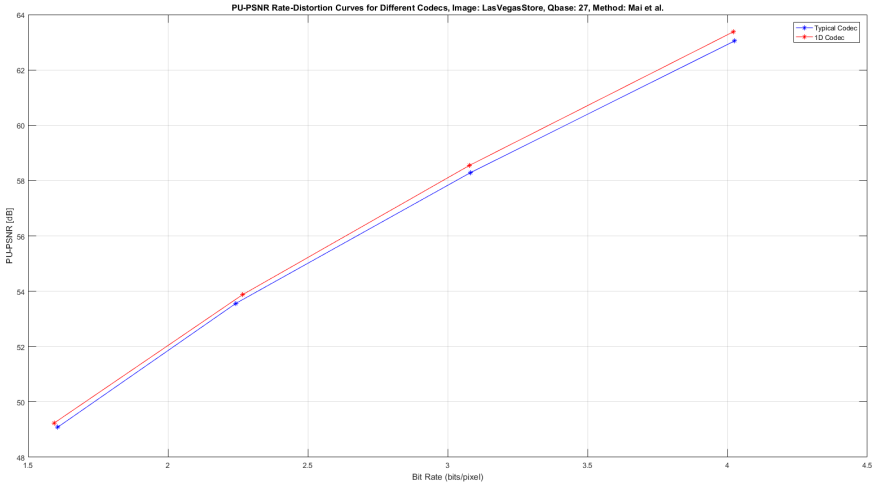

(b) *LasVegasStore*

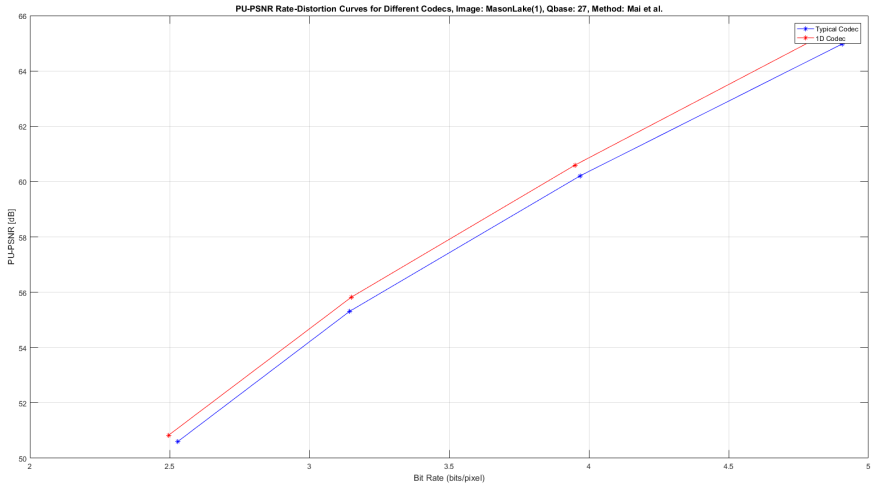

(c) *MasonLake(1)*

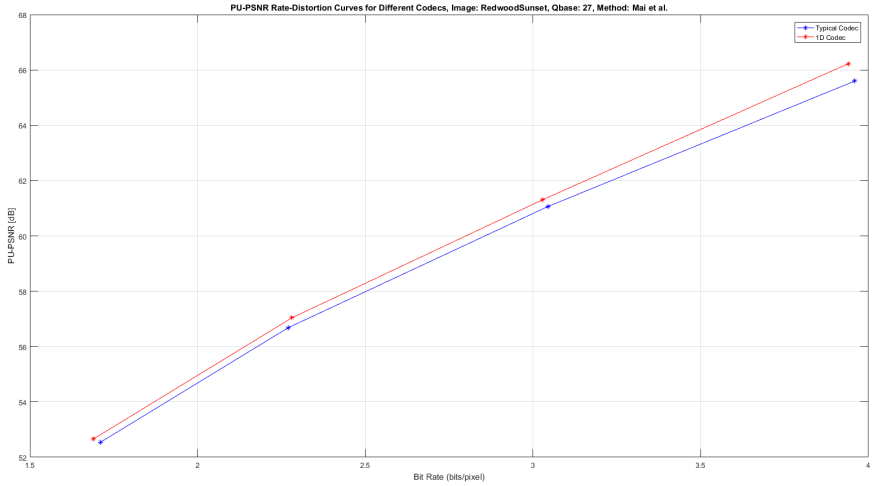

(d) *RedwoodSunset*

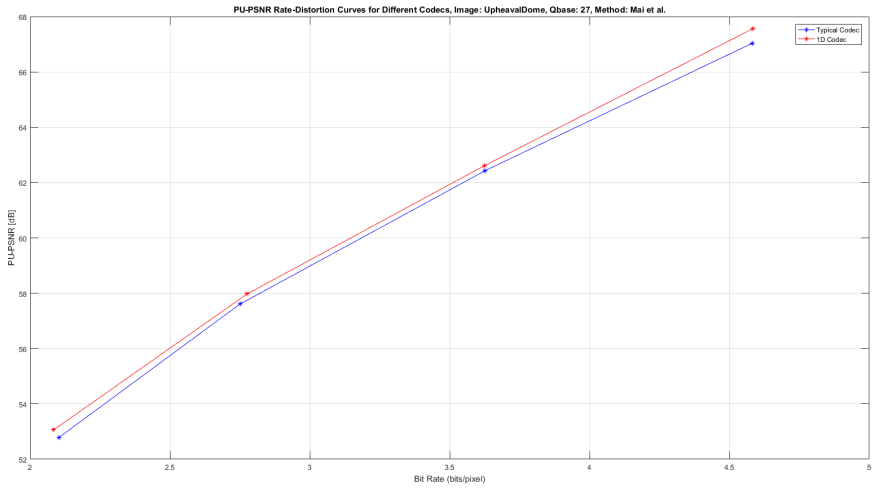

(e) *UpheavalDome*

Figure 6.4: PU-PSNR [dB] vs. bitrate (bits/pixel) rate-distortion performance plot results for the coding (the standard coding (blue) and the directional coding (red)) of 8-bit backward compatible HDR image coding residues for the selected five HDR images coded with the 8-bit conversion method of Mai *et al.* in the residue layer and a fixed base layer quantization parameter, QP = 27.

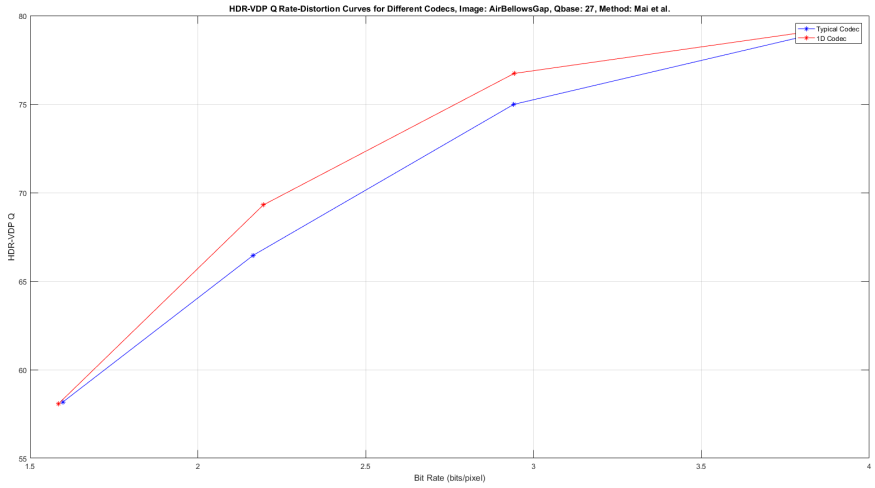

(a) *AirBellowsGap*

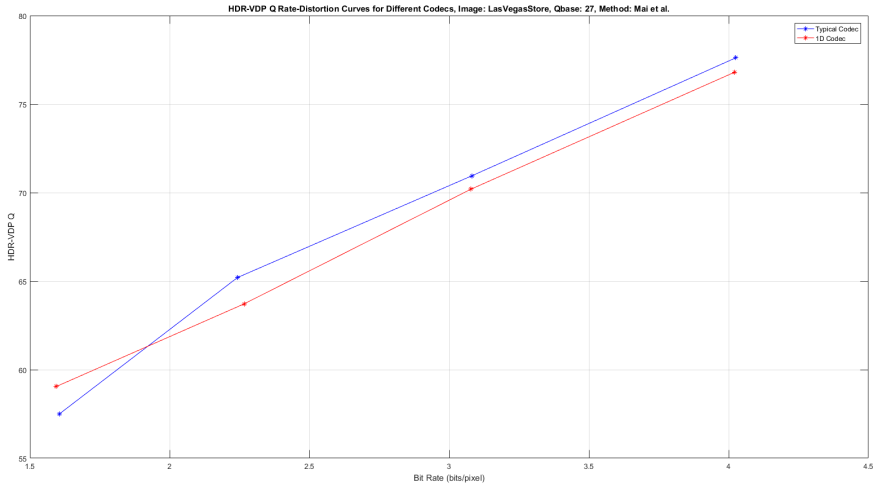

(b) *LasVegasStore*

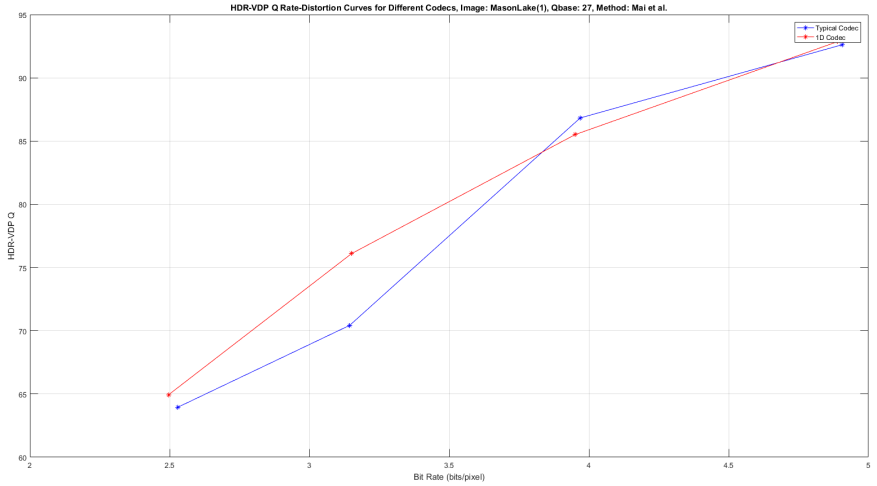

(c) *MasonLake(1)*

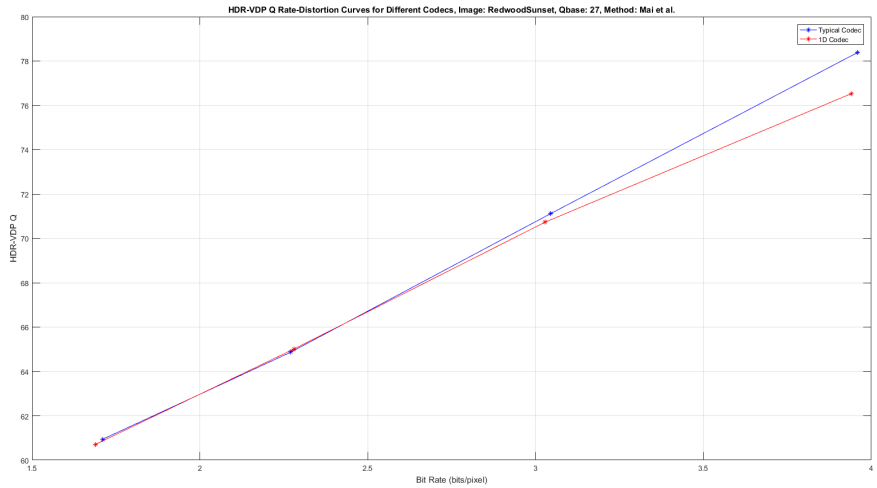

(d) *RedwoodSunset*

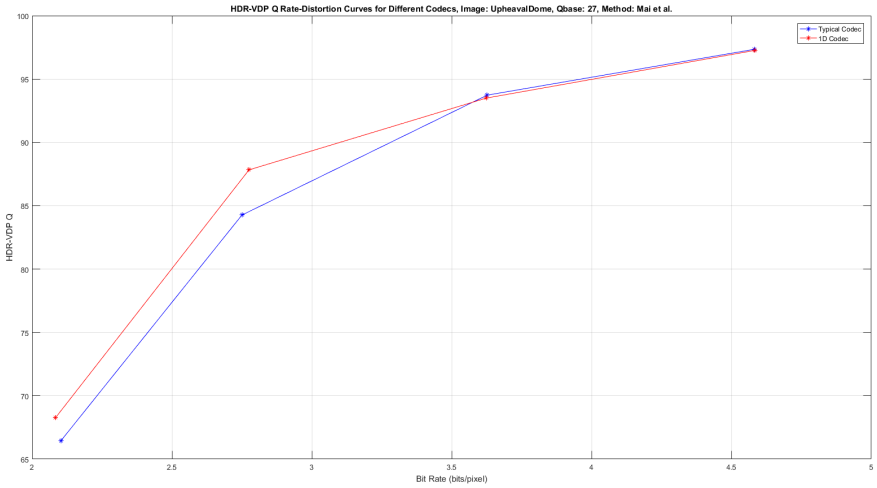

(e) *UpheavalDome*

Figure 6.5: HDR-VDP (Q) vs. bitrate (bits/pixel) rate-distortion performance plot results for the coding (the standard coding (blue) and the directional coding (red)) of 8-bit backward compatible HDR image coding residues for the selected five HDR images coded with the 8-bit conversion method of Mai *et al.* in the residue layer and a fixed base layer quantization parameter, QP = 27.

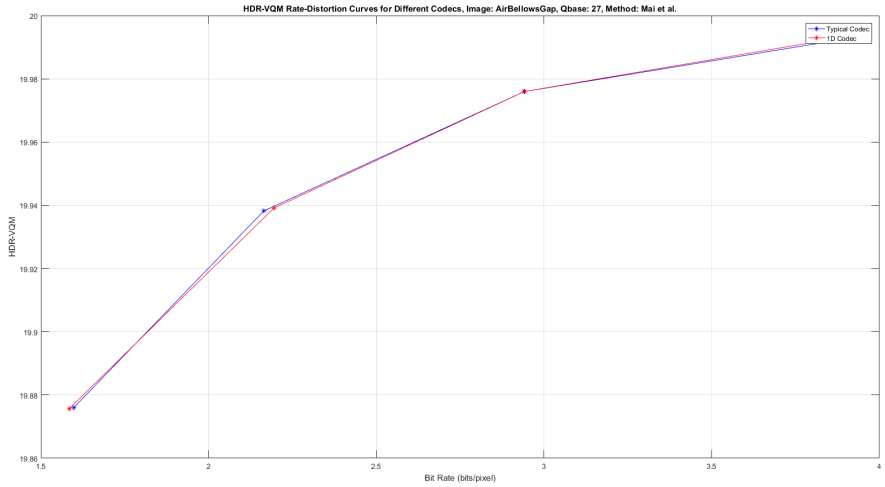

(a) *AirBellowsGap*

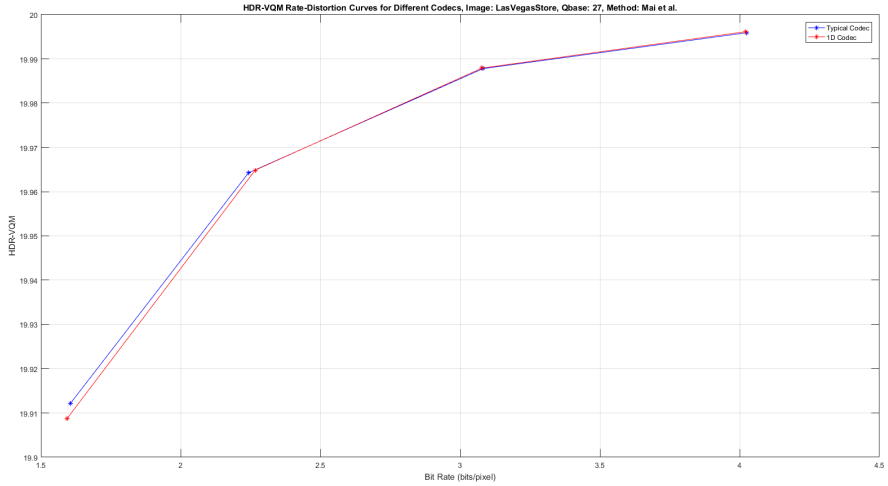

(b) *LasVegasStore*

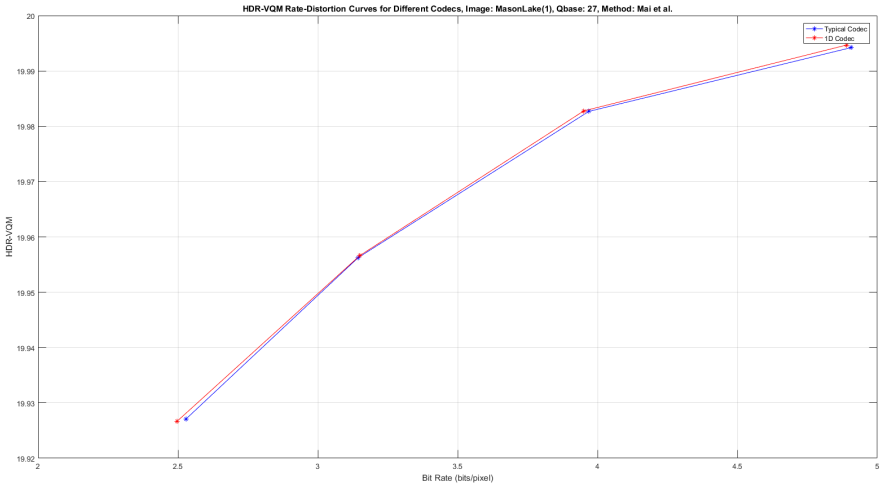

(c) *MasonLake(1)*

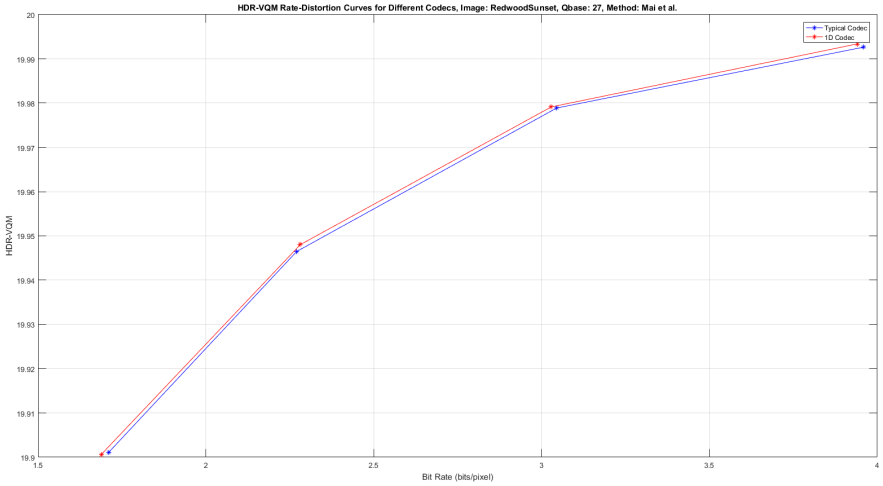

(d) *RedwoodSunset*

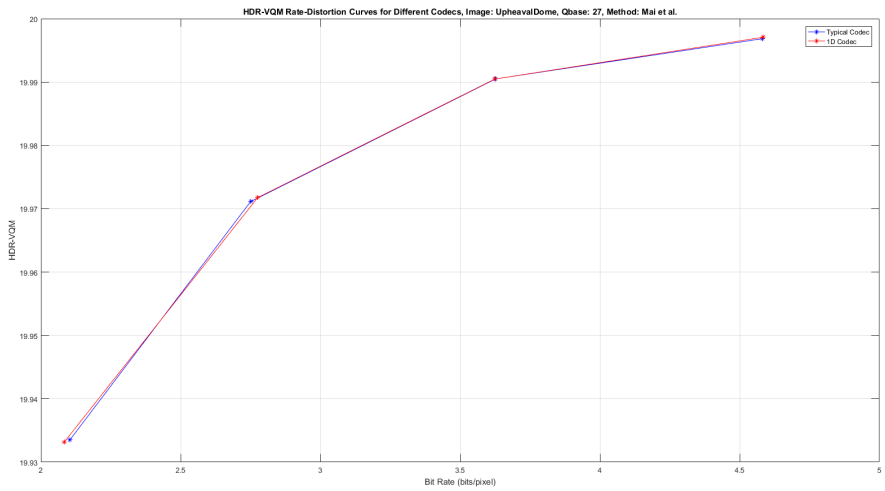

(e) *UpheavalDome*

Figure 6.6: HDR-VQM vs. bitrate (bits/pixel) rate-distortion performance plot results for the coding (the standard coding (blue) and the directional coding (red)) of 8-bit backward compatible HDR image coding residues for the selected five HDR images coded with the 8-bit conversion method of Mai *et al.* in the residue layer and a fixed base layer quantization parameter, QP = 27.

CHAPTER 7

CONCLUSIONS

In this chapter, summary of the thesis, conclusions and future work are provided.

7.1 Summary

In this thesis, a backward compatible high dynamic range (HDR) image coding system was proposed, designed and tested with the purpose of providing successful transition from widely accepted low dynamic range (LDR) technology, which has limitations to represent visual content of technological needs of progressive world, to HDR technology, which is proposed to overcome the limitations of LDR technology and encodes the whole luminance range of real world scenes which changes from extreme darkness (10^{-6} cd/m^2) to bright sunshine (10^{8} cd/m^2). For this purpose, a more efficient coding method for backward compatible HDR image coding residues, which are obtained as the differences between original HDR images and their predictions from corresponding base layer LDR images, was proposed and implemented. Firstly, spatial characteristics of backward compatible HDR image coding residues and spatial characteristics of LDR motion-compensated (MC) prediction residuals were associated with each other by visual inspection. Visually inspected similarities between spatial characteristics of backward compatible HDR image coding residues and LDR MC prediction residuals, which become more apparent on edges, object boundaries and textured regions, were quantified by performing the auto-covariance (AC) analyses on backward compatible HDR image coding residues. These analyses were followed by the implementation of the proposed coding method which is

more efficient according to spatial characteristics of backward compatible HDR image coding residues. The proposed coding method comprises two stages, which are the 8-bit conversion of backward compatible HDR image coding residues and the directional coding, which was used for the coding of LDR MC prediction residuals before. And finally, the rate-distortion performances of the proposed coding method were evaluated by the objective and perceptual quality metrics as well.

In Chapter 2, the general scheme of the proposed backward compatible coding of HDR image with the base layer and the residue layer was presented and the operations which were accomplished for each stage of both the layers were explained in detail.

In Chapter 3, the AC analyses of backward compatible HDR image coding residues were presented and explained in detail. In order to code backward compatible HDR image coding residues more efficiently as in the case of LDR MC prediction residuals, the study of their characteristics was a necessity before implementing the proposed coding method for backward compatible HDR image coding residues. With this purpose, in order to understand whether backward compatible HDR image coding residues exhibit also local anisotropic characteristics or not as in the case of LDR MC prediction residuals, backward compatible HDR image coding residues were investigated with respect to different bitrates (different quantization parameters (QPs)), spatial activities and dynamic ranges as the main variables in the HDR image coding. Firstly, spatial characteristics of backward compatible HDR image coding residues and spatial characteristics of LDR MC prediction residuals were associated with each other by visual inspection. After that, in order to quantify the visual inspected similarities, which were more apparent on edges, object boundaries and textured regions, between spatial characteristics of backward compatible HDR image coding residues and LDR MC prediction residuals, the utilized necessary AC models were explained. Finally, how to estimate the parameters of the utilized AC models was given at the end of the chapter.

In Chapter 4, the experimental results for the AC analyses of several backward compatible HDR image coding residues, which have different bitrates (different QPs), spatial activities and dynamic ranges as the main variables in the HDR image coding, were given and interpreted. With the resulting AC model parameters for a particu-

lar image with respect to these main variables, by analyzing the behaviours of these parameters, characteristics of the AC of local regions of backward compatible HDR image coding residues were investigated to conclude whether the directional coding methods could be applied for the coding of backward compatible HDR image coding residues or not.

In Chapter 5, afterwards the verification of existence of such local anisotropic characteristics in backward compatible HDR image coding residues in Chapter 3 and 4, the proposed coding method, which comprises two stages that are firstly 8-bit conversion of backward compatible HDR image coding residues and secondly directional coding of them, for backward compatible HDR image coding residues were presented and explained in detail. Also, the details of the utilized codec for this proposed coding method were clarified.

In Chapter 6, the experimental results, which are the rate-distortion performance results, for the proposed coding method with different 8-bit conversion methods and with different coding methods for several backward compatible HDR image coding residues, which have different bitrates (different QPs), spatial activities and dynamic ranges as the main variables in the HDR image coding, were given, compared and interpreted.

7.2 Conclusions

Backward compatible high dynamic range (HDR) image coding residues were analyzed whether they exhibit also local anisotropic characteristics or not as in the case of low dynamic range (LDR) motion-compensated (MC) prediction residuals by performing auto-covariance (AC) analyses on them. The experiments on the AC analyses of backward compatible HDR image coding residues have revealed that backward compatible HDR image coding residues obtained as the differences between original HDR images and their predictions from the corresponding base layer LDR images possess 1-D directional characteristics for several HDR images, which roughly cover a reasonable dynamic and spatial activity ranges. Furthermore, the 1-D directional structures in backward compatible HDR image coding residues become more salient

as the quantization in the base layer increases. The existence of such 1-D directional characteristics in backward compatible HDR image coding residues and its similarity between LDR MC prediction residuals indicate that the directional coding method, which uses diverse 1-D directional transforms in addition to the conventional 2-D transforms of the existing codecs and were used for LDR MC prediction residuals before, outperforms the standard coding methods, which use only the conventional 2-D transforms of the existing codecs, as a better solution for the coding of backward compatible HDR image coding residues. Moreover, rate-distortion performances of backward compatible HDR image coding residues vary with different 8-bit conversion methods. For instance, while some 8-bit conversion methods can give poor results such as the Logit function of the adaptive residual mapping method, the others can give good results such as the Sigmoid function of the adaptive residual mapping method and the adaptation of the optimum tone mapping method to backward compatible HDR image coding residues. It is verified that, the adaptation of the optimum tone mapping method to backward compatible HDR image coding residues remarkably surpasses the Sigmoid function of the adaptive residual mapping method in the meaning of rate-distortion performances for both the standard and the directional coding as an 8-bit conversion.

7.3 Future Work

The backward compatible or in other words the layer-based structure, which is used in this thesis, is composed of two layers, namely the base layer as the first layer and the residue layer as the second layer. In the experimental results of the proposed coding method for backward compatible high dynamic range (HDR) image coding residues, the bitrate used in the rate-distortion performance results is taken as the total bitrate of the base layer and the residue layer. However, question of how much bit is allocated for the each layer is not investigated. As a future work, bitrate allocation for each layer used in the backward compatible or in other words the layer-based structure can be studied. Furthermore, this research was conducted on backward compatible HDR image coding residues as a basis, for future work this research can be expanded to backward compatible HDR video coding residues or in other words sequential back-

ward compatible HDR image coding residues with incoming challenges as well. In addition, in this thesis, proof of the concept of whether the directional coding is a good candidate solution or not for the coding of backward compatible HDR image coding residues besides the standard coding is aimed mainly. Hence, the 1-D directional transforms are not integrated or the necessary modifications are not performed in the state-of-the-art codec at the time this research was conducted. As a future work, this research can be expanded to state-of-the-art codec at that time in order to see how much gain this brings.

REFERENCES

[1] G. W. Larson, "Real pixels in Graphics Gems II", J. Arvo (ed.), Academic Press, 1991.

[2] OpenEXR HDR File Format. [Online]. Available: http://www.openexr.com/

[3] G. W. Larson, “LogLuv Encoding for Full-Gamut, High-Dynamic Range Images”, J. Graph. Tools, Vol. 3, No. 1, pp. 15–31, 1998.

[4] F. Banterle, A. Artusi, K. Debattista, and A. Chalmers, "Advanced High Dynamic Range Imaging", AK Peters/CRC Press, 2011.

[5] E. François, C. Fogg, Y. He, X. Li, A. Luthra, and A. Segall, “High Dynamic Range and Wide Color Gamut Video Coding in HEVC: Status and Potential Future Enhancements”, IEEE Transactions on Circuits and Systems for Video Technology, Vol. 26, No. 1, pp. 63-75, January, 2016.

[6] Z. Mai, H. Mansour, R. Mantiuk, P. Nasiopoulos, R. Ward, and W. Heidrich, “Optimizing a Tone Curve for Backward-Compatible High Dynamic Range Image and Video Compression”, IEEE Transactions on Image Processing, Vol. 20, No. 6, pp. 1558-1571, June, 2011.

[7] J. Mir, A. Fernando, D. S. Talagala, and H. K. Arachchi, "Rate Distortion Analysis of High Dynamic Range Video Coding Techniques", in Proceedings of IEEE International Conference on Image Processing (ICIP 2015), Quebec City, QC, Canada.

[8] H.264/AVC JM Reference Software. [Online]. Available: http://iphome.hhi.de/suehring/tml/

[9] HEVC Reference Software. [Online]. Available: http://hevc.hhi.fraunhofer.de/

[10] A. Motra and H. Thoma, "An Adaptive LogLuv transform for High Dynamic Range Video Compression", in Proceedings of IEEE International Conference on Image Processing (ICIP 2010), Hong Kong, China.

[11] Y. Zhang, E. Reinhard, and D. Bull, "Perception-based High Dynamic Range Video Compression with Optimal Bit-depth Transformation", in Proceedings of IEEE International Conference on Image Processing (ICIP 2011), Brussels, Belgium.

[12] R. Mantiuk, G. Krawczyk, K. Myszkowski, and H. P. Seidel, "Perception Motivated High Dynamic Range Video Coding", ACM Transactions on Graphics, Vol. 23, No. 3, pp. 733-741, 2004.

[13] S. Liu, W. S. Kim, and A. Vetro, "Bit-depth Scalable Coding for High Dynamic Range Video", in Proceedings of SPIE, Visual Communications Image Processing, Vol. 6822, 2008.

[14] A. Segall, "Scalable Coding of High Dynamic Range Video", in Proceedings of IEEE International Conference on Image Processing (ICIP 2007), San Antonio, TX, USA.

[15] R. Mantiuk, A. Efremov, K. Myszkowski, and H.P. Seidel, "Backward Compatible High Dynamic Range MPEG Video Compression", ACM Transactions on Graphics, Vol. 25, No. 3, pp. 713–723, 2006.

[16] G. Ward and M. Simmons, "JPEG-HDR: A Backwards Compatible, High Dynamic Range Extension to JPEG", in Proceedings of the 13^{th} Color Imaging Conference, pp. 283-290, 2005.

[17] C. Lee and C. S. Kim, "Rate Distortion Optimized Compression of High Dynamic Range Videos", in 16^{th} European Signal Processing Conference, EUSIPCO, Lausanne, August, 2008.

[18] C. Lee and C. S. Kim, "Rate Distortion Optimized Layered Coding of High Dynamic Range Videos", Journal of Visual Communication and Image Representation, Vol. 23, No. 6, pp. 908-923, August, 2012.

[19] A. Koz and F. Dufaux, “Optimized Tone Mapping with Perceptually Uniform Luminance Values for Backward-Compatible High Dynamic Range Video Compression”, in Proceedings of Visual Communications and Image Processing Conference (VCIP 2012), San Diego, CA, USA.

[20] A. Koz and F. Dufaux, “Methods for Improving the Tone Mapping for Backward Compatible High Dynamic Range Image and Video Coding”, Signal Processing: Image Communication, Vol. 29, No. 2, pp. 274-292, February, 2014.

[21] I. R. Khan, “A Nonlinear Quantization Scheme for Two-Layer HDR Image Coding”, Signal, Image and Video Processing, Vol. 10, No. 5, pp 921-926, July, 2016.

[22] J. Mir, D. S. Talagala, H. K. Arachchi, and A. Fernando, “Adaptive Residual Mapping for an Efficient Extension Layer Coding in Two-Layer HDR Video Coding”, in Proceedings of IEEE International Conference on Image Processing (ICIP 2016), Arizona, USA.

[23] S. Choi, O.-J. Kwon, J. Lee, and Y. Kim, "A JPEG Backward-Compatible Image Coding Scheme for High Dynamic Range Images", Digital Signal Processing, Vol. 67, pp. 1-16, August, 2017.

[24] D. Gommelet, A. Roumy, C. Guillemot, M. Ropert, and J. L. Tanou, "Gradient-Based Tone Mapping for Rate-Distortion Optimized Backward-Compatible High Dynamic Range Compression", IEEE Transactions on Image Processing, Vol. 26, No. 12, pp. 5936-5949, August, 2017.

[25] S. Choi, O.-J. Kwon, D. Jang, and S. Choi, "Evaluation of Various Tone Mapping Operators for Backward Compatible JPEG Image Coding", KSII Transactions on Internet and Information Systems, Vol. 9, No. 9, pp. 3672-3684, September, 2015.

[26] P. Korshunov and T. Ebrahimi, "Context-Dependent JPEG Backward-Compatible High Dynamic Range Image Compression", Optical Engineering, Vol. 52, Issue 10, August, 2013.

[27] K. Feyiz, F. Kamışlı, E. Zerman, G. Valenzise, A. Koz and F. Dufaux, "Statistical Analysis of Residue Signal for Backward Compatible HDR Image Coding", in Proceedings of Signal Processing and Communications Applications Conference (SIU 2017), Antalya, Turkey.

[28] K. Feyiz, F. Kamisli, E. Zerman, G. Valenzise, A. Koz and F. Dufaux, "Statistical Analysis and Directional Coding of Layer-based HDR Image Coding Residue", in Proceedings of IEEE International Workshop on Multimedia Signal Processing (MMSP 2017), London-Luton, UK.

[29] D. Gommelet, A. Roumy, C. Guillemot, M. Ropert, and J. L. Tanou, "Rate-Distortion Optimization of a Tone Mapping with SDR Quality Constraint for Backward-Compatible High Dynamic Range Compression", in Proceedings of IEEE International Conference on Image Processing (ICIP 2016), Arizona, USA.

[30] R. Boitard, R. Cozot, D. Thoreau, and K. Bouatouch, "Motion-Guided Quantization for Video Tone Mapping", in Proceedings of IEEE International Conference on Multimedia and Expo (ICME 2014), Chengdu, China.

[31] F. Kamisli and J. S. Lim, "Transforms for the Motion Compensation Residual", in Proceedings of IEEE International Conference on Acoustics, Speech and Signal Processing, pp. 789-792, April, 2009.

[32] F. Kamisli and J. S. Lim, "1-D Transforms for the Motion Compensation Residual", IEEE Transactions on Image Processing, Vol. 20, No. 4, pp. 1036-1046, April, 2011.

[33] F. Kamisli, "Transforms for Prediction Residuals in Video Coding", Ph.D. Thesis, Massachusetts Institute of Technology, 2010.

[34] H. Zhang and J. S. Lim, "Analysis of One-Dimensional Transforms in Coding Motion Compensation Prediction Residuals for Video Applications", in Proceedings of IEEE ICASSP, pp. 1229-1232, 2012.

[35] N. Ahmed, T. Natarajan, and K. Rao, “Discrete Cosine Transform”, IEEE Transactions Comput., Vol. C-23, No. 1, pp. 90–93, January, 1974.

[36] J. S. Lim, "Two-Dimensional Signal and Image Processing", Prentice Hall, 1990.

[37] Meaning of Anisotropy. [Online]. Available: https://en.wikipedia.org/wiki/Anisotropy

[38] G. Valenzise, F. De Simone, P. Lauga, and F. Dufaux, “Performance Evaluation of Objective Quality Metrics for HDR Image Compression”, in Proceedings of SPIE, Applications of Digital Image Processing XXXVII, San Diego, CA, August, 2014.

[39] Ian E. G. Richardson, "H.264 and MPEG-4 Video Compression: Video Coding for Next-generation Multimedia", Wiley, 2003.

[40] D. Marpe, H. Schwarz, and T. Wiegand, "Context-based Adaptive Binary Arithmetic Coding in the H.264/AVC Video Compression Standard", IEEE Transactions on Circuits and Systems for Video Technology, Vol. 13, No. 7, pp. 620-636, July, 2003.

[41] T. O. Aydin, R. Mantiuk, and H. P. Seidel, "Extending Quality Metrics to Full Luminance Range Images", in Proceedings of SPIE, Human Vision and Electronic Imaging XIII, San Jose, California, United States, March, 2008.

[42] R. Mantiuk, S. Daly, K. Myszkowski, and H. P. Seidel, “Predicting Visible Differences in High Dynamic Range Images: Model and its Calibration”, in Proceedings of SPIE, Human Vision and Electronic Imaging X, San Jose, California, United States, March, 2005.

[43] M. Narwaria, M. P. D. Silva, P. L. Callet, “HDR-VQM: An Objective Quality Measure for High Dynamic Range Video", Signal Processing: Image Communication, Vol. 35, pp. 46-60, July, 2015.

[44] S. J. Daly, “Visible Differences Predictor: An Algorithm for the Assessment of Image Fidelity", in Proceedings of SPIE, Human Vision, Visual Processing, and Digital Display III, San Jose, CA, United States, August, 1992.